Assessing the Long-Term Performance of Tidal Turbines subject to Biofouling

By

Omid Afshar

B.E., Islamic Aziz University of Tehran (South Branch), Iran (2003)

M.E. University of Malaya, Malaysia (2013)

Submitted in Fulfilment of the requirements for the Degree of Doctor of Philosophy

School of Engineering

2018

Statement of originality and Authority of Access

This thesis contains no material that has been accepted for a degree or diploma by the University of Tasmania or other institution, and to the best of my knowledge and belief no material previously published or written by another person except by way of background and due acknowledgement is made in text of thesis.

Omid Afshar

Statement of Authority Access

This thesis may be available for loan and limited copying in accordance with the Copyright Act 1968.

Omid Afshar

Abstract

Among many sources of renewable energy available, tidal energy, has many attractive features as a clean energy resource. It is a sizable resource, distributed along coastlines and is considered to be one of the more promising renewable energy sources. However, a key concern associated with tidal turbines is their long-term reliability when operating in the hostile marine environment. Biofouling changes the physical shape and roughness of tidal turbine components, hence altering turbine performance. This represents a large stumbling block for adoption of the technology. Among the various types of fouling on man-made structures, barnacles are considered to be one of the most problematic organisms. Therefore, the main objective of this study was to determine the effect of barnacles on the performance of a twin-bladed horizontal axis tidal turbine. Three research questions were investigated: how barnacle roughness alters the performance of aerofoil sections of which tidal turbines are based; how barnacle fouling changes the long-term turbine performance of tidal turbines; and how the presence of barnacles affects drag on a flat plate.

The first two questions were investigated using Computational Fluid Dynamics (CFD). The geometry and density of the conical shaped barnacle elements for the adult sized *Amphibalanus Amphitrite* barnacle, were estimated to determine an equivalent sand-grain roughness. A commercial Reynolds Averaged Navier-Stokes (RANS) solver with Shear-Stress Transport (SST) turbulence model was used to simulate the flow around a two-dimensional NACA63-618 aerofoil with and without surface roughness. The model was validated against published experimental data for a smooth case. The results showed the presence of the adult barnacle fouling decreased the maximum lift coefficient by an average of 21% and lift-to-drag force ratio by an average of 60%. The performance of a twin-bladed horizontal axis turbine with rotors of the same aerofoil section was also studied. The barnacle roughness decreased

the peak power coefficient from 0.42 to 0.37 at the design tip-speed ratio of 6. This represents a decrease in turbine output power of 12%. The approximate time taken to reach adult size and establishment of this barnacle fouling community is approximately 8-12 months.

The effect of barnacle roughness on total drag force and the turbulent boundary layer on a test plate covered with artificial barnacles was studied experimentally in a water tunnel using a floating element force balance. The artificial barnacle models tested were obtained using a novel method of scanning real barnacles, 3D printing and then moulding them using an epozy resin. Three fouled plates were tested with low, medium and high barnacle fouling density. Based on roughness equations for cone shaped barnacle, a reduction in barnacle spacing (an increase in barnacle density) caused an increase in equivalent sand grain roughness. The results of roughness correlations indicated the equivalent barnacle roughness was 34.78 mm, 78.47 mm, and 112.9 mm for low, medium and high barnacle fouling density respectively. The testing showed the presence of artificial barnacles produced a maximum increase in the drag coefficient of 429% for the low density case.

Based on governing equations (geometrical formulations)for tidal turbine blade and single roughness elements, an increase in sand grain roughness causes a reduction in power coefficient results. According to theoretical hydrodynamic power of turbine, the smooth case gives the highest power coefficient. It is around 0.42. As shown and discussed, the lowest barnacle density produced an average 5% reduction in power coefficient over the clean case. For low density status, the power coefficient is around 0.4 and there is a slight difference between low density and smooth result with the same tip speed ratio. For a medium case, the percentage is over a 10% decrease in the power coefficient over the smooth case. An increase in sand grain roughness value causes a reduction in power generation from 0.38 to 0.34. For high-density status, the percentage of decreasing of power generation is 22%.

Acknowledgements

This project was funded by a Tasmania Graduate Research Scholarship (TGRS), with in-kind support from School of Engineering and ITC-UTAS.

This thesis would not have been possible without the assistance of a great number of people. I would like to particularly thank Dr.Alan Henderson for his supervision, support, friendship and inspiration during my PhD study. He taught me a lot of points about fluid mechanics. I inherited the UTAS Water Tunnel from Dr. Jessica Walker, who spent many hours teaching me how to use it, and also provided research papers for background reading. My co-supervisor, Associated Prof Xiaolin Wang, has shared his knowledge and enthusiasm for fluid dynamics, and provided much guidance over the course of this study.

My thanks goes to Dr. Ruth Erikson, at Institute Marine and Antarctica Study (IMAS), who gave me the opportunity to become familiar with some details about biofouling species. Dr. Neville Barret and Dr. Graham Edgar have also been great supporters. Dr. Michael Breadmore, Dr. Petr Smejcal and Mr. Sean Krisanski provided invaluable support in the field of 3-D printing technique.

The technical support staff at University of Tasmania have been invaluable throughout this project. I would like to thank in particular Calverly Gerard for his patience and guidance for calibration of equipment, setting up the data acquisition and Laser Doppler Velocimetry (LDV) system. Andrew Bylett, Peter Seward, David Morley and Rodrigo Ruffino provided much assistance in the Engineering workshop.

Finally, thanks to my partner, Nadia Azizabadi, who has been there for the whole journey and supported me all the way.

Contents

List of Figures

List of Tables

Nomenclature

Roman Symbols

A_f:	Frontal area of a single barnacle roughness	m^2
A_s:	Windward wetted area of a barnacle surface	m^2
b:	Width of test plate	m
B:	Smooth wall log-law intercept	-
c	Blade chord	m
C_D	Drag coefficient	-
C_f:	Friction coefficient	-
C_L	Lift coefficient	-
C_P:	Power coefficient	-
C_{press}:	Pressure coefficient	-
C_T:	Thrust coefficient	-
D	Drag force	N
d:	local diameter of turbine blade	m
Di:	Diameter of turbine blade	m
D_{theor}:	Theoretical drag force	N
f	Friction factor	-
g	Gravitational constant	m/s^2
h:	Height	m
H:	Height of artificial barnacle	m
h_f	Frictional loss	m
k:	Von karman constant	-
k:	Actual roughness height	m
k_s:	Sandgrain roughness height	m
$k_{s,p}$:	Sandgrain roughness height of prototype case	m

$k_{s,m}$:	Sandgrain roughness height of model	m
l	Section length of barnacle	m
l_p:	Length of test plate	m
L	Lift force	N
m	Cross sectional area of aerofoil	m
M:	Mass	kg
N:	Number of samples	-
p	Pressure	Pa
P	Power	W
p:	Local static pressure	Pa
p_0:	static pressure	Pa
Q:	Torque	N.m
r:	Blade radius of aerofoil	m
R	Blade radius	m
Re:	Reynolds number	-
s	Blade span	m
S:	Aerofoil surface area	m^2
S_f:	Total frontal area of barnacle roughness	m^2
S_i:	Generalized source term	-
t:	Thickness	m
T:	Temperature	°C
T	Thrust force	N
U	Flow speed	m/s
U^+:	Dimensionless velocity	-
u:	Local velocity	m/s
u_τ:	Friction velocity	m/s
u_i:	Velocity component of i direction	m/s
u_j:	Velocity component of j direction	m/s

y^+:	wall distance	-

Greek letters

σ	Tensile stress	Pa
τ	Shear stress	Pa
ρ	Density	kg/m^3
τ	Shear stress	Pa
μ:	Dynamic viscosity	kg/ms
υ:	Kinematic viscosity	m^2/s
τ_w:	wall shear stress	Pa
Λ_s:	modified roughness density and shape parameter	-
ω:	Angular velocity	rad/s
λ:	Tip Speed Ratio	-
α:	Angle of attack	°
β:	Twisted angle	°
φ:	Incident angle	°
θ:	Momentum thickness	mm
ε:	Virtual origin error	mm
δ:	boundary layer thickness	mm
δ^*:	displacement thickness	mm

Chapter 1

Introduction

1. Background

There is a growing market for green energy derived from sustainable resources throughout the world, with many countries offering incentives and targets. The oceans around the world offer a large energy sources that is yet to be significantly tapped [1,2].

The forms of ocean energy can be categorised into tidal, wave, current, thermal gradient and salinity gradient [3,4]. Of these five categories, the most significant developments of the past decade have been in both tidal and wave energy. Tides and waves are said to have great potential for providing predictable and consistent power generation, in comparison with solar and wind energy, which are subject to weather fluctuations that are much more difficult to predict [5,6].

Many countries surrounded by the oceans have rich marine energy resources and this represents a significant development potential for tidal and wave power turbines for electric power generation. Interest is growing in water current turbines as a clean power technology. High potential areas for tidal resources is provided in Fig.1.1.

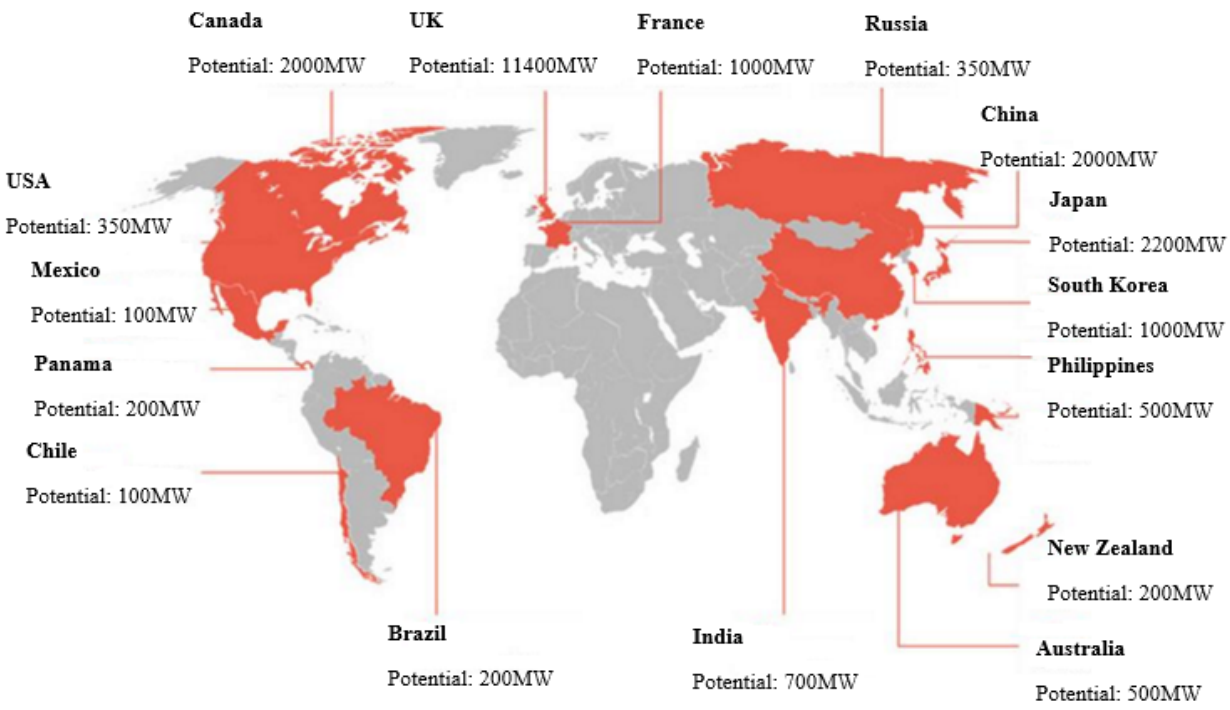

Fig.1. 1. High potential area for tidal resources [7].

In the field of tidal or ocean current energy, the Horizontal Axis Tidal Turbines (HATTs) have undergone intensive research in the past decades. Compared with other devices, currently HATTs appear to be the most technologically and economically viable one, and a number of large-scale marine current turbines have been deployed [1,2].

However, a key concern associated with tidal current turbines is their long-term reliability when operating in a hostile marine environment. Biofouling commonly occurs in the form of algae, mussels, and barnacles. Appropriate of materials can inhibit corrosion but is less easily to control the growth algae, mussels, barnacles. Biofouling changes the physical shape and roughness of turbine components, hence altering a turbine's overall performance.

2. Aims and Objectives

It is well understood that the biofouling effect has an adverse effect on ship hull performance [8]. There are many studies to indicate that increased roughness on the ship hull and propeller contributes to increased hull frictional resistance and decreased propeller efficiency, respectively [8-11]. Both translate into increased power consumption, or decreased speed [10]. However, there have been very few studies to investigate biofouling roughness on marine turbine performance.

Among the various types of fouling on man-made structures, barnacles are considered to be one of the most problematic organisms. Therefore, in this study, effect of barnacles on tidal turbine performance will be investigated. The main objective of this study is to determine the effect of barnacles on the performance of a twin-bladed horizontal axis tidal turbine. Three objectives are investigated:

1. How barnacle roughness alters the performance of aerofoil sections of which tidal turbines are based;
2. How barnacle fouling changes the long-term turbine performance of tidal turbines;
3. And how do the physical properties of barnacles such as density alter hydrodynamic performance marine surface.

1. Methodology of this study

These questions are answered using a combination of computational and experimental studies. At the first step, more specific information about barnacle characteristics and the relationship between the attachment process and associated roughness development on marine surfaces especially marine turbine blade will be reviewed. In order to better understanding of

aerodynamic performance on cross-sectional shape of turbine blade, flow around a two-dimensional NACA63-618 aerofoil shape with and without surface roughness will be investigated. Then the performance of a twin-bladed horizontal axis turbine with rotors of the same aerofoil section will also studied.

The numerical results of this research were conducted using the commercial ANSYS CFX 15 software. CFD can obtain various results at low cost and it used in a variety of fields. In addition, one of the biggest advantage of CFD over experiments is that the full-scale simulations can be carried out so that the scale effects mainly stem from relatively different boundary layers and flow separation can be avoided. The Reynolds Navier Stokes (RANS) equations with various turbulent models, including k-ε, k-ω and Shear Stress Transport (SST) have been used to simulate the flow around the turbine models. Key hydrodynamics results were extracted and validated against experimental results of Walker et al. [12].

In order to advance understanding of the effect of fouling density characteristics on drag force, a recirculating water tunnel with artificial barnacles (scale model) was used to investigate the flow over smooth and fouled test plates. There are three different fouling test plates: low, medium and high barnacle density. In order to generate the fouling density on a flat plate, artificial models were affixed and replicated with different fouling density on the flat plate. The height of single roughness element is constant for all fouling status.

The drag coefficient results were obtained by load cell drag equipment. The drag coefficient results of smooth case are compared with experimental data which was tested in the same water tunnel by Andrewartha [110]. The drag coefficient results, including artificial barnacles cases are compared with drag coefficient result of smooth case. In order to estimate the drag coefficient for fouling case, the equivalent sand grain roughness should be determined (based on Eq.5.10).

2. Novelty of this study

The main novelties of this study can be summarized as the following:

1. In order to develop a useful numerical model, the equivalent sand grain roughness parameter is used. This parameter is depending on surface reference area of roughness as well as three dimensional regular roughness element. Therefore, based on conical shaped barnacle elements and tidal turbine blade surface, the value of sand grain roughness for numerical method is estimated

2. In order to measure the drag force on fouled test plate, artificial barnacle method is used. The barnacle model was obtained by 3D scans of a real organism (*Amphibalanus Amphitrite),* which then was 3D printed and further replicated by a mould/resin technique. There has been a few studies carried out on investigation of roughness of plate by single roughness element. In this study, scaling method was used to replicate an artificial barnacle to measure roughness parameter.

3. The main feature of experimental work was to determine drag coefficient based on different fouling density. There have been a few studies to investigate fouling density characteristics on marine plate. In this research the height of artificial single roughness is constant and based on fouling density definition (the space between two neighbouring single roughness elements), low, medium and high fouling density were created. Based on these data and also single roughness dimension, the equivalent sand grain roughness for different fouling density of plate can be estimated.

1. Thesis structure

This thesis begins with a review of the literature on biofouling in Chapter 2, including barnacle roughness development, the relationship between barnacle characteristics and roughness, the effect of biofouling roughness on aerofoil and tidal turbine performance and the effect of biofouling roughness on boundary layer. In addition, there has been much discussion on long-term performance of marine turbine and some possible techniques of biofouling mitigation was provided in Chapter 2.

Chapter 3 answers the research question about effect of barnacle roughness on aerofoil performance. This objective was addressed using a computational approach. For this purpose, a 2D NACA 63-618 aerofoil was modelled for smooth and fouled cases. In order to illustrate the effect of cone shaped barnacle elements, equivalent barnacle roughness was estimated. Numerical results validated versus the experimental data from Walker et al.[12] and these results compared against the fouled case results. There has been much analysing on barnacle roughness development on aerofoil performance in Chapter 3.

Chapter 4 describes the effect of barnacle roughness on tidal turbine performance. A 3D turbine system which was previously investigated by Walker et al. [12] in a towing tank, was modelled by the commercial ANSYS CFX.15 software. Thrust and power coefficients were obtained and compared versus fouled case results. The pressure coefficient distribution of the NACA 63-618 aerofoil at 25%, 50% and 75% of the blade span were plotted and compared with roughened case.

All laboratory measurements were carried out in the hydrodynamic lab at the School of Engineering and ICT, University of Tasmania. Drag force over smooth and artificial fouled cases were obtained by a floating element force. The results of these laboratory investigations are presented in Chapter 5. The artificial barnacle sample was obtained by 3D scans of a real

organism (*Amphibalanus Amphitrite*), which then was 3D printed and further replicated by a mould/resin technique.

Finally, a conclusion for all chapters of this thesis is provided in chapter 6.

Chapter 2

Literature Review

This literature review is divided into five sections. The first part provides an introduction for biofouling and barnacle characterization. The second section reviews the effect of hard fouling roughness on aerofoil performance. The third and fourth sections comprise the effect of fouling roughness on hydrodynamic performance of marine current turbines. The last section is a discussion part and reviews some strategies for minimising the biofouling growth on tidal turbines blade.

1. Introduction

Due to the energy crisis and environmental pollution issues, interest in the development of alternative energy has increased tremendously in recent years. Among many sources of renewable energy available, tidal stream energy, which is driven by the ebb and flood of a tide due to the gravitational pull of the moon and the sun, has many attractive features as a clean energy resource [13]. A key concern associated with tidal turbines is their long-term reliability when operating in the hostile marine environment. Appropriate selection of materials can inhibit corrosion; however, control of the growth of algae, mussels and barnacles remains a challenge [12].

Fouling is the undesired deposition of material on surfaces, while the accumulation, deposition and growth of microorganisms on surfaces can be defined as biofouling [14]. Biofouling is a global problem for the marine industry and creates adverse effects on hydrofoil based turbines. Various factors contribute to the rate of the growth of microorganisms on surfaces [15] including salinity, temperature, nutrient levels, flow velocity, solar radiation intensity and depth [16]. Fig.2.1 shows various common macro fouling found on ships' hulls [17].

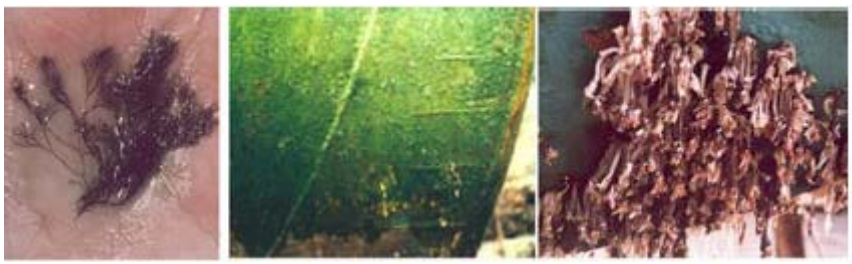

Fig.2. 1. Various common macro fouling [17].

Among different species of biofouling, barnacles are the most problematic marine organisms related to the biofouling of man-made structures [18-19]. Barnacles live exclusively

in the marine environment, and tend to live in shallow and tidal water. Most naval vessels and other watercraft are exposed to barnacle fouling when they are maintained long-term in port without any anti-fouling [20]. Adult barnacles on marine surfaces, for instance ships' hulls, will produce a significant hydrodynamic drag penalty and increase fuel consumption [8, 10, 21-25].

Barnacles grow rapidly following colonisation. Research by Wood and Allen [23] showed that macroscopic barnacles, such as acorn barnacles, are considerably more damaging compared with microscopic organisms. Of all the macroscopic organisms, barnacles from the arthropods group receive the widest attention as they are commonly found on ships' hulls and tidal turbines. For example, Katsuyama et al. [26] installed a three-bladed tidal turbine that was stationary on the sea bed at a depth of 7m for a period of 8 months. Fig.2.2 (a) shows the barnacle growth after 58 days and Fig.2.2 (b) shows the barnacle colonization after 238 days.

Fig.2. 2. Barnacle colonization on horizontal tidal turbine blade a) after 58 days b) after 238 days [26].

Biofouling is a unique type of surface roughness and leads to several adverse effects on marine turbine blades or ships' propellers. The development of increased roughness on a marine surface causes an increase in drag force and flow resistance. Biofouling induced roughness generates irregularities on smooth surfaces, and this perturbs the flow field around

the blade. As a result, tidal turbines affected by biofouling have lower efficiency than design [27].

This paper reviews the characterisation of marine barnacles in terms of surface roughness and the effect marine biofouling, especially barnacle roughness, has on the performance of horizontal-axis tidal turbines.

2. Characterization of barnacle

Many studies have revealed that barnacle attachment on marine surface reduces hydrodynamic performance [27-31]. Different types of barnacle characteristics, including adhesion, height, thickness and density, have a significant effect on the hydrodynamic parameters of surfaces colonised by barnacles. This section will review the relationship between roughness and barnacle development on marine surfaces.

An increase in barnacle dimension has huge consequences on hydrodynamic performance of marine devices. Results of experimental research by Demiral et al. [120] about effect of artificial barnacles on ship resistance showed that the effect of barnacle height on ship resistance is significant, since a 10% coverage of barnacles each 5mm in height caused a similar level of added power requirements to a 50% coverage of barnacles each 1.5mm in height. Orme et al [27], Khor and Xiao [31] showed that an increase the artificial barnacle height around 8 times on aerofoil surface led to increase drag coefficient by an average of 238% for low angle of attacks.

Barnacle colonization produces roughness and increases drag force on marine surfaces. Barnacle density is a roughness parameter and is a measure of how densely the barnacles, as roughness elements, are distributed over a surface. Growing barnacles will reduce the space

between themselves and this increases barnacle density on a surface. The drag force can increase sharply when the space between two neighbouring barnacles is reduced [27- 28].

Barnacle fouling development, and hence barnacle density, is dependent on feeding patterns. Adult barnacles use two basic feeding methods: feathery legs, called cirri, are beaten rhythmically to capture food from the water, or the cirri are extended into the moving water so that food is captured actively or passively [32].

Increasing barnacle density leads to a change in boundary layer flow and also has a complex effect on the hydrodynamic force. Thomason et al. [28] investigated the experimental specimen of *S. balanoides* barnacle colonies in a 5 m long seawater flume using tracer dyes, macro-video photography and image digitalization. In order to manipulate the density and pattern of barnacle colonisation, replicas of barnacles were glued to acrylic tiles with petroleum jelly. At low flow speed, cirral beating disturbed the boundary layer and the flow around downstream barnacles became turbulent. At higher flow velocity, beating of the cirri ceased and barnacles were permanently extended. Boundary layers around the upstream barnacles' cirral basket prevented flow between their cirri, although disturbance to the flow caused significant turbulence. Figs. 2.3 and 2.4 illustrate a graphical representation of the flow over a high density colony of barnacles and a small group of feeding barnacles, respectively. The width of the arrows indicates the coherence of the dye stream and the large arrow shows the flow direction.

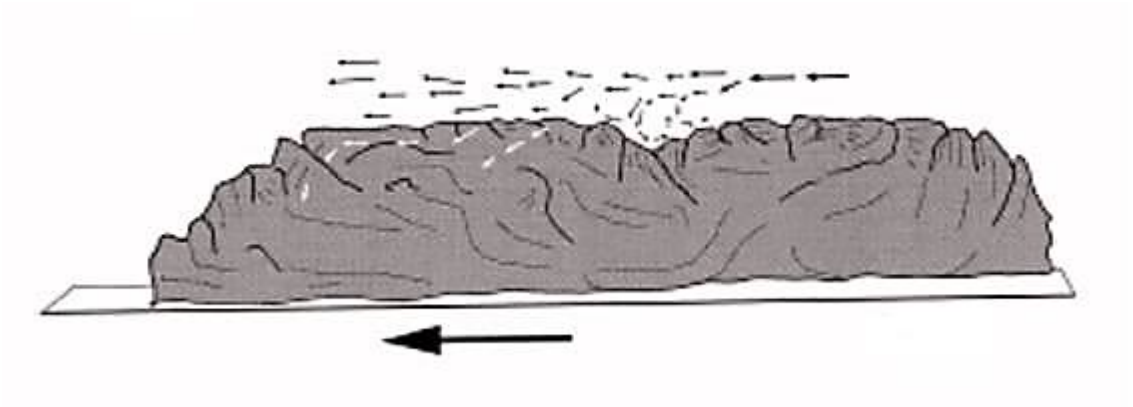

Fig.2. 3. Graphical representation of flow over a high density colony of barnacles [28].

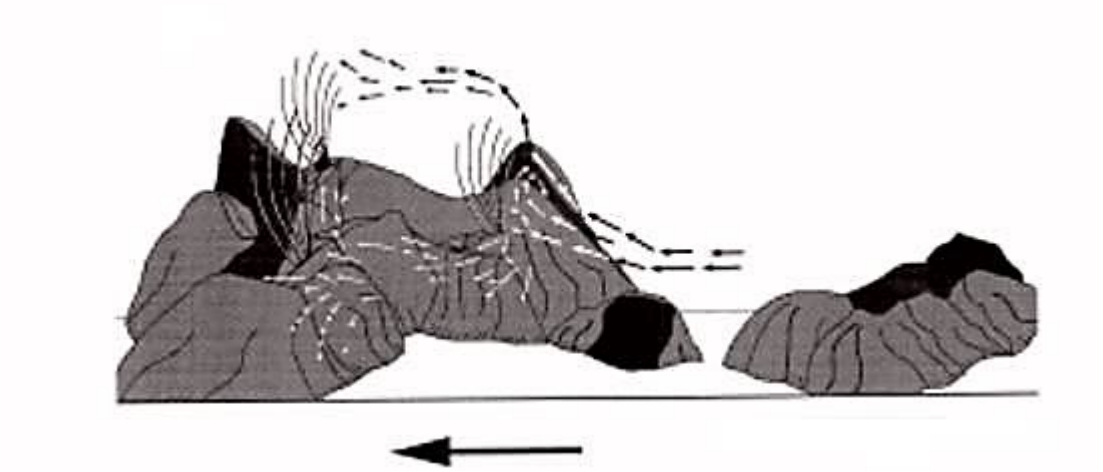

Fig.2. 4. Graphical representation of flow over a small group of feeding barnacles [28].

The type of marine surface roughness plays a vital role in barnacle growth. Thomason et al [28] indicated that the type of surface roughness can have a significant effect on barnacle size and density. Four different types of surfaces with varying textures were chosen as substrates to support barnacle colonies. The tiles were submerged in the Clyde Sea, UK, for a period of approximately 9 months, allowing the barnacles to reach adulthood. The resulting barnacle colony density was lowest for a smooth substrate, and highest for a substrate with a fine surface texture.

The head loss across a duct containing the tiles was measured and calculated based on a modified Darcy-Weisbach formula. This method was used to estimate the hydrodynamic response (head loss) of natural colonies of barnacles expressed in equation 2.1:

$$h_f = \frac{fl}{m}\frac{U^2}{2g} \tag{2.1}$$

where, f is the friction factor, l is the section length, m is the ratio of the cross sectional area to contact perimeter, U is the free stream velocity. The results showed that the head loss increased with increasing barnacle colony density, as shown in Table 2.1 [28]. They also found that the frontal area is important in terms of head loss, with staggered arrangements of barnacles producing greater head loss than aligned arrangements.

Table 2. 1. Frictional head loss for experimental barnacle colonies with different densities [28].

Barnacle colony density (substrate type)	Head loss h_f
Low (smooth tile)	0.0146
Medium (coarse tile)	0.0189
High (medium tile)	0.0224
Very high (fine tile)	0.0288

Once marine devices are exposed to barnacle fouling, the friction force increases [20]. This force increases dramatically as barnacles grow in size [33]. The actual roughness height can refer to the size of a single roughness element or an average of multiple roughness elements on a surface [34].

The frontal area or wetted area of a barnacle is functionally related to barnacle density by geometry. Schultz et al. [29] investigated the hydrodynamic forces on barnacles attached to a foil towed alongside a small skiff. The results indicated that an increasing barnacle height causes a reduction in lift force and an increase in drag force. In addition, increasing barnacle height leads to sheltering and wake interaction effects. Fig. 2.5 illustrates the loading on a single barnacle and Equations 2.2 and 2.3 represent an idealized model to predict the tensile and shear stresses at the base of the barnacle. These stresses can be used to predict the velocity at which barnacles will detach from a surface, based on their adhesion strength.

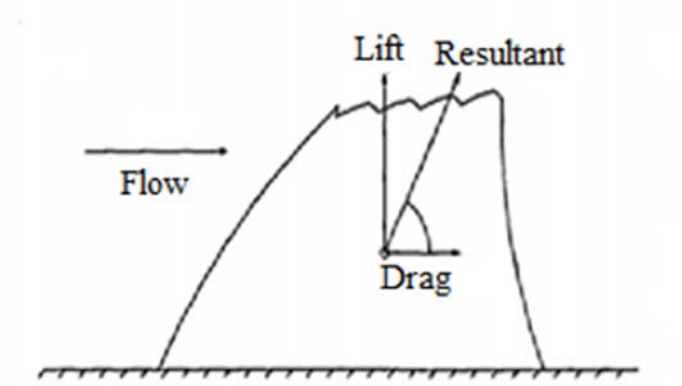

Fig.2. 5. Hydrodynamic forces on a barnacle [29].

$$\sigma_y = \frac{4L}{\pi d^2} + \frac{7.7D}{\pi d^2} \tag{2.2}$$

$$\tau_{xy} = \frac{4D}{\pi d^2} \tag{2.3}$$

3. Barnacle Development Roughness

Barnacles are the most comprehensively studied group of macrofoulers. Barnacles have different phases of fouling: temporary fouling occurs firstly, as the cyprid larva explores a surfaces. The cyprid explores various surfaces using a pair antennules [35]. Secondly, the larva

produces a settlement cement and grows up and changes to juvenile barnacles [36, 37]. Finally, juvenile barnacles changes to adult barnacles and they produces a stronger cement, leading to permanent settlement [36, 37]. Fig. 2.6 shows the life cycle of a typical barnacle with fouling production.

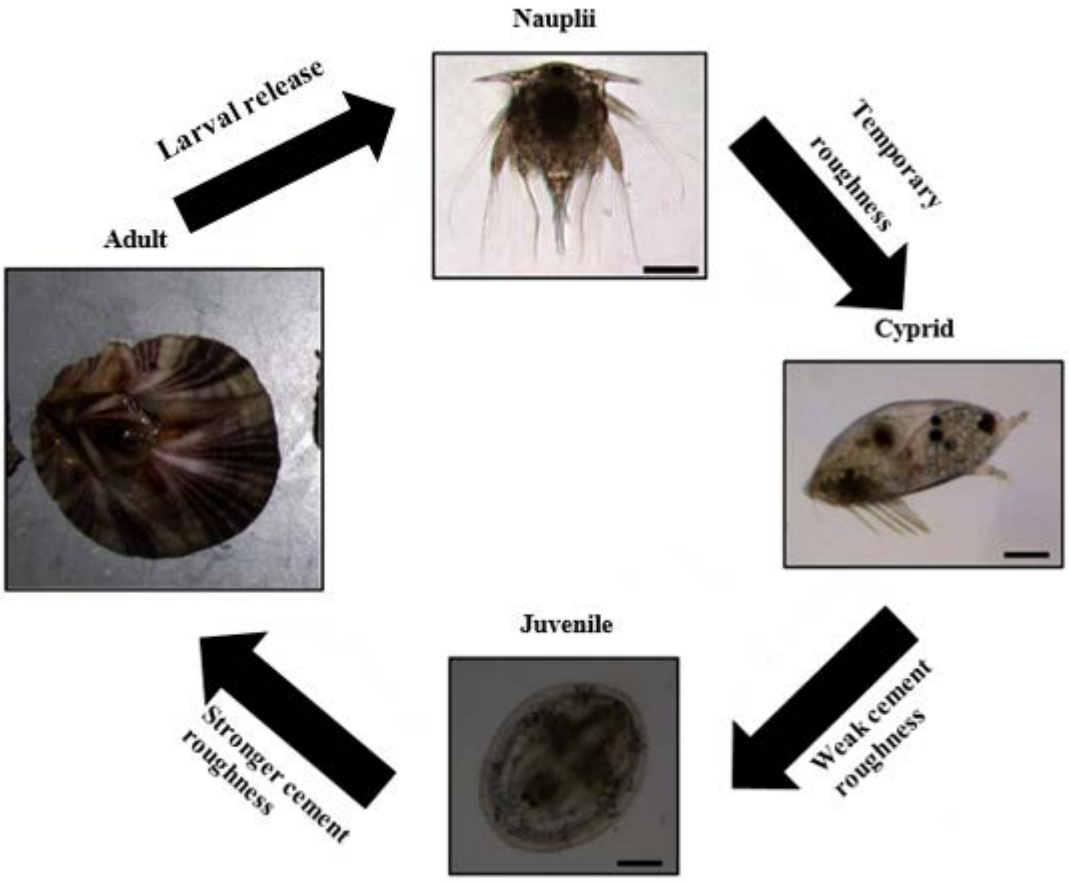

Fig.2. 6. Life cycle of barnacle and barnacle roughness development. Adapted from [38].

A typical adult barnacle has several shell plates around its body and moveable plates on its top part. Adult barnacles firmly attached to a surface and cannot move over surfaces independently like most other crustaceans. Various barnacle characteristics including adhesion, height, thickness and density have a significant effect on the hydrodynamic parameters of surfaces colonised by barnacles. The characterization of roughness in terms of height or density may only be identified when long-term barnacle attachment occurs.

Among different species of barnacles, striped barnacle *Amphibalanus Amphitrite* barnacle is among one of the more problematic species and is prevalent on ships and harbour structures [39]. It is approximately conical in shape and attaches to numerous surfaces including rocks, piers, metal and ships [39]. Fig.2.7 shows that sample of *Amphibalanus Amphitrite* barnacle.

Fig.2. 7. Real Amphibalanus Amphitrite barnacle samples [39].

4. Roughness function correlations

The development of correlations for the roughness function has been an area of active research for many years. Correlations range from simple models based on roughness height and pitch to more complicated relationships that include density and shape parameters.

Flack and Schultz [47] reviewed a functional relationship between the rough wall log-law intercept and a roughness spacing parameter λ which was determined by Bettermann [49], where λ= pitch/height of transverse bars. They also reviewed the relationship modification

which was obtained by Dvorak [123]. In this study, using a density parameter, λ= total surface area/total roughness area, which is equivalent to the spacing parameter of Bettermann [49] for square bars.

These correlations were developed using sand grain roughness surfaces, mesh screens, staggered rows of spheres, and square bars. Simpson [124] modified the parameter further using λ=total surface area/total roughness frontal area normal to the flow, showing reasonable agreement for spheres and cones, staggered hemispheres, and machined groves.

Driling]91] introduced a combined density and shape parameter. Roughness density is included as the ratio of the average element spacing to roughness height, whereas shape is accounted for in the frontal area of a single roughness element and the windward wetted surface area of a single roughness element. Van Rij et al. [93] investigated the use of roughness density parameter to three-dimensional regular roughness, using the results of Schlichting [116] for staggered patterns of spheres, and cones. The correlations for three-dimensional roughness stated that, an increase in roughness density caused a reduction in shape parameter and hence an increase in sand grain roughness parameter.

5. Effect of roughness fouling on ship hull and propeller

Roughness of a ship hull, which is often caused by marine coatings and biofouling, can dramatically increase a ship's frictional resistance and hence its fuel consumption and greenhouse gases emission. The surface condition of the hull is of primary importance in the performance of marine vehicles.

A large body of research has carried out to the effects of hull fouling on drag and powering. Results of most studies [33,105,108,110] about effect of fouling effect on friction coefficient indicated that even low-form algal fouling leads to a significant increase in frictional

drag, although the magnitude of the increase depends strongly on the fouling type and coverage. Frictional drag on some hull types can account for as much as 90% of the total drag even when the hull is free of fouling [21]. Demirel et al [121], used CFD method based unsteady RANS model which enables the prediction of the effect of marine coatings and biofouling on ship resistance. In order to model biofouling roughness on ship hull, equivalent sand grain roughness height which was estimated experimentally by Demirel et al. [120] based on wall function theory was used. Results of this research indicated the increase in the effective power of the hull was predicted to be 18.1% for a deteriorated coating or light slime whereas that due to heavy slime was predicted to be 38% at a same speed. Townsin [8] conducted a particularly through the investigation of the frictional drag increase resulting from barnacle fouling. Through this research, the simple predictions of the frictional drag penalty based on barnacle height and coverage were developed. The results of this research indicated a maximum drag penalty occurred when the barnacle coverage was 75%. However, when the coverage was reduced to 5%, the drag penalty was only reduced by one third from the maximum penalty. Schultz [108] noted that the height of the largest barnacles has the dominant influence on drag. In addition, in accordance with the findings of Schultz [108] observed that the effect of increased coverage of barnacles on frictional drag was largest for low values of coverage and smallest for high values of coverage.

Experimental, lab scale studies on flat plates provide reliable data since the uncertainties can be estimated to a degree. Therefore, several experimental studies have been devoted towards investigating the roughness effect on the skin friction of the flat plates. Based on review study by [117], which has studied on rotating disks covered with several different types of microbial slimes. This study indicated microbial slime led to an increase of 10% to 20% in the frictional resistance. Research by [24] conducted the extensive experimental study investigating the effect of fouling on frictional resistance. Flat plates were coated by anti-

corrosive paints and kept in sea water for a year. The plates were then towed with barnacles on them. The findings were remarkable since the resistance of the plates after 12months of sea exposure increased to 4times the resistance of an otherwise identical smooth plate. Andrewartha [110] measured an increase of 99% in the drag coefficients of test plates due to biofilms in a recirculating water tunnel. These findings clearly demonstrate that antifouling and hydrodynamic performances of coatings vary significantly depending upon operational conditions. A series of towing tests was carried out using flat plates covered with artificial barnacles by Demirel et al [120]. A real organism of *Balanus Improvises* barnacle scanned in 3-D printing and replicated with scale size. The results of towing tank test showed that the effect of barnacle size in significant, since a 10% coverage of barnacles each 5mm in height caused a similar level of added power requirements to a 50% coverage of barnacles each 1.25mm in height. Research by Townsin [8] on pontoons covered with shell fouling plate, indicated an increase of 66% in the resistance, even with only 5% coverage. Schultz [33] measured frictional resistance of plate with and without artificial slime experimentally by towing tank equipment. The results indicated that the frictional resistance of flat plates covered with artificial slime increased up to 18%.

The effects of propeller fouling on powering roughness on ship powering can also be very significant [118]. Mosaad [118] stated that although the effect of the propeller surface condition could be less important than the hull condition, it would be significantly more important in terms of energy loss per unit area. Owen et al. [119] investigated effect of biofouling roughness on ship propeller numerically. Equivalent sand grain roughness height was considered as main function of roughness on ship propeller and those values were estimated experimentally by Dermirel et al [120]. A Reynolds Averaged Navier-Stokes (RANS) solver with Shear Stress Transport (SST) turbulence model is used to model the flow around a

ship propeller surface. The results of research indicated the most fouling cases had a 11.9% efficiency loss at the advance coefficient of 0.6 compared to the smooth condition.

In economic terms, high return on a relatively cheap investment can be obtained by a properly set propeller maintenance strategy. This has further supported the idea of coating propellers using similar antifouling systems to those used on a ship's hull.

6. Effect of roughness on horizontal axis turbines

The effect of roughness and biofouling, especially barnacle roughness, on aerofoil and turbine performance and aerofoil boundary layer thickness is reviewed in this section. In addition, the long-term performance of tidal turbines that have been colonized by barnacles will also be discussed.

1. Characterization of roughness and fouling effect on aerofoil performance

The horizontal axis marine current turbines use blades with aerofoil shaped cross-sections to generate torque. It is well known that blade shape is critical to the aerodynamic performance of wind and tidal turbine blades [40]. In this section the characterization of roughness on aerofoil performance, which alters the geometry, is reviewed with regard to aerodynamic performance characteristics. Aerofoil performance is measured using the drag and lift coefficients, given in Equations 2.4 and 2.5, respectively, as a function of the angle of attack of the aerofoil.

$$C_D = \frac{D}{0.5\rho U^2 cs} \tag{2.4}$$

$$C_L = \frac{L}{0.5\rho U^2 cs} \tag{2.5}$$

Where, C_L and C_D are lift and drag coefficient, ρ is density, U is flow stream and cs is cross section area of aerofoil.

Many studies have revealed that, in order to produce accurate performance predictions from blade element momentum theory, accurate lift and drag coefficient curves for the aerofoil profile used for the turbine blades are needed [12, 27, 31, 41-42]. For tidal turbines, the blade profile used typically has a thick aerofoil cross-section, as the density of water is much greater than air, imposing larger structural loads across the rotor [43].

Surface roughness on aerofoils results in an increase in drag force and a reduction in the lift force. Petrone et al. [44] and Li et al. [45] investigated dust roughness on aerofoil performance. Results of research indicated aerofoil performance is dependent on height of actual roughness and location of roughness. The results revealed that the lift coefficient is reduced when the roughness height is increased. Khalfallah and Koliub [46] indicated that roughness on an aerofoil surface degrades aerodynamic performance by decreasing the maximum lift coefficient and increasing the drag coefficient.

Roughness can be characterized in terms of height, element density, pitch, shape and location [47]. Roughness height may refer to the size of a single roughness element or an average of multiple roughness elements. Roughness size can be defined by its height from the surface for randomly shaped elements and by its diameter for spherical elements. Roughness density refers to how densely the roughness elements are distributed on the surface [48]. Bettermann [49] indicated that pitch factor is a function of roughness spacing parameters. It is noted that roughness spacing parameters are estimated by the ratio of pitch to roughness height. Table 2.2 summarises experimental studies investigating the effect of various roughness types on aerofoil performance. These studies show that adding roughness to an aerofoil tends to increase the drag coefficient and decrease the lift coefficient.

Table 2. 2. Summary of studies investigating the effect of roughness on aerofoil performance

Type of roughness	Roughness description	Results	Reference
Ice layer	0.3mm roughness was applied to NACA 0012 aerofoil surface	Increase in C_D 40% decrease in C_L $C_{L\,max}$ is decreased from 1.5 to 1.1	[50]
Wrap around roughness	Roughness elements distributed over entire surface of NACA 64-4xx	20% decrease in $C_{L,max}$ 50% increase in C_D	[51]
Insect roughness	Several hypotheses about insect contaminations were examined on the aerofoil section of a wind turbine blade at a Californian site.	At the low speeds, power production is not significantly influenced by insect roughness. At high speeds, there is a decrease in power output due to insect roughness.	[52]
Glaze ice accretion	Distributed roughness consisting of hemispherical shapes in staggered rows near leading edge of NACA 0012	Early transition of the boundary layer.	[53]
Coarse grit	Wide double-tack tape was applied to one side of S809 aerofoil and	16% decrease in $C_{L,max}$ 41% increase in $C_{D,min}$	[54]

	grit was poured and brushed from the opposite side.		
Plastic strips	Plastic strips applied with different roughness height on leading edge of GA (W)-1 aerofoil	Small roughness height: Delay stall of aerofoil Large roughness height: Earlier aerofoil stall at a small angle of attack	[55]
Bulge tape	Bulge trip tape was mounted to the NACA 63-430 aerofoil surface to simulate the effects from leading edge roughness.	1. Separation point and transition are shifted to the leading edge when roughness was located at the front 25% of the chord length.	[56]
Tripping wire	1 mm dia tripping wire applied to suction side of Du300 aerofoil	Increase in C_D Overall C_L/C_D decreased	[57]
Zigzag roughness type	0.4mm and 0.6mm zigzag tapes applied to suction side of DU 300 aerofoil at 0.05c and 0.1c	C_L decreased significantly.	[57]
Grain carborundum	60-grain carborundum applied to leading edge of DU300 aerofoil	Early transition of boundary layer at the leading edge	[57]
Conical grid shape	An extrusion method was used to create small conical shape (model	1. Decreasing C_L/C_D by an average of 25%.	[27]

	height was 3.2mm) on NACA 4424 aerofoil surface		
Contact cement roughness	NACA63-618 aerofoil roughened with a thin layer of randomly applied contact cement to model barnacle growth	1. 2. 3.	Decreasing $C_{L,max}$ by [12] an average 11% Increased the stall angle from 10° for the smooth aerofoil to 16° for the roughened case. Increasing $C_{D,min}$ up to 153%

When hydrofoils are colonised by hard fouling such as barnacles, the performance response follows that of a roughened aerofoil. This is because the smoothness of surface is perturbed, especially at the leading edge, near the stagnation point. That is, the drag coefficient increases, and the lift coefficient decreases [12, 27, 31].

Orme et al. [27] and Khor and Xiao [31] investigated the effect of barnacles on a NACA 4424 aerofoil. Orme et al. [27] tested a two-dimensional aerofoil in a wind tunnel using three supporting struts connected to a force balance. An extrusion method was used to develop the barnacle roughness, with small, medium and large conical shapes used. Barnacles with the largest size produced the highest drag coefficient. In addition, results indicated that when the barnacle density increases, the drag coefficient is significantly increased and the lift coefficient is reduced. Fig.2.8 shows drag and lift coefficient results for different barnacle roughness density at various angles of attack.

Walker et al. [12] investigated the effect of roughness on a NACA 63-618 aerofoil in a wind tunnel. The two-dimensional aerofoil was roughened with a thin layer of randomly applied contact cement, both to the leading edge and to the entire aerofoil. The maximum lift coefficient was increased by an average of 11% for all roughness cases. The presence of roughness also increased the stall angle from 10° for the smooth aerofoil to 16° for the fouled aerofoils. The drag coefficient increased with increasing roughness. The minimum drag coefficient at Re = $5x10^5$ increased 49%, 59% and 153% for the leading edge roughness, light entire roughness and heavy roughness, respectively. The effect of roughness on the lift and drag coefficients is shown in Figs. 2.8 and 2.9 for the four different roughness conditions tested.

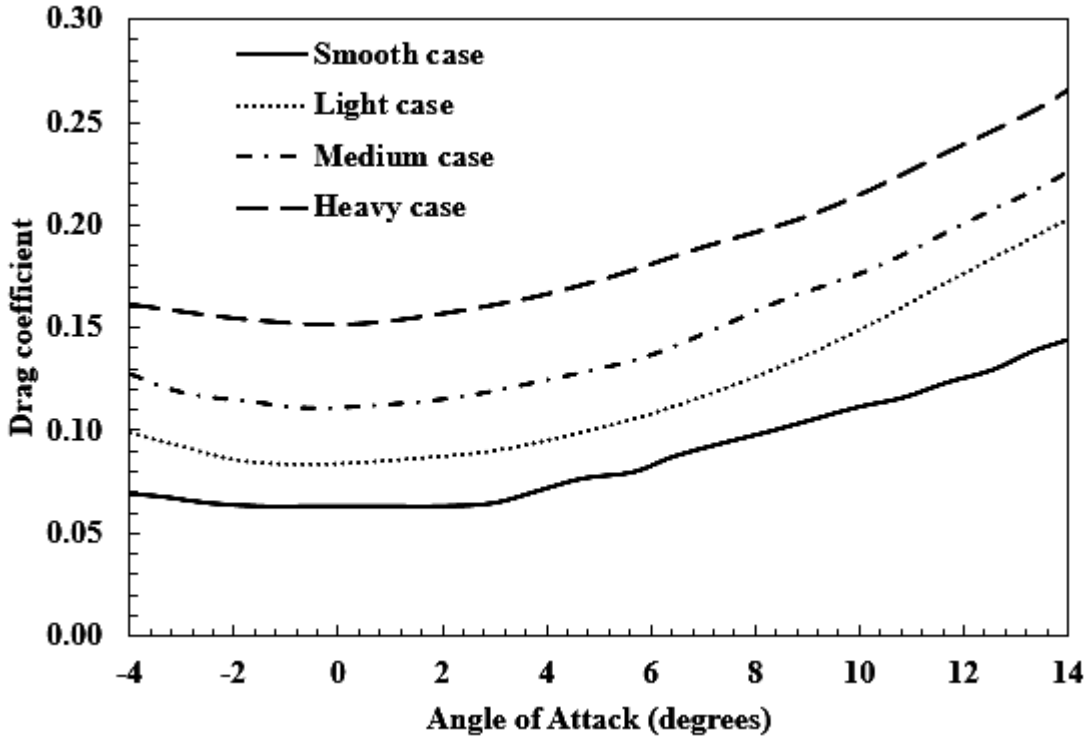

Fig.2. 8. Performance of a NACA 4424 aerofoil with different simulated barnacle density (Light case= 11389 barnacle/m2, Medium case=21389 barnacle/m2 and Heavy case=42253 barnacle/m2) at Re=6*106 adapted from Orme et al. [27] (a) Drag coefficient, (b) Lift coefficient

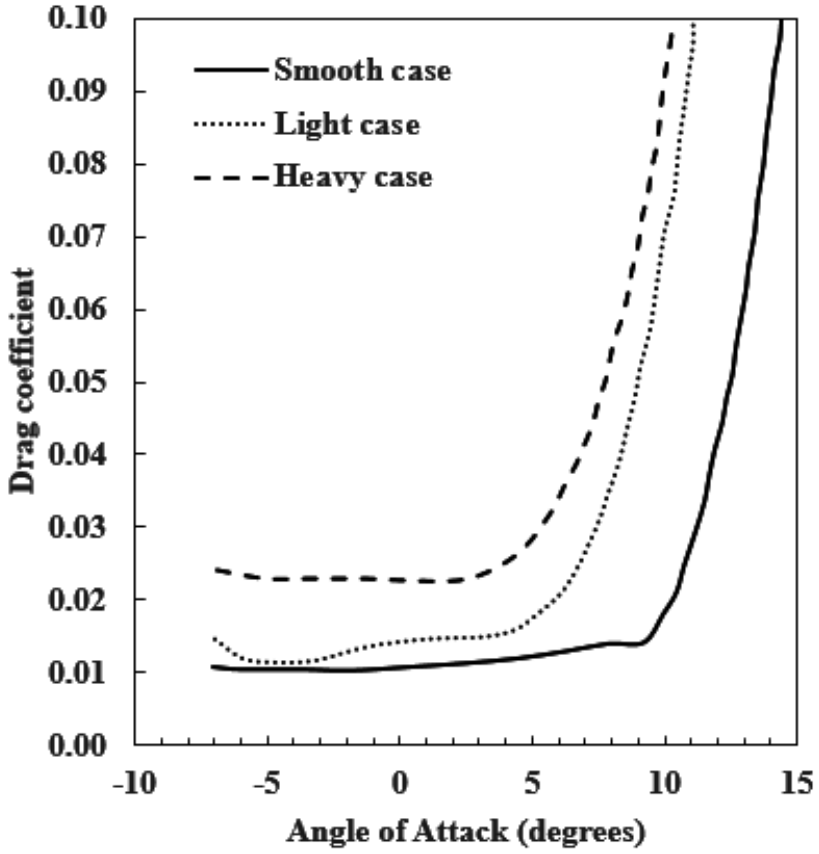
0.10
0.09
0.08
0.07
0.06
0.05
0.04
0.03
0.02
0.01
0.00
Drag coefficient
Smooth case
Light case
Heavy case
-10
-5
0
5
10
15
Angle of Attack (degrees)

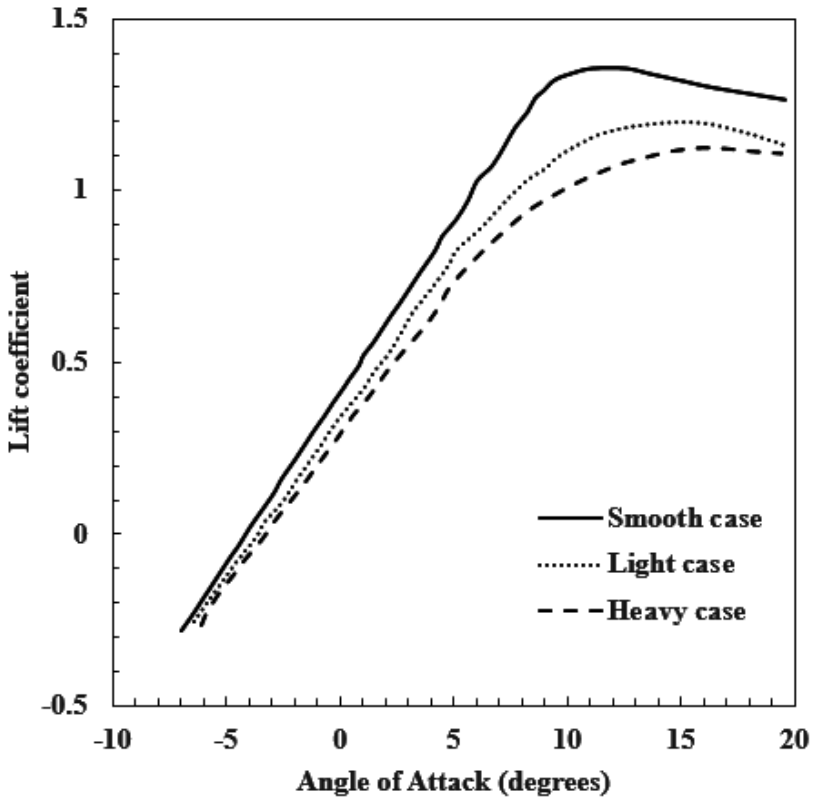

Fig.2. 9. Performance of a NACA63-618 aerofoil with different artificial fouled height. (Light case=1.1mm thick layer of lithium grease impregnated with diatomaceous, Heavy case=a thin layer of randomly applied contact cement) adapted from Walker et al [12].

The ratio of lift to drag C_l/C_D decreases when an aerofoil is coated with fouling. Results of research by Orme et al. [27], Khor and Xiao [31] indicated that the lift to drag ratio decreased both with increasing barnacle size and distribution density. Fig.2.10 shows that lift to drag ratio with different barnacle density on NACA4452 aerofoil surface. The highest lift to drag ratio is for the smooth aerofoil. Based on Fig.2.10, the lift to drag ratio is reduced when barnacle fouling is added to the aerofoil surface. It can be noted that the rate of lift coefficient reduction is greater than the rate of drag increase when barnacle height is increased.

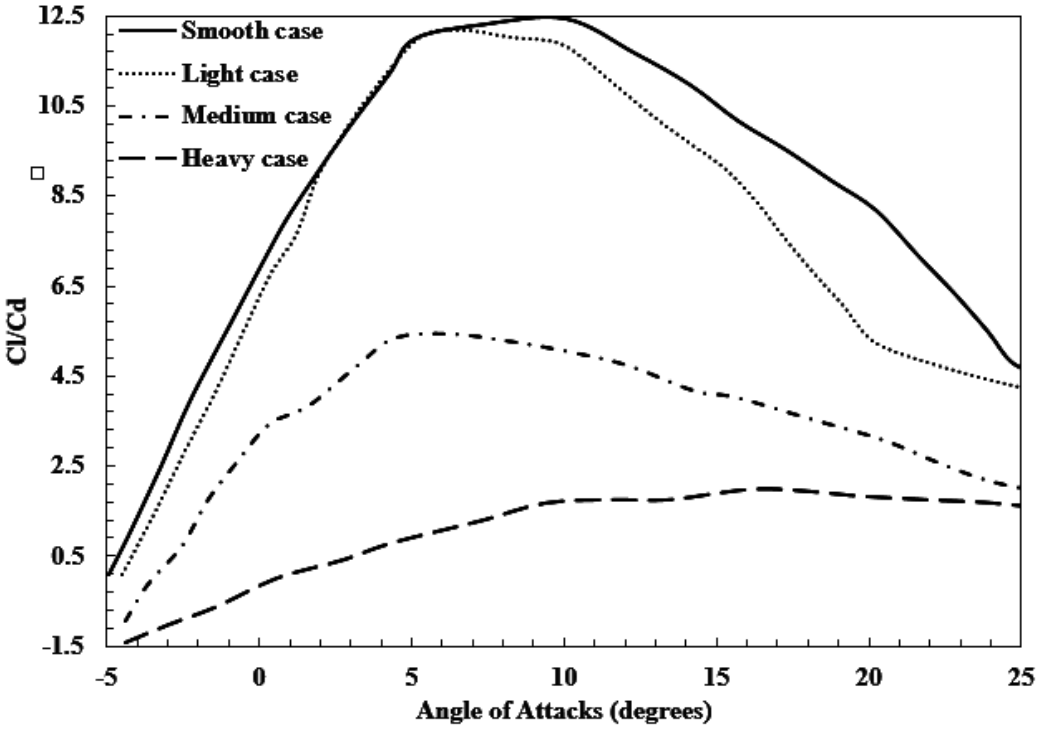

Fig.2. 10. Lift to drag ratio results for changes in barnacle size. Adapted from Orme et al. [27], Khor and Xiao [31].

1. Effect of biofouling roughness on aerofoil boundary layer thickness

An accurate boundary layer prediction of the flow over an aerofoil allows the calculation of hydrodynamic performance and the estimation of cavitation inception when such surfaces are roughened [58-60]. Efficient aerodynamic performance is best achieved when the flow remains attached to the aerofoil surface [61]. Flow separation can take place under a high angle of attack or due to the presence of roughness near the leading edge. In a low Reynolds number regime, the lift curve at a low angle of attack may have undesirable nonlinear features [62]. Research by Kerho [63] and Van Rooij and Timmer [64] indicated that laminar aerofoils are particularly sensitive to roughness because the improved aerofoil performance is obtained by tightly controlling the boundary layer behaviour. Any deviations of the boundary layer from

intended behaviour, such as that due to roughness, can result in significant deterioration in performance.

Roughness modifies the thickness of the boundary layer and the extent of its transitional characteristics, which depend on height, location and the Reynolds number. Research by Kerho and Bragg [63] and Bai et al. [65] indicated that the boundary layer velocity profile became fuller when roughness is added to the aerofoil surface and the transition area is close to the leading edge. Also, Montis et al. [66, 67] showed that the boundary layer upstream of the separation point became thinner with the presence of roughness on an aerofoil. The skin friction coefficient increases with disturbances to the boundary layer due to roughness and the transition location moves toward the leading edge. An increase in skin friction causes an increase in the drag coefficient and thereby affects the performance of the aerofoil. Flow visualization by Turner et al. [68] showed that an obviously turbulent boundary layer occurred over a rough surface Fig.2.11, whereas there was an obvious laminar-turbulent transition over a smooth surface Fig. 2.12.

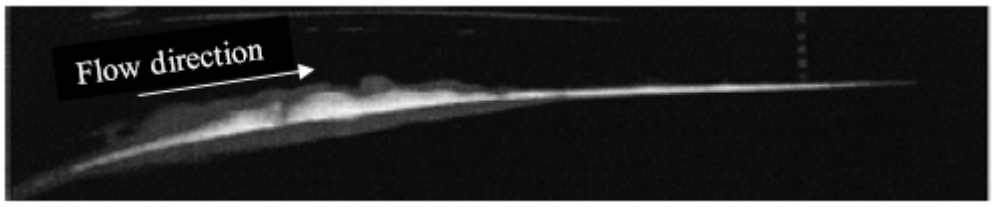

Fig.2. 11. Laminar-turbulent transition on a smooth aerofoil. Adapted from Turner et al. [68].

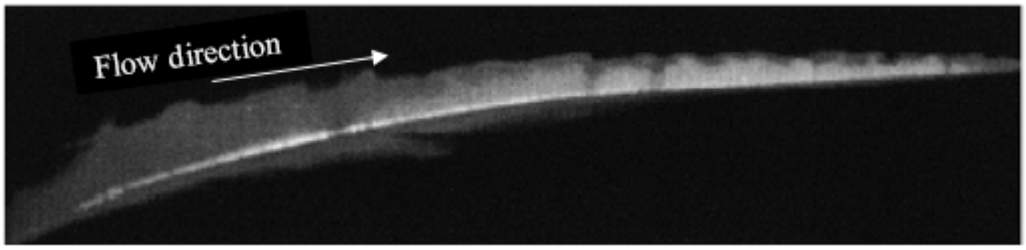

Fig.2. 12. Turbulent boundary layer on a rough aerofoil. Adapted from Turner et al. [68].

Biofouling roughness can also cause cavitation inception on the rotating surface. Results of research by Korkut and Atlar [69] indicated that propeller blade roughness stimulates the transition of the boundary layer from laminar to turbulent flow, causing cavitation inception. Wan et al. [70] concluded that the boundary layer displacement thickness can have an effect on ship propeller performance. The results indicated that an increase in roughness thickness in the ship propeller blade causes an increase in the boundary layer displacement thickness, which is characteristic of increased skin friction loss and decreased propeller performance.

2. Effect of fouling on thrust and power coefficient

The performance of a tidal turbine is characterised in terms of the power and thrust coefficients, given in Equations 6 and 7 below. Studies by Kojima et al. [71], Huang et al. [72], Sagol et al. [48] and Walker et al. [12] indicated that roughness on a horizontal axis turbine blade can significantly reduce the lift coefficient and increase the drag coefficient of the aerofoil and, hence, reduce hydrodynamic turbine performance.

$$C_p = \frac{P}{0.5\rho U^3 \pi R^2} \tag{2.6}$$

(2.7)

Where, C_P and C_T are power and thrust coefficient, ρ is fluid density, U is flow stream and R is the radius of blade.

There have been few studies to investigate the effects of fouling on marine current turbine performance. Batten et al. [73] conducted a numerical study on tidal turbine performance, including an investigation of the effects of blade fouling. The numerical codes for this research were based on Blade Element Momentum theory and were adapted from a programme for wind turbine design developed by Barnsely and Wellicome [122]. They assumed that the presence of fouling might increase the drag coefficient by up to 50%. The effect of surface roughness does not tend to have much effect on the lift slope but can alter the angle at which stall can occur. The proposed model predicted a decrease in the power coefficient of 6-8%. Goundar and Ahmed [74] and Ng et al. [75] revealed that the presence of marine macro-organisms alters the hydrodynamic design of the tidal turbine blade and significantly affected rotor performance.

Walker et al. [12] investigated the effect of light and heavy biofouling roughness on tidal turbine performance by testing a model-scale two-bladed horizontal axis tidal turbine in a towing tank. The tidal turbine blades were tested under three conditions: smooth, coated with a thick layer of lithium grease impregnated with diatomaceous earth to approximate slime fouling, and roughened with a thin layer of contact cement to increase blade roughness, as would occur with barnacle fouling. Results indicated that the attachment of soft fouling did not have significant effect on turbine performance, as most of the material sheared off the blades, whereas the presence of artificial hard fouling adversely affected hydrodynamic performance. The results showed approximately 20% reduction in the maximum power coefficient with the contact cement roughness. In addition, the thrust coefficient was significantly reduced when

roughness material was present. Fig. 2.13 shows the reduction in the power coefficients with a roughened turbine blade.

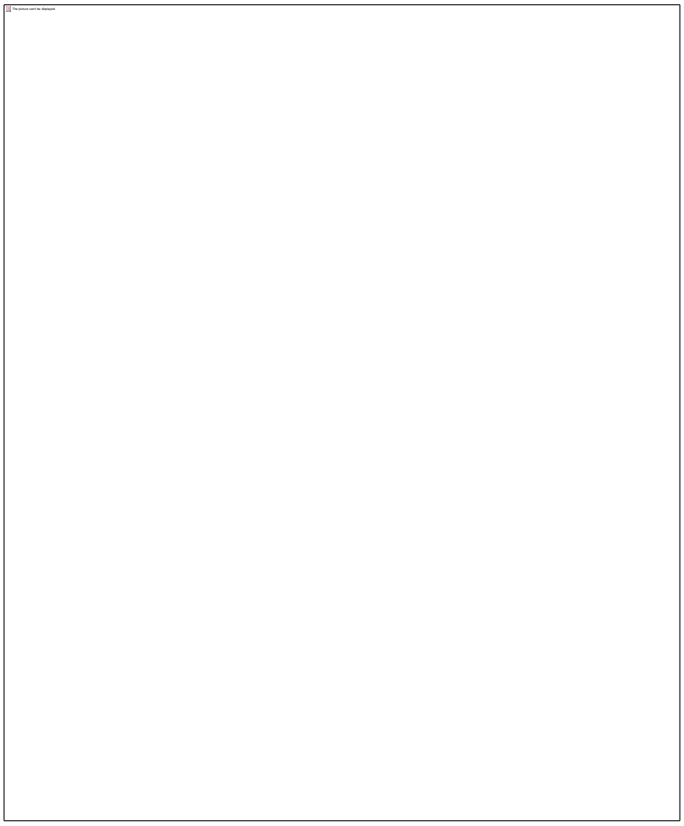

Fig.2. 13. Power coefficient curves for smooth and different fouled roughness height for a two-bladed horizontal axis tidal turbine (○ smooth, ▪ lithium grease impregnated with diatomaceous earth, ▲ roughened with a thin layer of contact cement) [12].

3. Effect of biofouling on long-term turbine performance

It is well understood that the presence of roughness has a significant effect on energy loss. Wind and marine turbines are unavoidably exposed to the environmental conditions that prevail in the location where they are erected. Chen and Lam [76] and Soares et al. [77] indicated that the rotor part of the tidal current turbine is affected by biofouling which may

contain a high content of corrosive minerals. In addition, marine fouling settlement can accelerate the corrosion rate through the thin layer of a turbine blade.

Rough sites produced by biofouling roughness on a turbine rotor can create hydrodynamic imbalance. Since tidal current turbines and wind turbines have a similar support structure, wind turbines are used as benchmarks to study the hard fouling growth effect on the hydrodynamic parameters. Antikainen and Peuranen [78] found that added hard roughness such as ice could cause an imbalance in the turbine rotor and thus cause a significant effect on the aerodynamic balance of turbine blades. Jasinski et al. [79] and Talhaug et al. [80] investigated the effect of long-term roughness on turbine performance experimentally and numerically. Jasinski et al [79] investigated wind turbine performance under ice roughness. For typical supercooled fog conditions found in cold northern regions, four rime ice accretions on the S809 wind turbine aerofoil were predicted using the NASA LEWICE code. The resulting aerofoil/ice profile combinations were wind tunnel tested to obtain the lift, drag and pitching moment characteristics over the Re range $1\text{-}2*10^6$. These data were used in the PROPID wind turbine performance prediction code to predict the effects of rime ice on a 450kW rated power. The results revealed that long-term roughness can cause a reduction in annual power in the range of 20-50%.

Yebra et al. [17] tested turbine blades with three different biofouling heights. The tidal turbine type was a bi-directional ducted horizontal axis turbine. The turbine was installed at a depth of 19 m on the sea bottom in Race Rocks ecological reserve, Canada. The first sample developed a thin slime (R_z = 100 micron) over five years, the second sample developed a thick slime (R_z = 500 micron) over the same period and the third sample consisted of algae filaments (R_z = 5 mm). There were some assumptions as tidal currents took place 12 hours a day on average and during that time the turbine ran at 90% of its rated power. The results indicated

that power loss for a period of one year for a 1MW full size commercial turbine would be less than 5% for filamentous algae. The power loss for a period of five years was more than 15% for blades coated with filamentous algae, while there were 8% and 4% power losses for heavy slime and light slime coatings, respectively. Fig.2.14 shows the sample of thin and thick slime layers on a tidal turbine blade.

Fig.2. 14. Sample of slime thin slime (left) and thick coating (right) on a tidal turbine blade [17].

Katsuyama et al. [26] compared the long-term performance of tidal turbines with and without anti-fouling coatings. The blade materials were steel and were coated with a long-term anti-corrosion epoxy resin. The turbine blade dimensions were 150 × 50 mm. Two stationary three-bladed tidal turbines were installed at a depth of 7 m on the sea bottom off Ikitsuki I, Japan for period of eight months. After one month both cases were fouled by *Megabalanus rosa*, a common species of barnacle. The results indicated that a significant barnacle density of up to 3-4 kg/m^2 developed over the entire turbine blade without the anti-fouling coating, which would generate a mass imbalance. The entire tidal turbine surfaces (blades and hub surfaces), without the antifouling coating, were covered by *Megabalanus rosa* barnacle after eight months and disruption of aerodynamics was reported. The hub section of the tidal turbine without an anti-fouling coating only incurred barnacle growth and its blades were protected against

barnacle colonization. Fig. 2.15 shows the extent of barnacle growth on experimental model turbines with and without anti-fouling coatings.

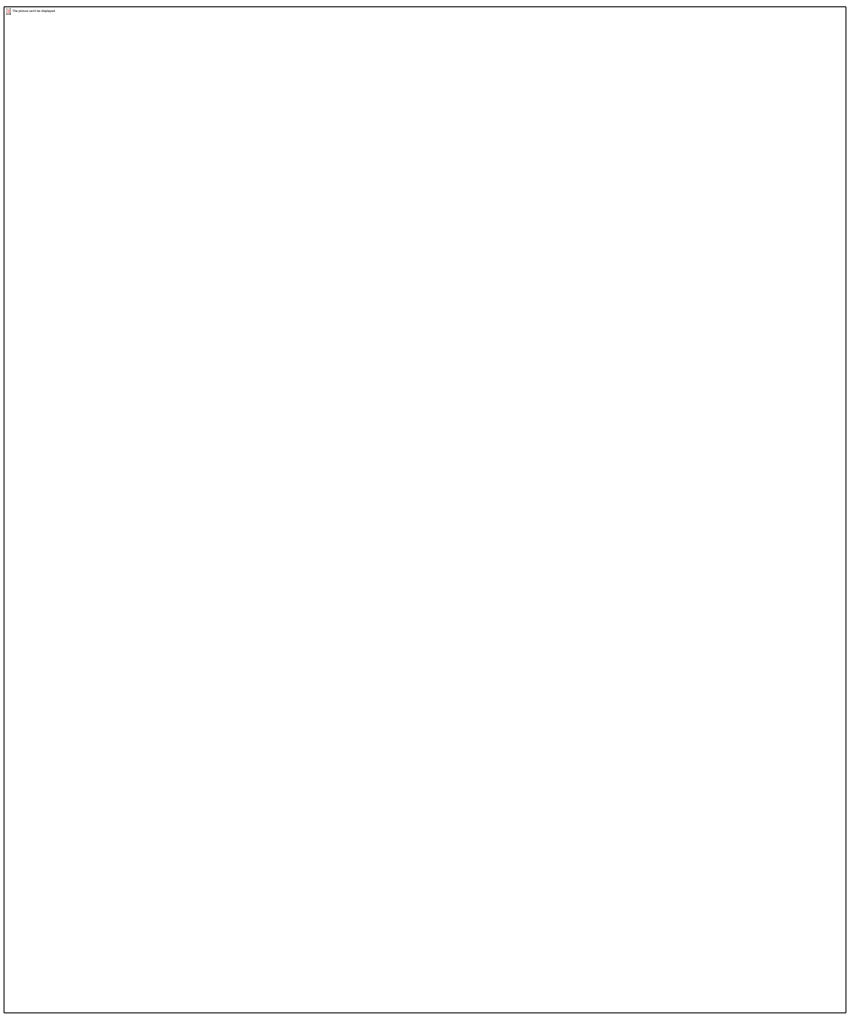

Fig.2. 15. Three bladed tidal turbines, 238 days after initial installation in the sea A) with anti-fouling coating. B) without anti-fouling coating [26].

In order to minimise biofouling development on marine turbines, biofouling prevention techniques can be used. In the context of a tidal turbine system, a critical issue is to evaluate biofouling impact on the different components. Indeed, marine renewable energy devices are composed of several materials and each of them will have a different impact [81]. The tidal turbine rotor and hub are the most important components of a tidal turbine device; their materials can play an important role in tidal turbine performance. Polagye and Thomson [82]

installed some plates with different materials which might be used in the different parts of turbine components at a depth of 55 m on the seabed in-situ in Washington in a period of 10 months. The results revealed that among different materials, glass fibre composite performed well, with limited surface fouling after 10 months of deployment. In addition results of research by Titah-Benbouzid et al [81] indicated that Carbon Fibre Composite material can be used for the turbine rotor. This material can develop minimal surface fouling after up to 10 months of deployment. Another suitable material is enamelled metal. Results of research by Hills and Thomason [83] on seven different surfaces with the same size revealed that no barnacles settled on enamelled metal after two months, whereas other materials such as wood and rusty metal were colonised with barnacles after the same time.

2. Discussion

This review has shown that biofouling has a significant impact on marine current turbine performance. Among different species of marine animal biofouling, the barnacle is one of the most problematic marine biofouling groups. Barnacles can survive in different environmental conditions and colonize a variety of surfaces. As discussed in the section on barnacle characteristics, density and height are the most important parameters that affect the hydrodynamic performance of marine turbines. Barnacle fouling development, and hence barnacle density, is dependent on feeding patterns.

Small particles of hard fouling can be transported by the tide and wave to the height of tidal turbine rotor. These particles generate irregularities on the rotor blade and the smoothness of the blade surface is perturbed. Hard fouling colonization can make an erosion and mass imbalance on the blade surface. Increasing barnacle roughness changes the boundary layer flow on turbine blade surfaces, leads to a reduction in the lift coefficient and a significant increase in the drag coefficient, thereby reducing the performance of the aerofoil and the turbine rotor.

The best approach to mitigate the effect of biofouling on marine current turbine performance is to slow the growth of barnacles in the first instance. This can be achieved through the use of anti-biofouling materials or the application of protective surface coatings. This review has shown that using different materials, such as carbon fibre composites, may be beneficial in slowing the development of biofouling. There is a considerable body of research on marine protective coatings for use in the shipping industry; however, the use of such coatings on marine current turbines is an area for further research.

Once fouling is established, there are several ways to remove it from marine devices. Dry-docking operations are commonly used to remove barnacles from large marine surfaces (i.e. ships' hulls). Some marine current turbines, such as SeaGen, can be cleaned and maintained above sea level [84]. Due to the challenges of cleaning turbines in-situ, it is important that the maintenance of marine current turbines, including the removal of biofouling, is considered at the design phase.

This review has also shown that biofouling is a significant issue for the long-term performance and viability of marine current turbines. However, there have been few detailed studies that investigated the effect of biofouling roughness on marine current turbines. Further research is needed to understand the complex flow physics involved in barnacle growth on turbine rotors. Areas for further study include accurately representing barnacles as a roughness, the effect of barnacles on the boundary layer flow, lift and drag characteristics, power and thrust performance, and fatigue issues from rotor imbalances caused by uneven fouling growth.

3. Conclusion

The effect of biofouling on horizontal-axis tidal turbine performance has been reviewed in this paper. Surface roughness from barnacles increases with the height and density of the

barnacles on marine surfaces increases. Hard fouling production increases the surface roughness on turbine blades leading to decreases in hydrodynamic performance. Areas of increased roughness can cause a mass imbalance in the rotor system, leading to potential fatigue issues. The presence of roughness on a turbine can cause up to a 20% reduction in the power coefficient. Barnacle roughness development represents a significant potential economic issue for commercial tidal turbine operation and a barrier to large scale uptake of the technology. However, further studies on turbine blade profile design, rotor materials and maintenance technology can help to reduce biofouling growth on marine turbines and improve long-term performance.

Chapter 3

Effect of Simulated Barnacle Roughness on Aerofoil Performance

1. Introduction

Many studies have revealed that, in order to produce accurate performance predictions from blade element momentum theory, accurate lift and drag coefficient curves for the aerofoil profile used for the turbine blade sections are needed [12, 27, 31, 41-42]. For tidal turbines, the blade profile used typically has a thick aerofoil cross-section, as the density of water is much greater than air, imposing larger structural loads across the rotor [43].

Roughness can be defined as a surface extension of a body that penetrates into the viscous layer. Consequently, momentum and energy transfer between the surface and the flow will increase which will affect the aerodynamic performance of aerofoil. In the previous chapter (Characterization of roughness and fouling effect on aerofoil performance section), results of many studies about roughness indicated aerofoil performance is dependent on height of actual roughness and location of roughness [44-57].

It is well understood that barnacles are among the most problematic marine organism which have an adverse effect on marine surface performance[18-19]. Once marine devices are exposed to barnacle fouling, the skin friction increases significantly [8]. This force increases dramatically as barnacles grow in size [33]. Roughness height can refer to the size of a single roughness element or an average of multiple roughness elements on a surface [34]. Schultz et al. [29] investigated the hydrodynamic forces on a hydrofoil with barnacles that was towed alongside a small skiff.

In order to estimate the performance of Horizontal Axis Turbine blade, torque generation by aerofoil shaped cross-sections of blade can play a vital role. Thus, the prediction of aerofoil performance of turbine with roughness case can help to estimate the hydrodynamic performance of turbine blade. Obviously, aerofoil performance is measured using the drag and

lift coefficients. In the previous chapter, the results of some experimental and numerical studies on 2D aerofoil studies showed increased roughness height caused a reduction in lift force and an increase in drag force. Therefore, the effect of barnacle roughness on 2D aerofoil performance will be investigated in Chapter 3.

As the size of marine turbine grows, it is becoming more difficult and too expensive to perform full-scale experiments. Therefore, computational tools are preferred for analysis of tidal turbines. Several efforts [56, 85-90] have been made to model roughness on aerofoil surface by using Reynolds Average Navier- Stocks (RANS) equations. Ferrer and Munduate [85] have performed numerical simulations on an S814 aerofoil using the commercial CFD code ANSYS Fluent. Transition is modelled using Menter-Langtry correlation, and fully turbulent flow is modelled using the k-ω SST turbulence model. For the rough configurations, flow is assumed to be fully turbulent. Comparisons of numerical simulations against experimental data show that the commercial code predicts lift coefficients well for both clean and rough surfaces. However, for the rough case, at higher angles of attack have not yet yielded converging results.

Equivalent sand grain roughness is one the best method to develop the numerical simulation for fully roughness surface. Knopp et al [89] applied a roughness correction to the Shear Stress Transport (SST) turbulent model for 2D aerofoil study. To quantify the characteristic roughness, they estimated and applied equivalent sand grain roughness to the NACA 65-215 aerofoil model. Comparison of lift coefficient for smooth and roughness cases (for angle of attack of 4°to 12°) indicated there was a good agreement between SST model and experimental results.

There have been few studies to investigate the effect of barnacle roughness on 2D aerofoil performance by using computational method. Khor and Xiao [31] investigated the

effect of barnacle roughness on a NACA4424 aerofoil by using k-ε turbulent model. Fouling was modelled by setting small conical shapes on the surface of aerofoil as proposed in the experimental study of Orme et al. [27]. In computational model, small conical shapes (artificial barnacles) was simplified by using the spikes resembling fouling on aerofoil model shape. . The lift and drag coefficients were obtained and validated for different sizes and distribution densities. The results indicated that an increase in fouling density and fouling size caused an increase in turbulent kinetic energy and moved the separation point closer to the leading edge.

The present study applies previously quantified relations between barnacle characteristics (special barnacle dimension) and sand grain roughness height to study the effect of barnacle biofouling roughness on 2D aerofoil performance. A commercial RANS solver using a Shear Stress Transport (SST) model is used to study different simulated barnacle roughness on a NACA63-618 aerofoil. In addition, the normal force coefficient of aerofoil for smooth and roughness cases will be analysed by the pressure coefficient curves for each case. The lift and drag coefficient results for the smooth and rough cases are compared with experimental results from Walker et al. [12].

2. Equivalent barnacle roughness

In order to develop a useful numerical model, the effect of the conical shaped barnacle elements on a boundary layer may be represented using equivalent sand grain roughness as this also used to represent many other types of fouling in literature. A commonly used description of a turbulent boundary layer profile on rough walls may be written as

(3.1)

However, the limitation of the equation is that it includes all aspects of roughness but does not allow for a separation of the contributing causes of the roughness effects. For barnacles, this includes height, pitch, density and element shape. In addition, in this study, the reference surface area of roughness is an aerofoil shape. Therefore, above equations may not be useful for evaluating cone shaped barnacle roughness on aerofoil surface. Bons [34] revealed that many of the specific correlations are valid on two and three dimensional regular roughness, including bars, blocks, cones and hemisphere, etc. Bons [34] related roughness of a surface with cone shaped elements to equivalent sand grain roughness by:

(3.2)

Where Λ_s is shape roughness parameter and k_s is equivalent barnacle roughness. In order to estimate roughness shape parameter, the height of roughness elements, and spacing between them should be considered. Dirling [91] introduced a combined density and shape parameter Λ_s (Eq. 3.3), where roughness density (S/S_f) is included as the ratio of the average element spacing to roughness element height k. Sigal and Denberg [92] indicated that roughness geometry such as wetted area and frontal area of single roughness element over a test surface, can play a vital role to determine the equivalent sand grain roughness. The element shape is accounted for in the frontal area of a single roughness element A_f and the windward wetted surface area of a single roughness element A_s.

(3.3)

This shows that sand grain roughness k_s is functionally related to roughness shape parameter Λ_s. As the ratio A_f/A_s increases, the roughness shape parameter decreases. In fact, an increase in barnacle dimension geometry (height and diameter) causes a reduction in

roughness shape parameter and hence an increase in sand grain roughness k_s. In addition, an increase in roughness density parameter (S/S_f) causes an increase in roughness shape parameter and hence an increase in sand grain roughness. Thus, as expected, the value of sand grain roughness for adult barnacle is greater than for juvenile barnacles.

The study by Van Rij et al [93] describes the numerical procedures employed to determine Λ_s from three-dimensional cone shaped roughness elements. The sand grain roughness values determined with this approach are then compared with and verified by sand grain roughness magnitudes determined using analytic geometry for uniformly shaped roughness elements arranged in a regular pattern on a test surface. The results indicated there was a good agreement between numerical results and experimental data for sand grain roughness. According to Sigal and Danberg [92] and Van Rij et al [93], three-dimensional roughness consists of arrangements of spheres, hemispherical elements, cones, pyramids, and bars along a test surface. Each roughness element is placed on the surface perpendicular to the flow direction. With this approach, equivalent barnacle roughness, k_s is determined entirely from single roughness geometry and the surface parameters. These studies suggest that it is acceptable to represent the conical barnacle fouling this approach.

In this study, *Amphibalanus Amphitrite* barnacle with cone-shaped was chosen. According to Poore [39], the range of *Amphibalanus Amphitrite* barnacle height is between 5 to 13.5mm and the range of dimeter is between 6 to 20mm. According to Shkedy et al [139] and Shalla et al. [140] adults diameter typically range from 7 to 20mm. According to life cycle of barnacle (explained in section2-3), juvenile barnacles are attached on marine surfaces and fouling development will be started.

It is worth to mention that fouling with the minimum size in height or density can have an adverse effect on marine performance. Orme et al. [27] and Khor and Xiao [31] investigated

the effect of barnacles on a NACA 4424 aerofoil. Orme et al. [27] tested a two-dimensional aerofoil in a wind tunnel using three supporting struts connected to a force balance. An extrusion method was used to develop the barnacle roughness, with small, medium and large conical shapes used. The results revealed that the drag coefficient was increased by an average of 50% for all low barnacle density (11389 barnacle/m^2). Therefore, in order to show the effect of presence of fouling on aerofoil performance, the minimum size of barnacle height and diameter were chosen to estimate sand grain roughness in this section.

In order to estimate the sand grain roughness height, density parameter (S/S_f) and ratio A_f/A_s should be determined. According to Orme et al [27], fouling density can be defined as space length between two neighbouring barnacles. In fact, there is a space between two single roughness. Based on this definition, the space between two neighbouring barnacles is around a barnacle diameter for low density. In addition, in order to generate low fouling density, minimum height and diameter of barnacle should be considered (Fig. 3.1). It is because of barnacle dimension (height and diameter) is functional of barnacle density. There was some assumptions to evaluate these parameters. According to Van Rij et al [93], S_f can be defined as a total frontal area of roughness on surface area. Thus, based on low-density status assumption, the total number of barnacles can be estimated. The surface reference area of a NACA 63-618 aerofoil, S, was detailed by Walker et. al. [12].The second assumption is related to A_f/A_s. based on single barnacle geometry, $A_f=0.5h*D$ and $A_s=0.5\pi D/2(h^2+(D/2)^2)^2$. Based on these assumptions the shape parameter and sand grain roughness can be found in the following table:

Fig.3. 1. Schematic diagram of low fouling density (a barnacle diameter space between two barnacles) (frontal view).

Table 3. 1. sand grain roughness parameters for Amphibalanus Amphitrite barnacle

h(mm)	*D(mm)*	$A_f(mm^2)$	$A_s(mm^2)$	*Space between two barnacles*	*N*	$S_f\ (mm^2)$	$S((mm^2)$	Λ_s	k_s *(mm)*
7	9.5	33.25	63	9.5	42	1382	181700	366	0.41

1. Dimensionless similarity approach

In order to determine the impact of a given very small coating roughness material on the frictional drag of a plate, some non-dimensional analysis which are related to drag coefficient, can be appropriated. Schultz [21] investigated on the predictions of full-scale ship resistance with roughness coating material. The predictions were based on results from laboratory-scale drag measurements and boundary layer similarity law analysis. The total drag force of ship model is (R_{Tm}=R_{Rm}+R_{Fm}) where R_{Rm} is the residuary resistance and R_{Fm} is the frictional resistance. Gillmer and Johnson [133] indicated that the total drag of ship resistance is functional of Reynolds number and Froude number, if two sides of above equation is divided by reference dynamic pressure. Schultz [21] also indicated it is desirable to have dynamic similarity between ship and the model if the resistance of the full-scale ship is predicted.

However, the above approach is not able to use for turbine blade application of this study as the type of roughness in this study is single roughness elements. The dimensionless similarity for single roughness element would be different. Schlichting [116] revealed that the ratio of the height of the roughness element to the boundary layer thickness, h/δ, is an important parameter for the application of such results to actual conditions on a ship's hull or an aeroplane.

As the experimental turbine model in this study, used in this investigation was a $1/25^{th}$ scale model of a prototype turbine, and based on this, a computational model was created. In order to find sand grain roughness for aerofoil model $k_{m\text{-}s}$, the equivalent barnacle height for turbine model is needed. Therefore, dimensionless similarity (*height of single roughness element/boundary layer thickness*) between turbine prototype and model cases should be applied.

3. Computational Approach

A two-dimensional NACA63-618 aerofoil with a chord of 0.23m, a span of 0.79m and an aspect ratio of 3.4 was selected to allow for a comparison with the experimental study of Walker et al. [12] .The upstream inlet is 10c (chord length) from the leading edge of the aerofoil and the outlet boundary is placed 15c downstream of the trailing edge of the aerofoil. The far-field simulation was set from the aerofoil because its effect on the flow around the moving aerofoil was negligible [125]. Upper and lower sides of fluid domain and the aerofoil surface are walls. The geometry of the NACA 63-618 aerofoil section is shown in Fig. 3.2. The NACA63-618 aerofoil points coordinates are presented in Appendix.1. The solid blockage ratio as the ratio of the turbine diameter and the domain width is around 0.05.

Fig.3.3 shows the fluid domain and boundary condition around the aerofoil. The Reynolds number is 1.1×10^6 based on inlet speed. Based on experimental research by Walker

et al [12], all drag data collapse and agreed well with XFOIL results. Therefore, the flow region on the surface of the aerofoil is considered as predominantly turbulent at this Reynolds number. The upper and lower sides of domain featured a no slip boundary condition (the fluid velocity is zero relative to the boundary). Symmetry was applied to the left and right sides of domain to keep the simulation two-dimensional.

For the roughness cases, equivalent barnacle roughness, $k_{m\text{-}s}$, which was determined by equations. 3.2and 3.3, is applied on aerofoil surface. Based on Table3.1, the value of sand grain roughness was estimated 0.41mm for the minimum height of *Amphibalanus Amphitrite* barnacle. The roughness height is held constant it was applied on aerofoil surface uniformly (the roughness density value is constant). In order to employ the sand grain roughness value on aerofoil surface, the NACA63-618 aerofoil surface was chosen as a wall boundary condition. Symmetry boundary conditions were set at the sides and top of the fluid domain. Then a steady state solution is carried out for roughness case.

Fig.3. 2. geometry of NACA 63-618 aerofoil

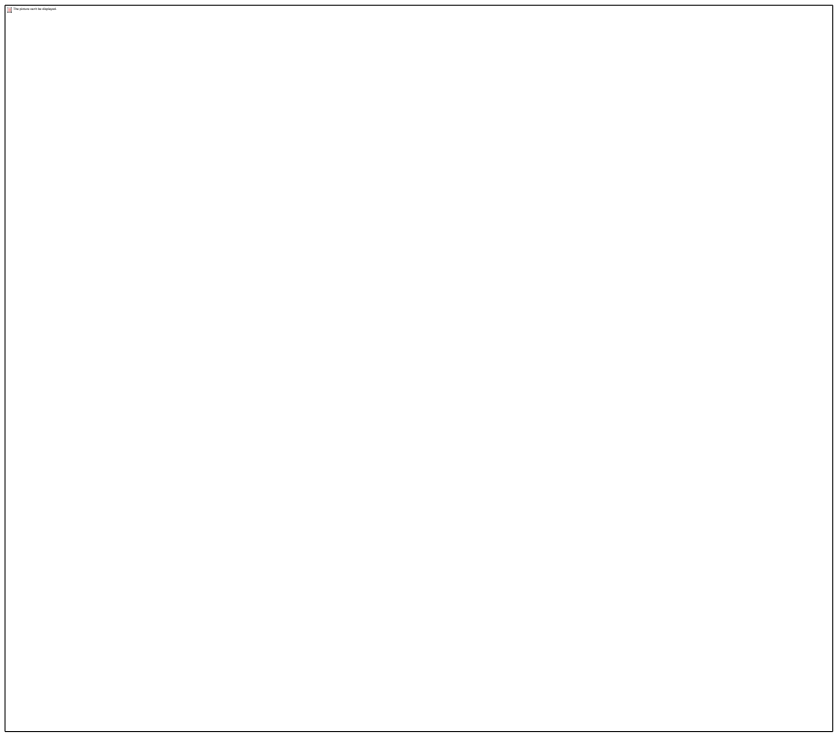

Fig.3. 3. Schematic of the computational domain and boundary conditions

The commercial ANSYS CFX 15 solver was used to investigate the performance of the aerofoil. The model used was a two dimensional second-order multi block structured Reynolds-Averaged Navier-Stokes (RANS) solver. This solves the continuity equation, RANS equations (momentum equations) in conjunction with a turbulence model using a finite volume approach:

The low Reynolds number model is considered to be effective and robust for $y^+=1$ and $30<y^+<300$ for smooth and roughened cases, respectively. Due to its accuracy and reliability for a wide range of flow types, including flows with adverse pressure gradients and separation,

the Shear Stress Transport (SST) model with fully turbulent model. The details of the model are provided by [94].

A spatial discretization of the computational domain was achieved using swept hexahedral elements. A C-type structure grid was used for the region around the surface of the aerofoil. In order to capture the transition boundary layers correctly, the grid must have a y^+ of approximate to one [95]. y^+ is a non-dimensional distance which indicates the degree of fineness of grid in near-wall region. It is defined by the formula:

(3.4)

Therefore, the maximum later of nodes from aerofoil surface is chosen 30 with growth rate of 1.2. The distance between the nodes of the first layer and the aerofoil surface (Δy) is around 1.2×10^{-5}m. Figs.3.4 shows wall distance from aerofoil surface to the first row of mesh in leading edge of aerofoil.

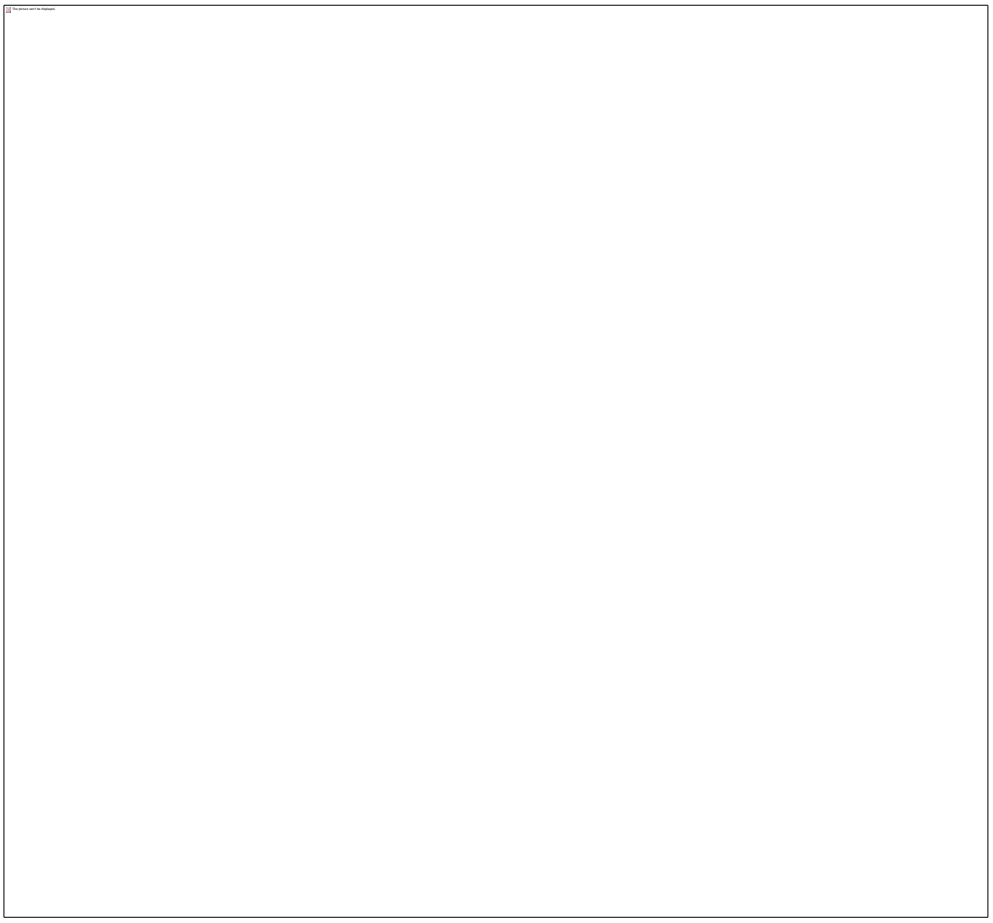

Fig.3. 4. wall distance from aerofoil surface to the first row of mesh in leading edge

The mesh independence was verified using the Richardson extrapolation method [96-98]. Richardson extrapolation is used to calculate a higher-order estimate of the flow fields from a series of lower order discrete values. The mesh error estimation based on Richardson extrapolation method can be found by the following equations:

(3.5)

(3.6)

(3.7)

(3.8)

(3.9)

(3.10)

Where r_i is convergence ratio, ε_n is force coefficient difference, δ is error estimate of finest mesh, C_R is Richardson extrapolated value and ε_R is relative error estimate.

The simulations were conducted at 2° Angles of Attack (AOA) with three different grids for the fully turbulent case with no roughness. Coarsening and refinement was made by halving and doubling the number of elements respectively in all directions, without changing the adjacent to the wall cell height (y^+=1). The coarse grid has 75000 elements and the refined grid has 300000. Figure 3.5 shows the grid dependence study in comparison with drag coefficient for smooth case data [12] at an angle of attack 2°. The drag coefficient converges to the experimental value when the number of cells reaches 300000 cells. In addition, the difference is below 5% for 300000 cells. As a result, a 300000 cell mesh was chosen for all angle of attacks.

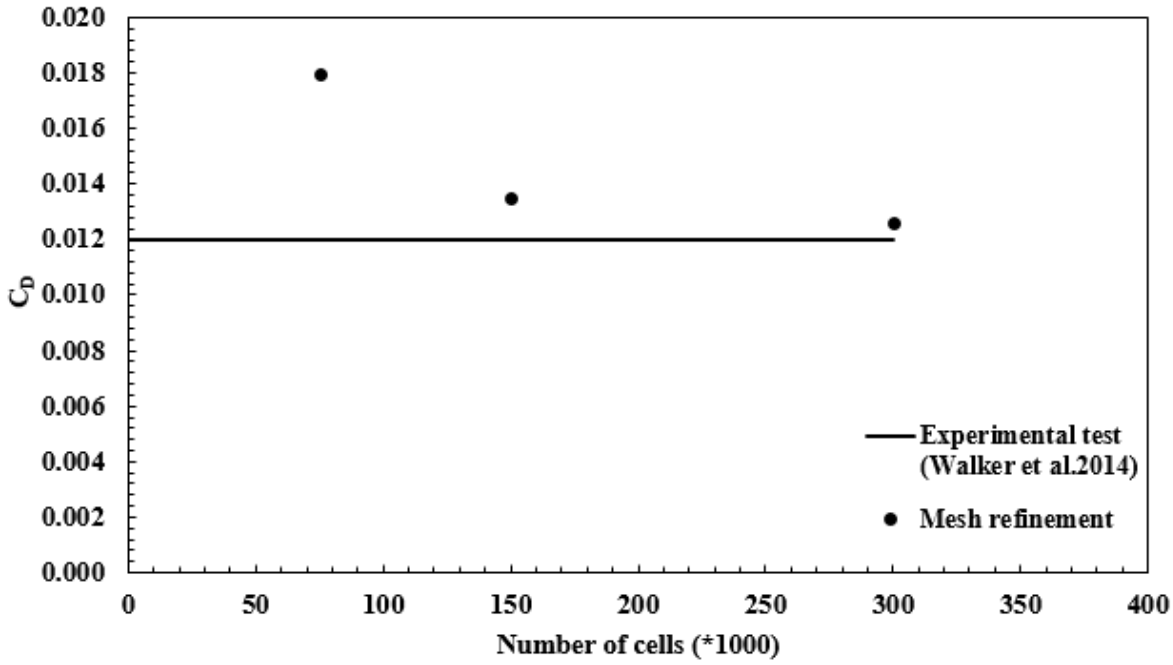

Fig.3. 5. Mesh sensitivity study at angle of attack 2°

A grid sensitivity study was performed to ascertain whether the selected grid density was of sufficient resolution and that the spatial discretization errors were minimal. The total number of elements of the original mesh was halved and doubled to generate two additional meshes for this study. Table 3.2 shows grid dependence parameters based on extrapolation's theory;

Table 3. 2. grid dependence parameters based on Richardson extrapolation's theory

r_i	ε_{32}	ε_{21}	p	δ	C_R
2	0.005	0.001	2.32	2.5E-5	0.011975

Based on above parameters, the value of relative error for three different mesh cases can be found in Fig. 3.6.

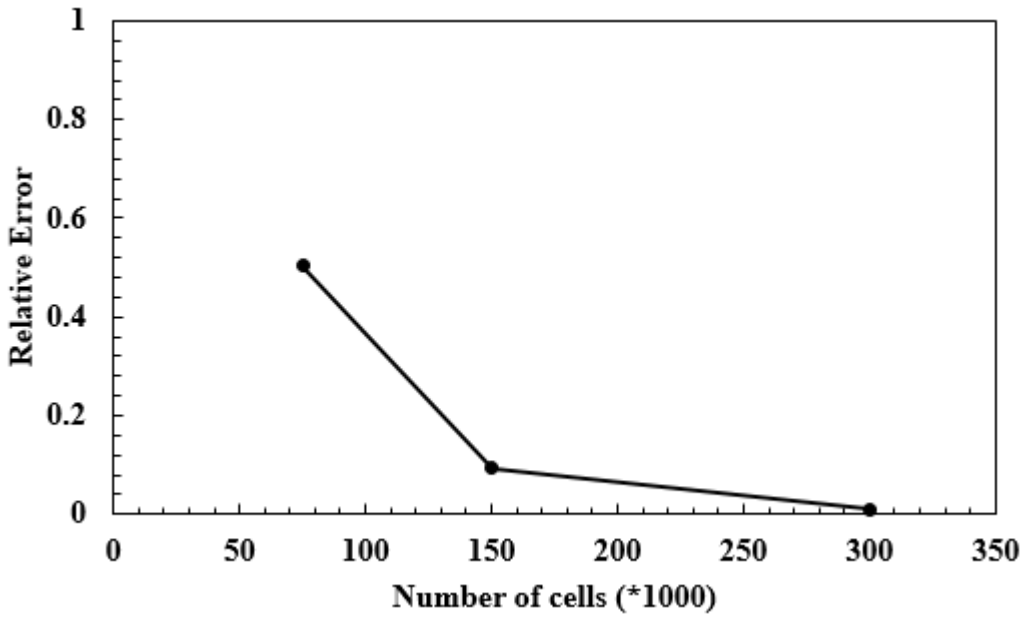

Fig.3. 6. Relative error for three different number of cells

4. Results and Discussion

1. Lift and drag coefficients

The value of lift and drag coefficients with angle of attack for smooth and roughened (minimum size of barnacle) cases are shown and numerical smooth case compared with smooth experimental results from Walker et al [12] in Fig. 3.7 and Fig. 3.8 respectively.

Fig.3. 7. Results of drag coefficient with Re=1.1×106

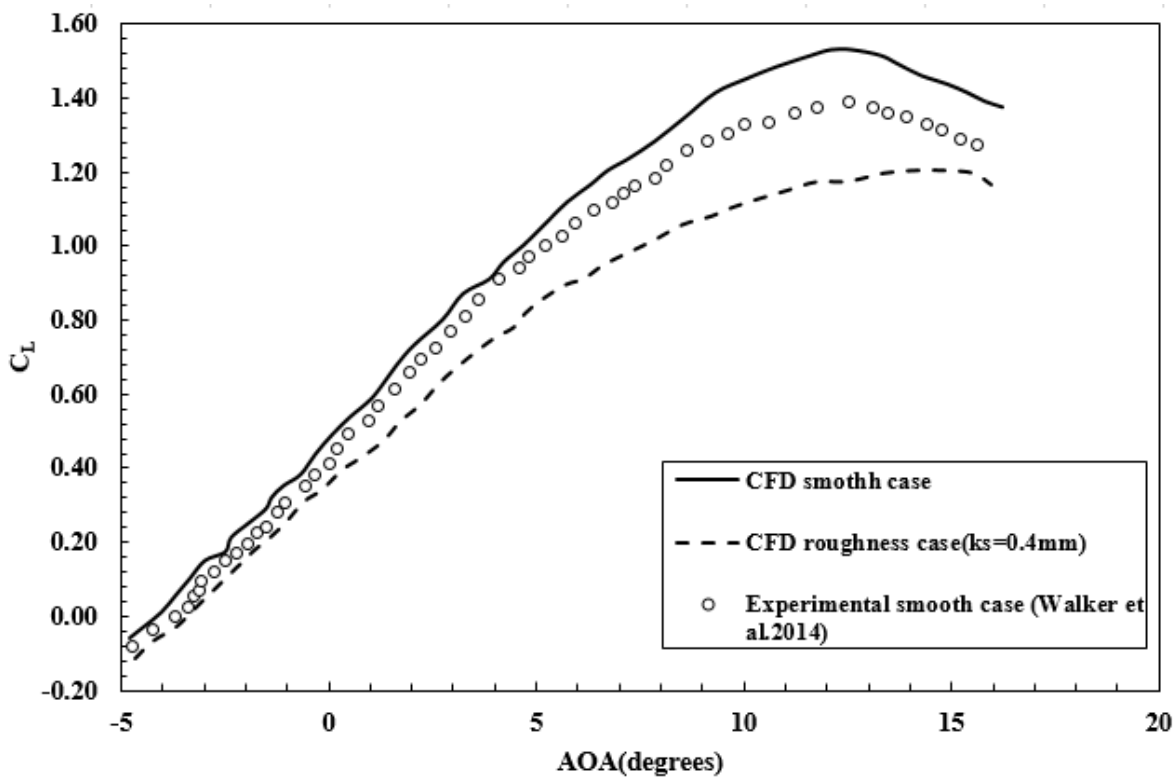

Fig.3. 8. Results of lift coefficient with Re=1.1×106

The smooth aerofoil lift and drag coefficients determined from commercial ANSYS CFX. 15 solver were compared to the data from Walker et.al. [12]. In the above two figures, it is obvious that the smooth numerical results show good agreement with the experimental study of Walker et al. [12].

The roughened aerofoil case is compared to the smooth aerofoil case and Walker et al. [12] data in Fig. 3.7 and 3.8. Based on barnacle geometry (Table3.1) and governing equations for evaluating equivalent barnacle roughness (Equations3. 2 and 3.3), the ,minimum sand grain roughness (k_s=0.4mm) was chosen for barnacle fouling case.

The drag coefficient increased with presence of roughness. The minimum drag coefficient at Reynolds number of 1.1×10^6 increased 112% for k_s=0.4mm. The effect of roughness was to decrease the lift coefficient curve. The maximum lift coefficient reduced by an average of 21% for the maximum equivalent barnacle roughness (k_s=0.4mm). In addition, based on Fig.3.8, the effect of roughness increases the stall angle from 10° for the smooth aerofoil to 14° for the roughened aerofoil.

The variation of C_L/C_D with angle of attack is shown in Fig. 3.9. The ratio of lift to drag ratio decreases when the aerofoil is coated by fouling. These results indicates that the lift to drag ratio decreases with presence of roughness. The highest lift to drag ratio is for the smooth aerofoil and the effect of fouling was to decrease the $(C_L/C_D)_{max}$ by an average of 60%.

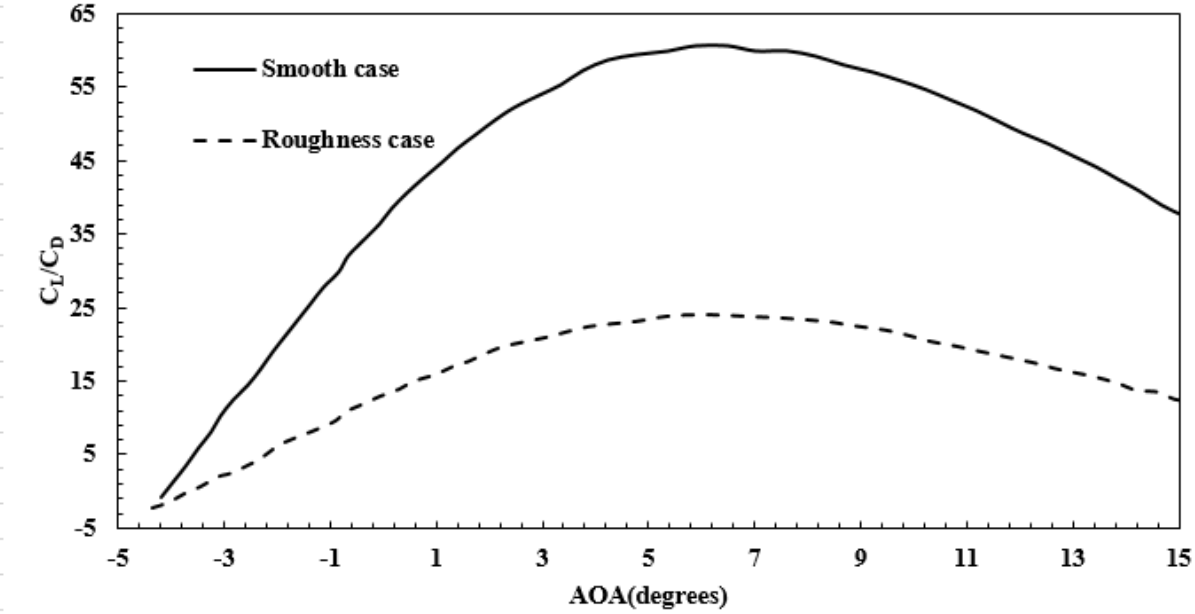

Fig.3. 9. The variation of CL/CD with various angle of attack

2. Flow field over aerofoil

In order to illustrate the roughness effect on separation phenomena or turbulent flow, pressure distribution around the aerofoil were visualized. Pressure coefficient for NACA 63-618 aerofoil at 0° and 8° of angle of attack have been plotted for smooth and fouling cases as shown in Figs. 3.10 and 3.11 respectively.

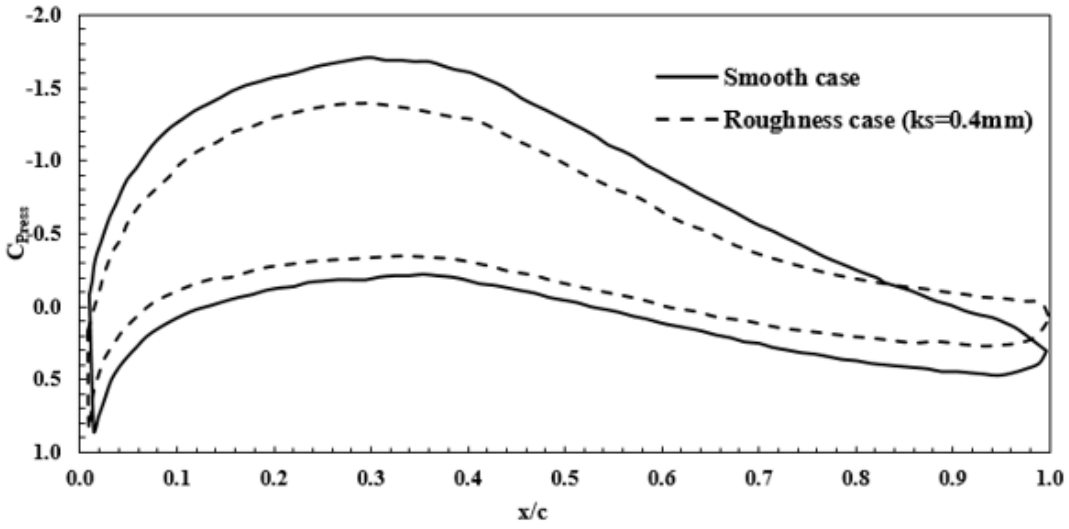

Fig.3. 10. pressure coefficient graph for smooth and roughness cases at AOA=0°.

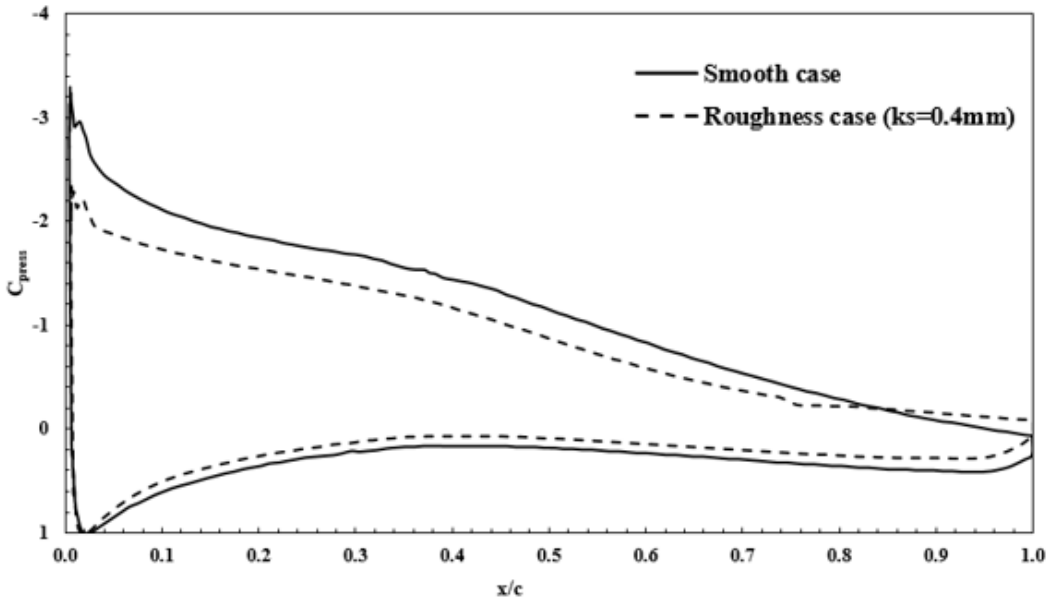

Fig.3. 11. pressure coefficient graph for smooth and roughness cases at AOA=8°.

As can be seen in Figs. 3.10 and 3.11, the enclosed pressure coefficient area decreases with presence of the sand grain roughness. The enclosed area between the pressure coefficient curves for each surface is equal to the normal force coefficient of aerofoil. It can be noted that an increase in fouling height causes a reduction in normal force coefficient of aerofoil. This

contributes to a reduction in lift force by an average of 22% and 25% for fouling case at angles of attack of 0° and 8° respectively.

At low angle of attack (Fig.3.10), except 0.85<x/c<1, the pressure coefficient for roughness graph is lower than pressure coefficient for smooth case in suction side. At the 85% of chord length, the pressure distribution curve is approximate constant and pressure coefficient is more than the value for smooth case. As angle of attack increases (Fig.3.11), it can be seen that separation occurs on the suction side over the region of 0.75<x/c<1 due to adverse pressure gradient.

The turbulent kinetic energy contours for NACA 63-618 aerofoil at 0° and 8° of angle of attacks have been plotted for smooth and fouling cases as shown in Figure 3.12.

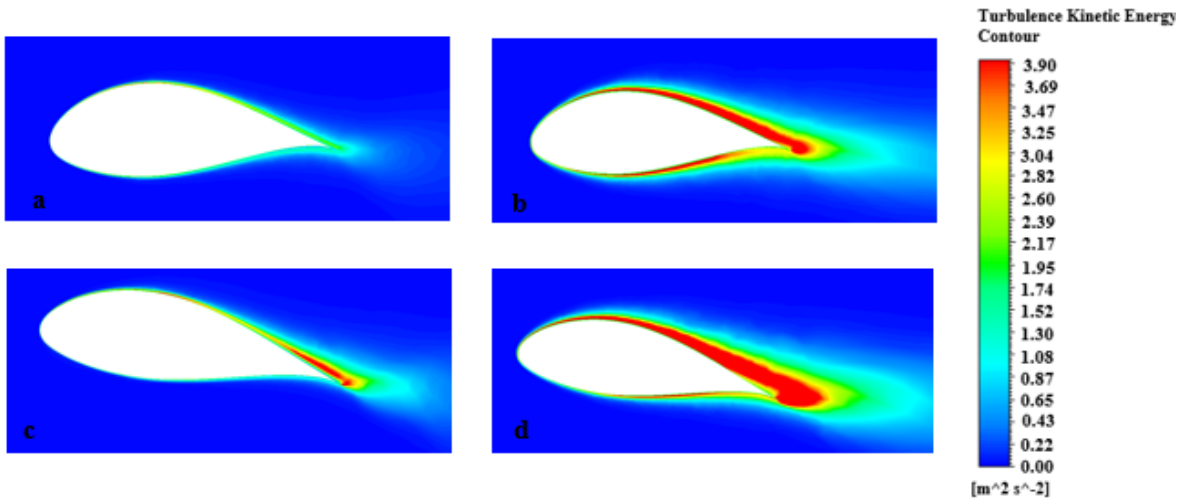

Fig.3. 12. Turbulent Kinetic Energy contours for smooth and roughness case ((ks=0.4mm) with Re=1.1×106 a) smooth case, α=0° b) roughness case α=0° c)smooth case, α=8° d) roughness case α=8°

Fig. 3.12 shows the turbulence kinetic energy at low (0°) and high (8°) angle attacks for 1.1×10^6. The turbulent kinetic energy increases with fouling height and produces a greater

region of turbulent activity in the wake. As shown in these figures, the absolute value of turbulence kinetic energy increases over the upper surface of aerofoil when sand grain roughness is added on surface. In fact a thicker turbulent boundary layer is apparent on the upper aerofoil surface when sand grain roughness is present (Fig. 3.12.b and 3.12d). With increase in turbulence kinetic energy, the separation point moves to the leading edge and turbulence flow occurs over most of the upper surface.

3. Effect of barnacle roughness on long-term aerofoil performance

In this study, barnacles which survive in different environmental conditions and colonize a variety of surfaces, were described as one of the most problematic causes of marine animal biofouling. This is because a barnacle fouling community can appear on marine surfaces in a short-time after marine deployment. According to Polagye et al. [82] and Titah-Benbouzid et al. [81], some materials like carbon fibre composite or Aluminium can be colonised by juvenile barnacle within 3 months of deployment. Based on research by Mineur et al. [99], establishment of adult barnacle fouling community can take place less than one year after surface deployment.

In this study, the *Amphibalanus Amphitrite* barnacle with the minimum size (Table. 1)was chosen for evaluating the effect of equivalent barnacle roughness, k_s, (Equations. 3.2 and 3.3) on aerofoil performance. Based on available literature, it is possible for adult barnacles to develop on aerofoil surfaces within one year.

The hydrodynamic results showed that the NACA 63-618 aerofoil with the minimum k_s, produced a reduction in the lift coefficient and significant increase in the drag coefficient. The computation results indicated that the maximum lift coefficient reduced by an average of

21% after 10 months of barnacle fouling attachment. In fact, presence of fouling represents a reduction in the performance of aerofoil and consequently marine turbine rotors based on aerofoil sections.

Barnacle roughness development is a significant issue for the long-term performance and viability of marine current turbine. Experimental research by Katsuyama et al. [26] in Japan showed that barnacle colonization on a three-bladed tidal turbine produced a mass imbalance on the rotor section and the marine turbine stopped after eight months.

5. Conclusion

The effect of simulated *Amphibalanus Amphitrite* adult barnacle roughness on NACA63-618 aerofoil was studied using RANS-based solver. According to sand grain roughness equations, equivalent barnacle roughness depends on single roughness geometry and surface parameters. As adult barnacles with the minimum size have the most significant effect on hydrodynamic performance of marine surface, the adult barnacle with the minimum size was chosen in this study.

In this study, barnacles were described as one of the most problematic causes of marine animal biofouling. This is because a barnacle fouling community can produce the roughness on marine turbine surfaces. In addition, hard fouling colonization can make an erosion and mass imbalance on the blade surface. Thus these fouling sites on rotor areas can produce a reduction in the lift coefficient and significant increase in the drag coefficient and hence reduction in hydrodynamic performance.

The simulation indicated that barnacle fouling development changes the boundary layer flow on suction side of aerofoil and leads to a reduction in the lift coefficient and a significant increase in the drag coefficient. The effect of roughness was to decreases the maximum lift

coefficient by an average of 21% for roughness case. In addition, a thicker turbulent boundary layer is apparent on the upper aerofoil surface when sand grain roughness is present. With increase in turbulence kinetic energy, the separation point moves to the leading edge and turbulence flow occurs over most of the upper surface.

Barnacle roughness development is a significant issue for the long-term performance and viability of marine current turbines. As discussed, minimal barnacle fouling on surface and then establishment of fouling community can take place less than a year. Therefore, strategies concerning maintenance technology can help to reduce fouling growth and improve long-term performance.

Chapter 4

The performance of a Horizontal Axis Tidal Turbine (HATT) with Simulated Barnacle Roughness

1. Introduction

Horizontal Axis Tidal Turbines (HATTs) operate using the aerodynamic lift principle and the rotor blades are commonly designed using aerodynamic section data. However, the flow fields encountered by HATT turbine blades are complex and difficult to predict [100-101]. However, blade shape is critical to the aerodynamic performance of wind and tidal turbine blades. Therefore, the aerodynamic performance of turbine rotor blades can help to interpret the turbine performance. In the previous chapter, it was concluded that biofouling roughness has significant effect on aerofoil performance. An increase in roughness element causes an increase in drag force and a reduction in lift force.

Although obtaining the marine performance of tidal turbine experimentally can obtain highly reliable data, this kind of method is expensive and requires a great deal of experience and time. On the other hand, CFD can obtain various results at low cost and most of the flow phenomena can be simulated around the blade easily. Several efforts [43,128-130] have been made to evaluate the performance of turbine based on steady state three-dimensional analysis by using Reynolds Average Navier- Stocks (RANS) equations. Jo et al[128] investigated the hydrodynamic performance of full-scale marine turbine with the ANSYS CFX programme. The Shear Stress Transport (SST) turbulence model was used as a turbulence closure. The model was assumed to be incompressible, three dimensional and steady state. The numerical results showed a good agreement versus the experimental results. Tian et al [129] studied on inflow profiles for predicting wind turbine wake. The steady state three-dimensional Naiver Stokes equations were solved. Based on wind wake simulation results the shape and magnitude of wake velocity and wake turbulence profiles were significantly affected by different inflow profiles.

Small particles of dust, dirt and contamination can be transported by the wind and water to the height of the turbine rotor. As these particles hit the rotor blade, the smoothness of the surface is perturbed, especially at the leading edge, near the stagnation point. In the study by Khafallah and Koliub [46], the effects of dust accumulation on a 300kW pitch regulated wind turbine, over various operational periods, was examined. As expected, the dust accumulation pattern follows the blade profile, with the highest concentration of particles on the leading edge and tip of the blade.

Several researchers [44, 46, 50-52, 57, 85, 102] have investigated the effect of roughness on wind and tidal turbine blades. A study by Corten and Veldkamp [52] on insect contamination roughness on wind turbine blades at wind farms in California indicated a reduction in turbine rotational speed. In addition, an increase in insect contamination density can produce a mass imbalance on rotor surface and hence a reduction in power outputs of these turbines. In the study by Freudenreich et al [57], clean and rough configurations of a thick state of the art wind turbine blade were investigated experimentally and numerically. Three different roughness configurations were examined on the wind turbine blade and aerofoil surface: a trip wire 1mm in diameter, 0.6mm zigzag tapes and 60 grain carborundum. Results indicated the presence of roughness causes a reduction in the power production of the wind turbines.

The two largest performance issues for marine current turbines are the roughening of the turbine blades due to impact, cavitation or scour due to particulates, and the fouling of the turbine blades by marine growth [75]. Biofouling is a unique type of surface roughness and leads to several adverse effects on marine turbine blades or ship propellers.

Hard fouling production by barnacles on tidal turbine rotors increases the surface roughness on the blade leading to the losses of hydrodynamic performance and producing mass turbine imbalance in the rotor system. Walker et al. [12] investigated the impact of blade

roughness on the performance of a two-bladed horizontal axis marine current turbine using a combined experimental and numerical approach. In order to model barnacle growth on a tidal turbine blade, a thin layer of randomly applied contact cement was applied to a three-dimensional two bladed turbine which was tested in a towing tank. The towing tank testing revealed a 19% reduction in maximum power coefficient from the baseline smooth case, which was supported by numerical modelling. Katsuyama et al. [26] compared the long-term performance of tidal turbines with and without anti-fouling coatings. Their results indicated that the entire tidal turbine surfaces (blades and hub surfaces) without the antifouling coating was covered by *Megabalanus rosa* barnacle after 8 months and disruption of aerodynamics were reported. On the other hand, the hub section of tidal turbine with an anti-fouling coating only incurred barnacle growth and its blades were protected against barnacle colonization

One of the best methods to investigate the barnacle development roughness on tidal turbine blade is by representing the roughness as a sand grain roughness. This allows the performance to be assessed using wall functions and a computational fluid dynamics. However, there have been few studies to investigate the relationship between barnacle growth and sand grain roughness height. The irregular distribution of fouling is much harder to model. For instance, Khor and Xiao [31] ignored the sand grain roughness parameter in their study. The artificial fouling which was applied by setting small conical shapes on the surface in the experimental study of Orme et al [27], was modelled and simplified by using the spikes resembling in the design section on that study.

The main aim of this study focuses on the relationship between barnacle characteristics and sand grain roughness height to study the effect of barnacle biofouling roughness on turbine performance. A commercial RANS solver using a k-ω model is used to study different simulated barnacle roughness on twin-bladed turbine. The numerical results for the smooth

case are validated with experimental results from Walker et al. [12] and then compared with the rough surface case results. In addition, the relationship between the tip speed ratio and surface pressure distributions on the rotor for smooth and roughened cases are investigated.

2. Equivalent barnacle roughness

In order to quantify the effect of the conical shaped barnacle roughness on a boundary layer of a turbine blade, an equivalent barnacle roughness is used to represent the actual fouling roughness. Equivalent barnacle roughness was explained well in section 3.2.

It is worth to mention that the experimental turbine model in this study, used in this investigation was a $1/25^{th}$ scale model of a prototype turbine, and based on this, a computational model was created. In order to find sand grain roughness for aerofoil model $k_{m\text{-}s}$, the equivalent barnacle height for turbine model is needed.

Many studies [21,133-135] revealed a similarity law scaling procedure for the prediction of the effects of a particular roughness on the frictional resistance of any arbitrary body covered with the same roughness, utilising the experimentally obtained roughness functions of such surfaces. This procedure allows on the predict the impact of a given roughness on the frictional drag and roughness function of a plate covered with the same roughness.

However, for some roughness method such as single roughness element on turbine blade, the scaling procedure can have different approach. Schlichting [116] revealed that the ratio of the height of the roughness element to the boundary layer thickness, h/δ, is an important parameter. In this study, dimensionless similarity (*height of single roughness element/boundary layer thickness*) between turbine prototype and model cases should be applied.

It is worth to mention that fouling with the minimum size in height or density can have an adverse effect on marine performance. Orme et al. [27] and Khor and Xiao [31] investigated the effect of barnacles on a NACA 4424 aerofoil. Orme et al. [27] tested a two-dimensional aerofoil in a wind tunnel using three supporting struts connected to a force balance. An extrusion method was used to develop the barnacle roughness, with small, medium and large conical shapes used. The results revealed that the drag coefficient was increased by an average of 50% for all low barnacle density (11389 barnacle/m^2). Therefore, in order to show the effect of presence of fouling on aerofoil performance, the minimum size of barnacle height and diameter were chosen to estimate sand grain roughness in this section.

In order to estimate the sand grain roughness height, density parameter (S/S_f) and ratio A_f/A_s should be determined. According to Orme et al [27], fouling density can be defined as space length between two neighbouring barnacles. In fact, there is a space between two single roughness. Based on this definition, the space between two neighbouring barnacles is around one and half barnacle diameter for low density. In addition, in order to generate low fouling density, minimum height and diameter of barnacle should be considered (h=5mm and D=6mm). It is because of barnacle dimension (height and diameter) is functional of barnacle density. There was some assumptions to evaluate these parameters. According to Van Rij et al [93], S_f can be defined as a total frontal area of roughness on surface area. Thus, based on low-density status assumption, the total number of barnacles can be estimated. The surface reference area of a turbine blade, S, was detailed by Walker et. al. [12].The second assumption is related to A_f/A_s. based on single barnacle geometry, $A_f=0.5h*D$ and $A_s=0.5\pi D/2(h^2+(D/2)^2)^2$ (Fig.4.1). Based on these assumptions the shape parameter and sand grain roughness can be found in the following table.

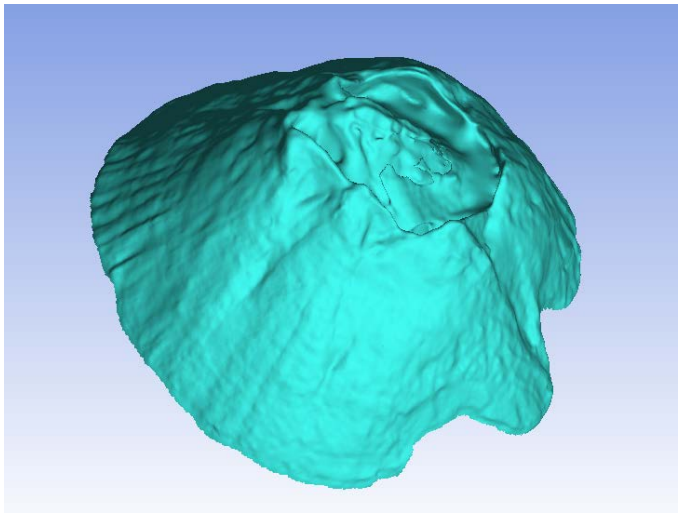

Fig.4. 1. Computer model of Amphibalanus Amphitrite barnacle.

Based on the typical dimensions of *Amphibalanus Amphitrite* barnacle [39], turbine blade geometry [12] and governing equations (Eq. 3.2 and 3.3), equivalent barnacle roughness for blade can be determined for juvenile and adult *Amphibalanus Amphitrite* barnacle in Fig.4.2

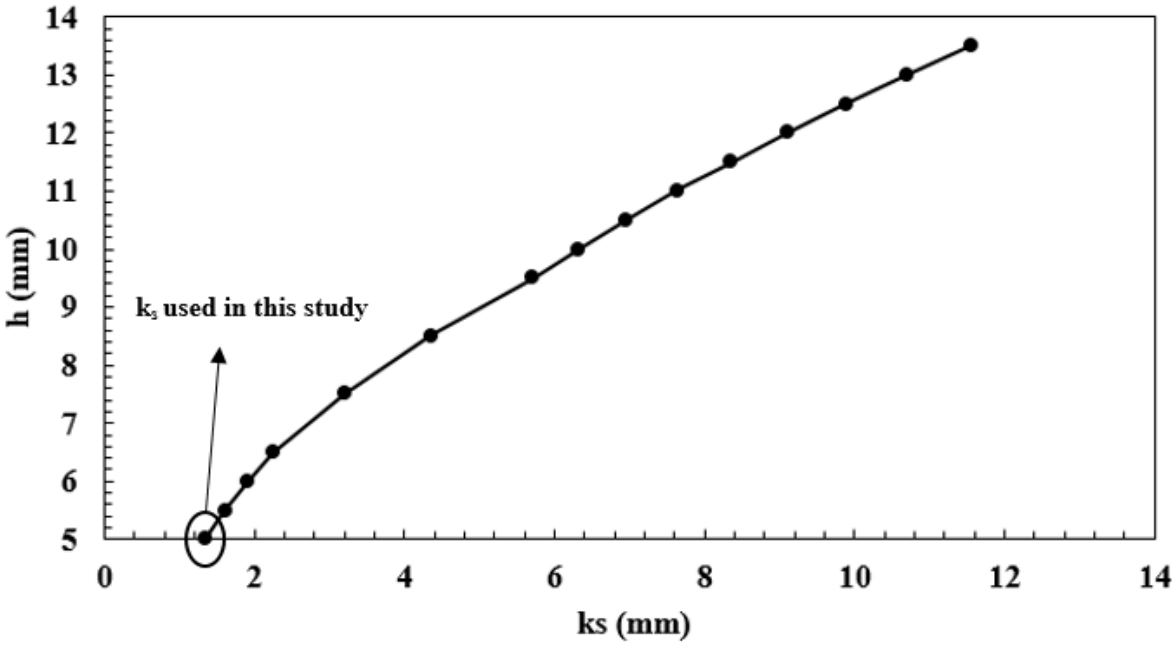

Fig.4. 2. Sand grain roughness result for turbine blade

3. Turbine model geometry

The marine current turbine model consisted of a two-bladed rotor with a diameter of d=0.8m. This is representative of a 1/25th scale model of a full size turbine. The rotor blades are based on a NACA63-618 aerofoil cross section and it was detailed in section (3.3). The blades are constructed of 6061 aluminium and were anodised for corrosion resistance [12]. The blade geometry is detailed by Walker et al. [12].

Point coordinates required to visualize a 3-D model were obtained and the schematic diagram of tidal turbine blade was plotted as shown in Fig. 4.3 from the design information of Walker et.al. [12] by using ANSYS-Geometry, a 3-D modelling program. The blade geometry is detailed in Appendix.2.

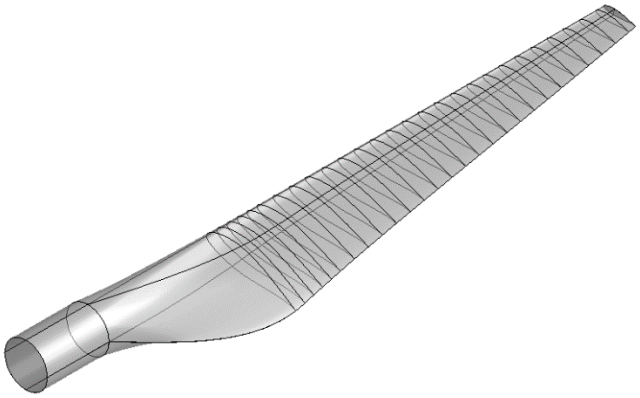

Fig.4. 3. schematic diagram of tidal turbine blade

4. Performance analysis

1. Mesh and grid system

The numerical analysis based on 3-D Reynolds-Averaged Navier-Stokes (RANS) equations has been widely used for the flow analysis of turbomachinery. A CFD analysis was conducted to estimate the performance of the turbine. The ANSYS commercial CFD code (version 15.0) was used for the simulations, focusing on the turbine in the analysis domain.

Grid generation was carefully conducted for smooth convergence and reliable results. The thickness of the near-wall grid layers was considered according to the application of the turbulence model for smooth and roughness cases. An inflation layer (boundary layer) was employed to capture the boundary layer on surface of the blade. The number of layers is then increased slowly to obtain an appropriate y^+. The parameter y^+ is a non-dimensional distance which indicates the size of the first element within a boundary layer.

However, inflation option for smooth and roughness case are different. As the flow is turbulent, first layer thickness with 10 layers were chosen for smooth case to capture the boundary layer. The distance between the nodes of the first layer and the blade surface (Δy) is around 1.1×10^{-4}m. For roughness case, on the other hand, as the flow is fully turbulent, the total thickness option with 20 layers was selected to capture the boundary layer. The growth rate for both cases was chosen 1.2. It is worth to mention that the y^+ is significantly higher than the value of sand grain roughness, k_s, on turbine blade. This fact allows the chosen turbulence model to achieve thoroughly and reasonably [126].

The key areas of interest occurred around the rotating blades and hub for accurate estimation of the torque and thrust coefficients. Thus, the prism-layer was composed around the blade and the mesh generated for rest of fluid domain was an unstructured tetrahedral grid. The total number of elements and nodes are 1197785 and 270809 respectively.

2. Mesh independence study

Grid generation was carefully conducted to investigate the influence of mesh resolution on simulated turbine performance. A grid sensitivity study was performed to ascertain whether the selected grid density was of sufficient resolution and to minimise spatial discretization errors.

The mesh independence was verified using the Richardson extrapolation method [96-98]. Richardson extrapolation is used to calculate a higher-order estimate of the flow fields from a series of lower order discrete values. The mesh error estimation based on Richardson extrapolation method can be found by Eqs (3.5-3.10).

Based on mesh refinement theory, Richardson extrapolation has been used with grid refinement ratios of r=2 [127]. Thus, the total number of elements of the original mesh was halved and then doubled to generate additional meshes. Fig. 4.4 shows grid dependence study compared to experimental data [12] at a tip speed ratio of 6. According to Richardson extrapolation parameters (Based on Eqs. 3.5-3.10), the value of relative error for three different mesh cases can be found in Figs. 4.4 and 4.5 respectively.

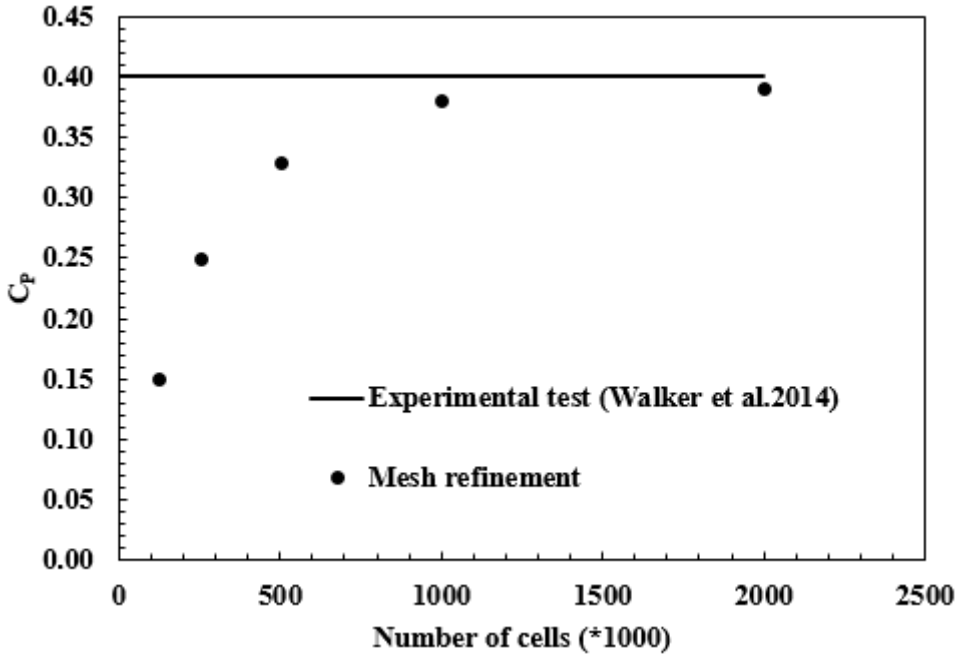

Fig.4. 4. Mesh sensitivity study at λ=6

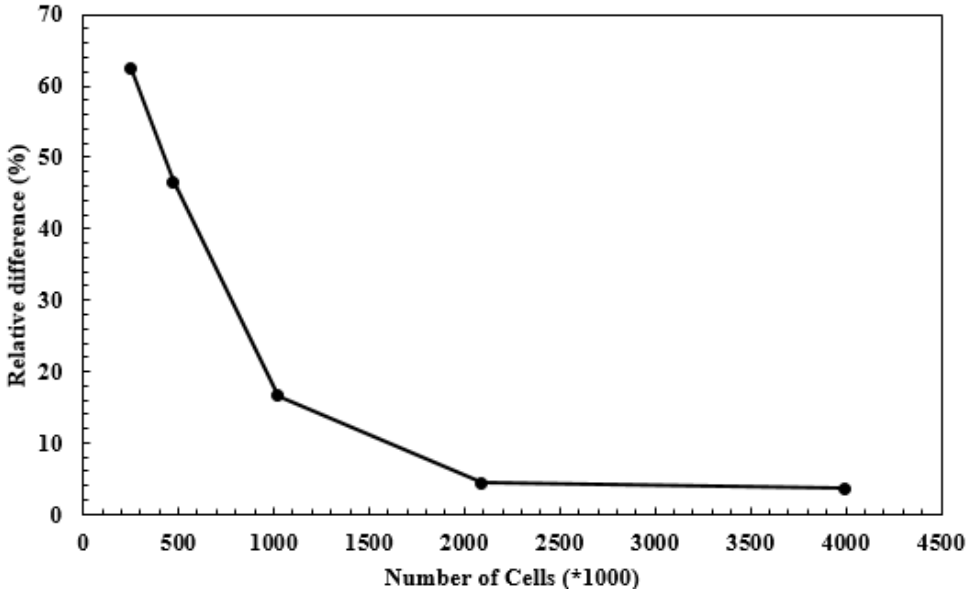

Fig.4. 5. Relative errors of meshing cases

As can be seen in Figs. 4.4 and 4.5, the power coefficient converges to the experimental value when the number of cells reaches 1million. In addition, the relative error is below 5% when number of cells is 2 million.

3. Boundary conditions

The analysis field was assumed to be incompressible water, three dimensional, and steady state. The analysis field was composed of two fluid domains: an internal rotating domain encompassed the turbine and an outer domain covered the remaining area of the flow channel, as shown in Fig. 4.6. The blockage ratio that is defined as the ratio of the rotor swept area to the external domain cross-section are, is approximately 0.05.

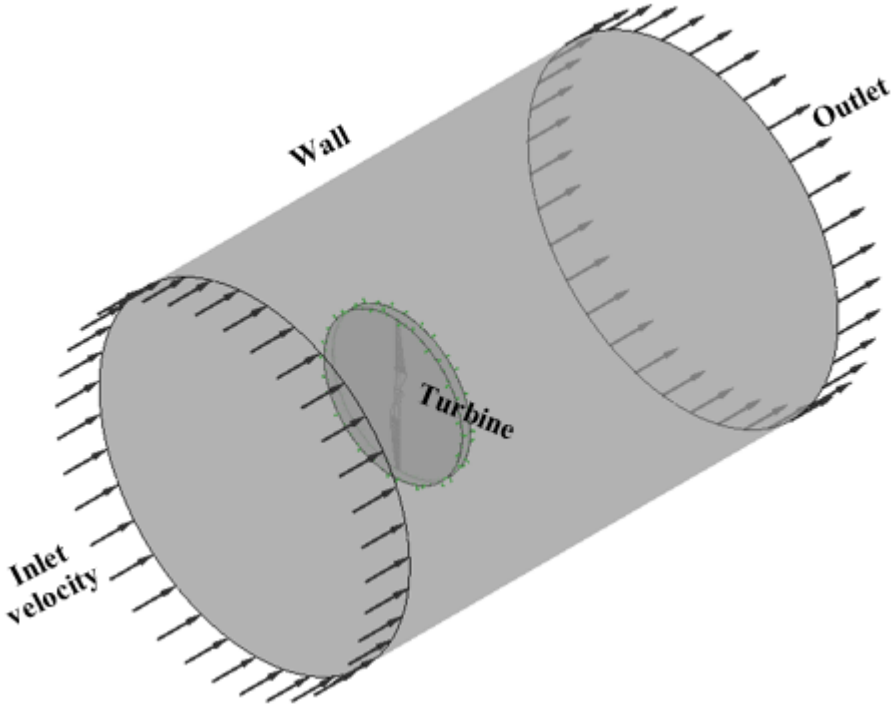

Fig.4. 6. Computational model for performance analysis.

The outer stationary domain area used an opening condition that was similar to the environment of the towing tank. The rotor was represented by a wall condition with non-slip surface as the sand grain roughness is applied on that. A free stream velocity was applied to the inlet for smooth and roughness cases. A speed of 1.68 m/s was chosen to match the experimental condition [12]. In the rotating domain, the rotation velocity and upstream velocity are linked by tip speed ratios. As the inlet velocity is constant, the angular speed can be adjusted

to the required tip speed ratio over the range of $5<\lambda<10$. An interface was used to connect the two domains. The turbulence model performed analysis by considering the steady flow field around the aerofoil using the k-ω model. The k-ω model is well regarded for predicting the size and onset of flow separation in an adverse pressure gradient [126]. Finally, sand grain roughness is applied as wall roughness application on turbine blades for fouled case. Table.4.1 shows the defined boundary conditions.

Table 4. 1. Boundary conditions

Description	Analysis condition
Working fluid	Water (isothermal, 25°C)
Inlet	Velocity (1.68m/s)
Wall	Non-slip wall
Outlet	Normal pressure (1 atm)
Interface area	Frozen rotor
Turbine	Wall (double blades)
Turbulence model	k-ω

4. Hydrodynamic performance of turbine

Since tidal turbines convert the energy of a free flowing water to mechanical power, their performance can be evaluated by calculating the energy conversion efficiency. The turbine power characteristic is affected by factors including the current speed, rotor diameter, blade area and rotational speed. The power and thrust coefficients of a HATT are defined by equations 4.1 and 4.2. The tip speed ratio is a dimensionless value representing the ratio of the rotational speed to the inflow velocity, as shown in equation 4.3. The pressure distribution around the aerofoil can be defined using equation 4.4.

$$C_P = \frac{Q\omega}{0.5\rho A U_\infty^3} \tag{4.1}$$

$$C_T = \frac{T}{0.5\rho A U_\infty^2} \tag{4.2}$$

$$\lambda = \frac{R\omega}{U_\infty} \tag{4.3}$$

$$C_{press} = \frac{p - p_0}{0.5\rho U_\infty^2} \tag{4.4}$$

Where, C_P, C_T, and C_{Press} are power, thrust and pressure coefficient respectively. R is radius of blade, ρ is fluid density, U is fluid velocity, A is cross section area, Q is torque, ω is angular velocity and P is static pressure.

5. Results and discussion

1. Performance curves

The value of thrust and power coefficients with tip speed ratio for smooth and roughened (minimum size of barnacle) cases are shown and compared with smooth case of experimental results for [12] in Figs. 4.7 and 4.8 respectively. In addition, the output power of two bladed tidal turbine for smooth and roughness cases is plotted in Fig. 4.9.

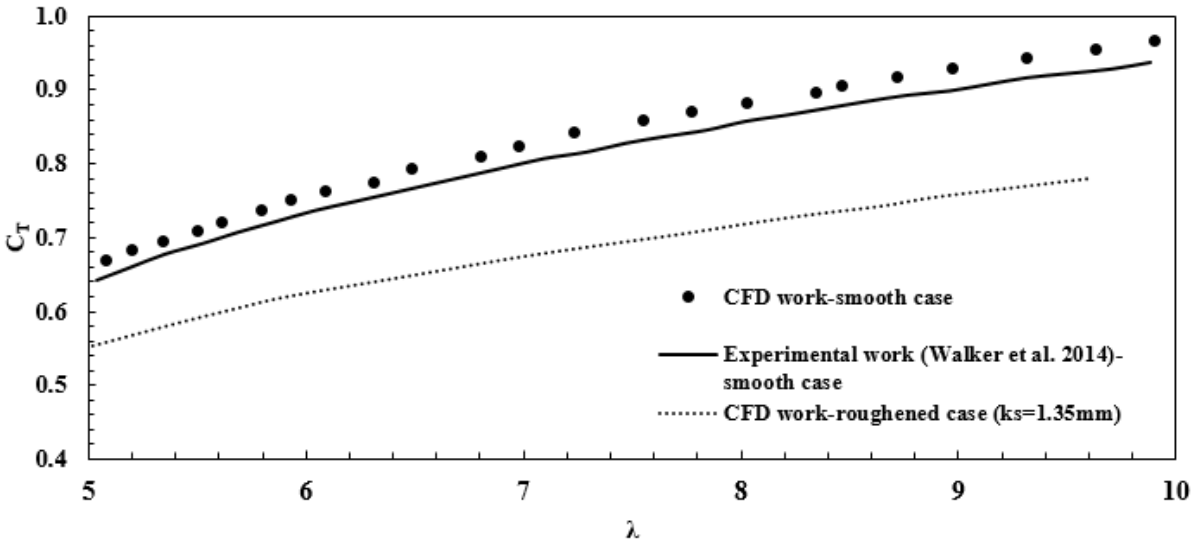

Fig.4. 7. Thrust coefficient at U=1.68m/s

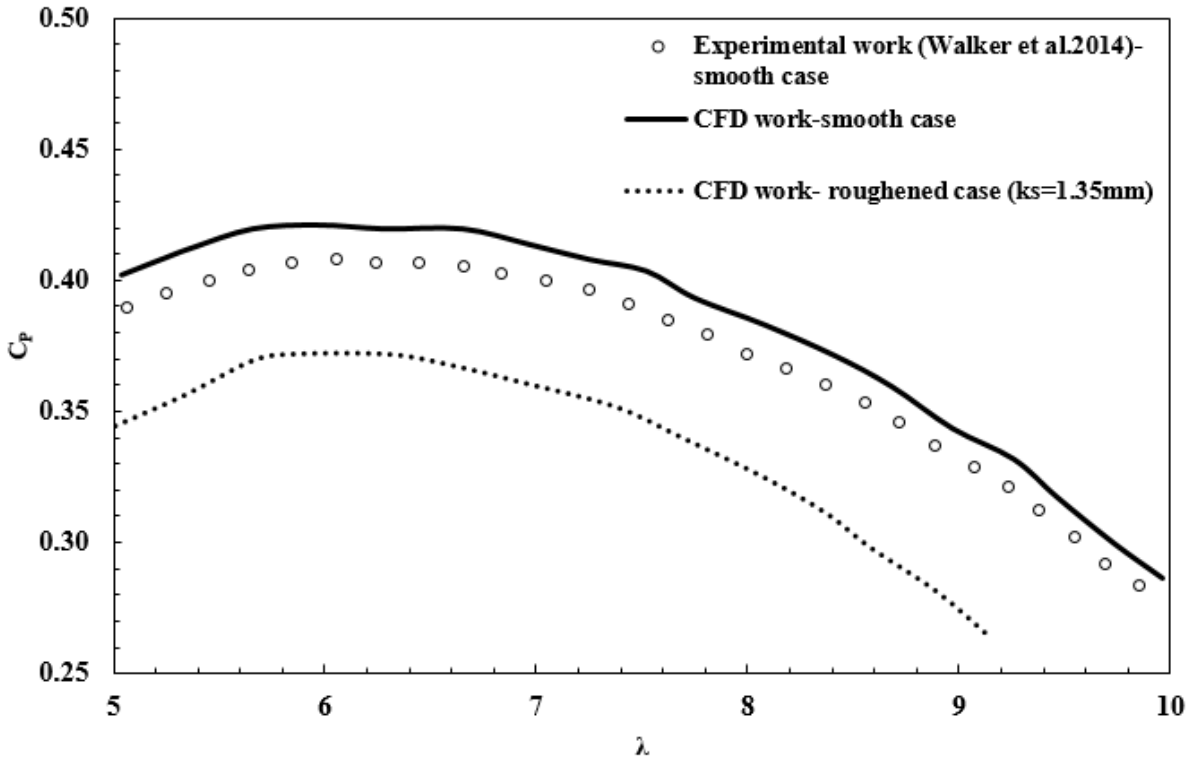

Fig.4. 8. Power coefficient at U=1.68m/s

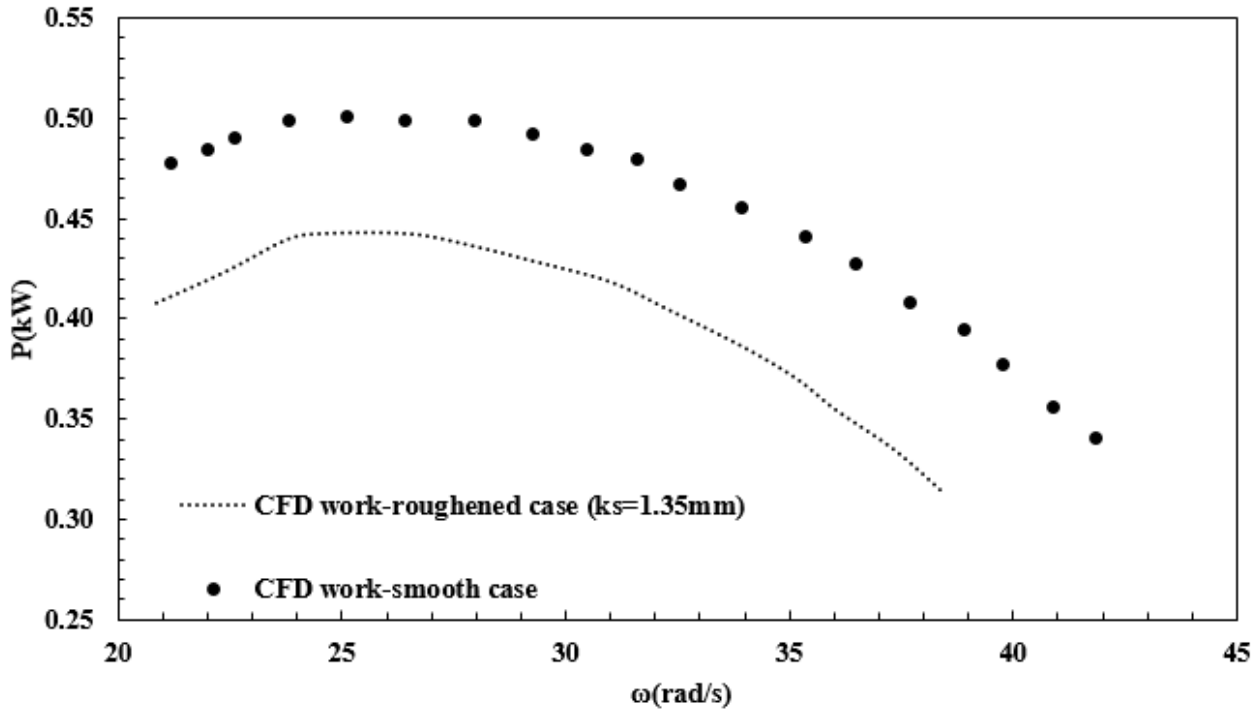

Fig.4. 9. Power curve at U=1.68m/s

The numerical turbine performance curves as a function of tip speed ratio are compared with experimental data which was tested in towing tank [12]. As can be seen in two figures (Figs 4.7 and 4.8), it was obvious that the numerical results show good agreement with the experimental data for smooth case. Based on numerical results, the relative difference for thrust and power curves are estimated 3.1% and 3.4% respectively.

The numerical turbine performance curves including equivalent barnacle roughness, k_s, case is compared to the smooth case and Walker et al. [12] data in Figs. 4.7 and 4.8. Based on barnacle geometry (Fig.4.2) and governing equations (Eq. 3.2,3.3), the minimum equivalent barnacle roughness, $k_{s\text{-}max}$, was chosen for barnacle fouling case.

The thrust coefficient decreased with presence of roughness. According to Fig.4.7, the average thrust coefficient reduced by an average of 16% for the minimum equivalent barnacle roughness. At tip speed ratio of 6, the trust coefficient was reduced from 0.72 to 0.59, a reduction of 18% in numerical curves. In addition, the effect of roughness was to decrease the

power coefficient curve (Fig.4.8). The maximum power coefficient reduced by an average of 12% when roughness is presence. The maximum power coefficient reduced from 0.42 to around 0.37 at λ=6 when sand grain roughness was added on rotor.

The output power curves including equivalent roughness case is compared to the smooth case in Fig. 4.9. The effect of sand grain roughness was to drop the power curve. As can be seen the maximum power was generated at tip speed ratio of 6 for both cases(ω=25rad/s). the maximum power was reduced from 0.5kW to 0.41kW.

2. Surface Pressure Distribution

The simulated pressure on the front and back sides (pressure and suction sides) of the turbine blade for smooth and roughness cases are visualized in Figs. 4.10 and 4.11. These cases are representative of high and low rotor blade loading and are shown here to highlight the effect of roughness on the surface pressure distributions.

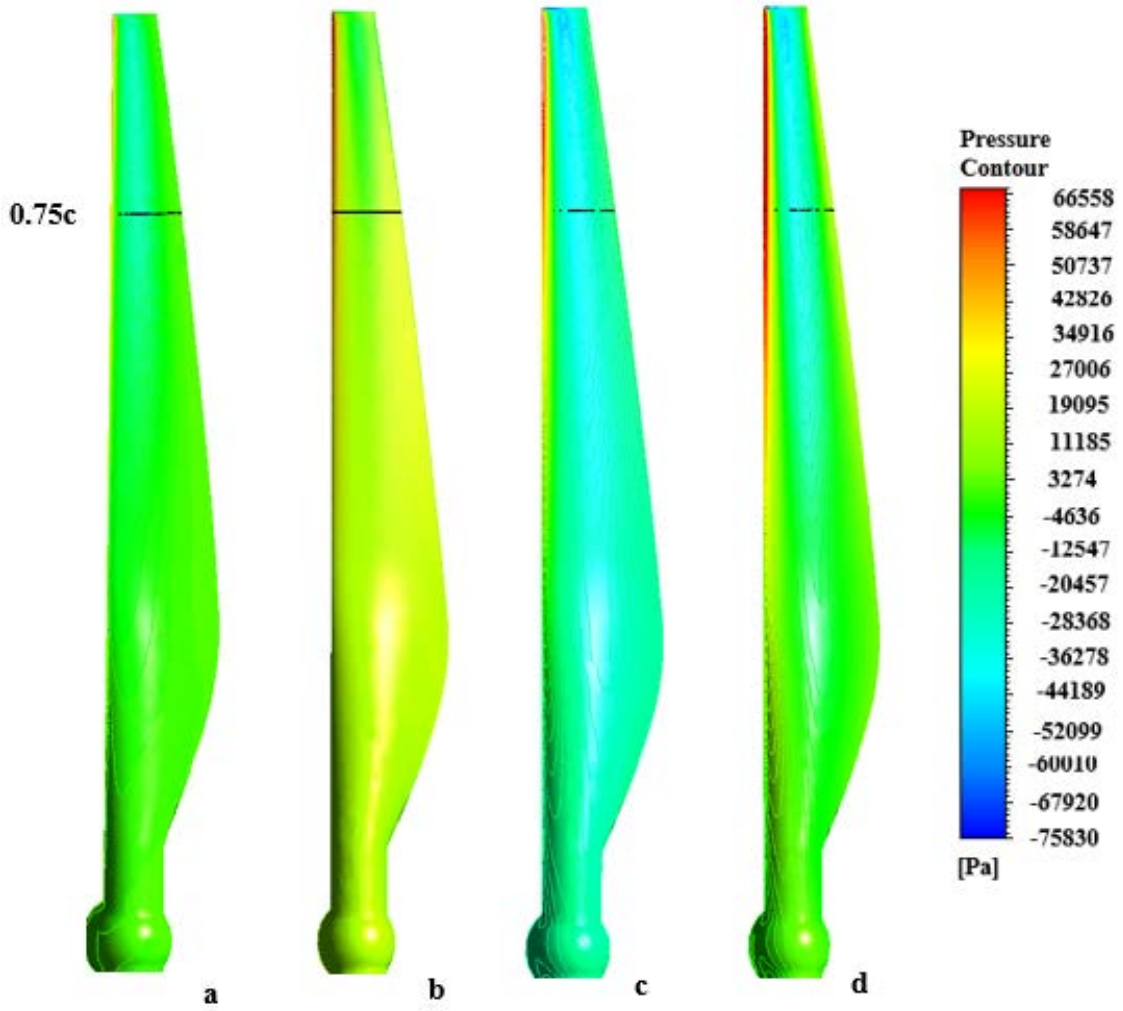

Fig.4. 10. Rotor pressure distribution: a) smooth case, λ=5 b) roughness case (ks=1.35mm), λ=5 c)smooth case, λ=9 d)roughness case (ks=1.35mm), λ=9 (Pressure side).

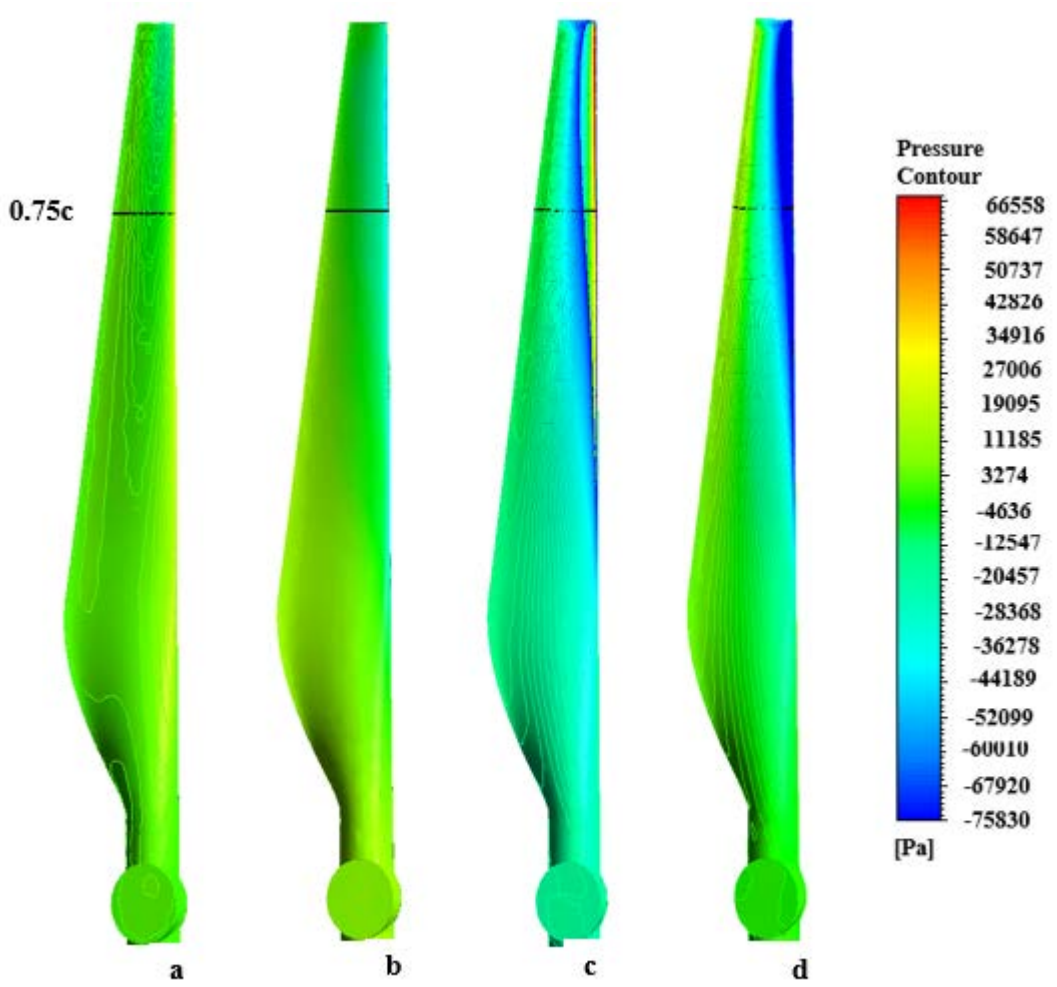

Fig.4. 11. Rotor pressure distribution: a) smooth case, λ=5 b) roughness case (ks=1.35mm), λ=5 c)smooth case, λ=9 d)roughness case (ks=1.35mm), λ=9 (Suction side).

For the acting face of turbine shown in Fig4.10.a and Fig.4.10.c (smooth case only), as the tip speed ratio increases, the pressure in the region near the tip and the leading edge continues to increase. At tip speed ratio 9 (Fig. 4.10.c), low pressure occurs towards the rotor tip. The angle of attack on the rotor blade reduces as tip speed ratio increases and this corresponds to reduce turbine load. For the suction side of the turbine (Fig. 4.11.a, Fig.4.11.c), low pressure continues to increase by increasing tip speed ratio.

Fig.4.10.b and Fig.4.10.d show the simulated pressure in the pressure side of turbine including the sand grain roughness. Comparing the smooth case, the pressure near the tip and leading edge of blade for roughness case increases gradually (Fig.4.10.b). In the suction side, low pressure increases around the leading edge when sand grain roughness was added on the blade surface (Fig4.11.b and Fig.4.11.d). As tip speed ratio increases, low pressure continuous to increase (Fig. 4.11.d).

Based on turbine blade geometry [12], the region between 25% to mid span of blade is the thickness foil. Therefore, the tip speed region can be the critical area for hydrodynamic performance. 75% of blade span which indicates the low pitch angle, for both pressure and suction sides was highlighted by black line in Figs. 4.10 and 4.11. As can be seen, the low pressure increases considerably for the suction side when sand grain roughness was added on the blade. Comparing the pressure side with the suction side, the maximum pressure difference occurs in this region for roughness case.

Pressure difference between pressure side and suction side can be higher by increasing of sand grain roughness height. In fact, the maximum pressure difference between both sides can be related to barnacle colonization in the tip blade. Barnacle colonization of the area can have an adverse effect on turbine rotor such as corrosion. The corrosion rate can be accelerated in the thin area (tip area) of a turbine blade when roughness material is presented.

3. Effect of fouling on marine turbine performance

In this study, two-bladed tidal turbine for smooth and fouled cases was modelled in the commercial ANSYS CFX. 15 software. In computational model, strong cement roughness of barnacle was presented by equivalent barnacle roughness parameter, k_s,. Based on governing equations (Eq.4.1 and 3.3), equivalent barnacle roughness is functionally related to barnacle

geometry size, A_f and A_s, and also associated with ratio of roughness density, S/S_f. According to life cycle of barnacle, the adult barnacles produce a stronger cement for themselves and a stronger cement causes an increase in barnacle dimension [37, 105-106]. Procedure of life cycle of barnacle can be related to equivalent barnacle roughness parameter. Therefore, real barnacle roughness development may be represented by the equivalent barnacle roughness, k_s,. In addition, a stronger cement shell leads to permanent settlement on marine surfaces

In the case of marine renewable energy equipment, barnacle roughness has an adverse effect on long-term performance. A kind of strong cement which was produced by larva in backside of barnacles, causes the high frictional resistance and leads to an increase of weight and subsequent potential speed reduction and loss of annual performance. Results of experimental research by Katsuyama et al. [26] in Japan revealed barnacle roughness development make a mass imbalance profile on rotor profile of tidal turbine and tidal turbine is stopped if barnacle colonization continues.

For that purpose, short-term cleaning and maintenance of tidal turbine system may be required to ensure long-term performance. In order to barnacle removal technique, some marine current turbines, such as SeaGen, can be cleaned and maintained above sea level [84]. Designing and manufacturing tidal turbine rotor with the materials with limited surface fouling like Carbone Fibre Composite material can minimise corrosion rate through the thin layer of a turbine surface [81-82].

6. Conclusion

The effect of *Amphibalanus Amphitrite* barnacle roughness on a two-bladed horizontal tidal power turbine was studied using ANSYS CFX, a commercial CFD code. A numerical approach for three dimensional regular roughness shape is described to calculate the equivalent

barnacle roughness, k_s, rough surfaces with cone shaped size. Based on surface roughness density and single barnacle geometry, the equivalent barnacle roughness is determined. The results indicated that an increase in barnacle geometry and roughness density ratio, S/S_f, causes an increase in equivalent barnacle roughness , k_s,.

The thrust and power coefficient curves show that the numerical results of smooth case agree well with experimental data for Walker et al. [12]. Presence of fouling causes a reduction in thrust and power coefficients. Effect of roughness was to decrease the thrust curve by an average of 16% for roughness case. Additionally, the maximum power coefficient reduced from 0.42 to around 0.37 at λ=6 when sand grain roughness was added on rotor surface.

Numerical results from fouling case revealed that the presence of equivalent barnacle density, k_s, causes a reduction in power and thrust coefficient of tidal turbine. Based on the governing equations for evaluating sand grain roughness (Eqs 3.2 and 3.3), sand grain roughness is functional of fouling density and single roughness dimension. In fact, low fouling density or presence of barnacle causes a reduction in power performance of tidal turbine.

Chapter 5

Drag Measurements on a Flat Plate with Artificial Barnacle Fouling

In order to advance understanding of the effect of fouling density characteristics on drag force, a recirculating water tunnel with artificial barnacles (scale model) was used to investigate the flow over smooth and fouled test plates. There are three different fouling test plates: low, medium and high barnacle density. In order to generate the fouling density on a flat plate, artificial models were affixed and replicated with different fouling density on the flat plate. The height of single roughness element is constant for all fouling status. Fouling density is defined as a ratio of the total barnacle surface area to the surface area of a flat plate. Artificial barnacle samples were used to generate the fouled plates.

The drag coefficient results were obtained by load cell drag equipment. The drag coefficient results of smooth case are compared with experimental data which was tested in the same water tunnel by Andrewartha [110]. The drag coefficient results, including artificial barnacles cases are compared with drag coefficient result of smooth case. In order to estimate the drag coefficient for fouling case, the equivalent sand grain roughness should be determined (based on Eq.5.10). As single roughness element roughness method was chosen to generate fouling for flat plate, the equivalent sand grain roughness is functional of physical dimension of single roughness element and fouling density. Therefore, it is necessary that the sand grain

roughness of experimental results compare versus the sand grain roughness of geometrical formulation.

It is worth to mention that the equivalent sand grain roughness for 2D aerofoil surface and 3D tidal turbine blade (CFD chapters) were determined by geometrical formulation. Therefore, this comparison can show the connection between geometrical technique used for computational method and classical equations used in experimental test. In addition, this comparison can help to reveal the importance of some roughness characteristics of roughness communities such height and density.

1. Introduction

In the previous chapters, the effect of biofouling roughness (barnacle roughness) on marine renewable energy surfaces was reviewed and analysed numerically. However, detailed analysis of turbulence structure around groups of barnacles and also the relationship between the fouling density community and drag coefficient is lacking.

Much research has been used the sand grain material to show the effect of biofilm on drag in the marine environment [12, 17, 21, 27, 31, 107, 105-109], Schultz and Swain [105] Schultz [106] made turbulent boundary layer measurements on the surfaces in a recirculating water tunnel. A smooth surface, two sandpaper surfaces with different grits and two surfaces covered with filamentous green algae grown over a 30 day period were tested. A significant increase in the skin friction coefficient was measured for both of the fouled plates (125% and 110% increase on smooth plate values). Andrewartha [110] conducted detailed boundary layer measurements on freshwater biofilms in a recirculating water tunnel. A painted sand grain roughened test plate was developed to investigate biofilm growth over rough (coarse) surfaces. Significant increases in local skin friction coefficient were measured (210% for a rough plate) when compared with a smooth case.

However, there have been few studies to create an artificial biofouling on plates due to ecological challenges. High resolution Particle-Image Velocimetry was used to measure the flow over barnacles immersed in a turbulent boundary layer by Barros et al [111]. Two configurations were investigated: single barnacle configuration and a regular array of barnacles. Quadrant analysis revealed important structural behaviour, especially when only considering the strongest Reynolds shear stress events. It is likely that these events are linked to contribute to both larval settlement and waste removal.

Therefore, the last method (creating the artificial biofouling material on a test plate) can have some benefits. Understanding the flow around these fouling communities will provide insight regarding the roughness scales that contribute significantly to the drag, with the aim of developing predictive models of drag increase due to specific fouling communities. This study aims to quantify the drag coefficient of rectangular plates fouled with artificial *Amphibalanus Amphitrite* barnacles using a force balance load cell in a recirculating water tunnel. Based on barnacle density characteristics which are defined as the ratio of the total barnacle surface area to the test plate area, three different densities will be investigated: low, medium and high densities and their results will be compared with the smooth plate data.

Based on drag measurement results and single roughness dimension parameters, the sand grain roughness value for each plate will be estimated. It is worth mentioning that the drag coefficient results for the rough test plates is functional of the virtual origin of boundary layer. Because of conditions of test in this study are same, as test conditions of Andrewartha [110], thus the correction for the virtual origin of the boundary layer by Andrewartha [110] will be used. In addition, an equivalent sand grain value for cone shaped roughness element was estimated using an empirical correlation for three dimensional roughness element. Based on these parameters, equivalent sand grain roughness will be predicted for turbine blade and power generation for different fouling density will be calculated numerically.

2. Barnacle roughness density

Many studies have revealed that barnacle attachment on marine surface reduces hydrodynamic performance [27-28, 30-31, 105]. Different types of barnacle characteristics, including adhesion, height, thickness and density have a significant effect on the hydrodynamic parameters of surfaces colonised by barnacles.

Barnacle colonization on a marine surface leads to permanent settlement. Permanent settlement helps to produce a stronger cement for adult barnacles. In addition, permanent settlement has a significant effect on the increase of the development of cypris larvae. An increase in the number of barnacles and the rate of barnacle growth causes an increase in barnacle fouling density. Thus, barnacle density is one of the most important fouling characteristics and has a significant effect on marine surface roughness.

Increasing barnacle density leads to an increase in drag coefficient force and a reduction in aerofoil performance. Orme et al. [27], Khor and Xiao [31] investigated the effect of barnacles' roughness density on a NACA 4424 aerofoil. Orme et al [27] tested a two-dimensional aerofoil in a wind tunnel using three supporting struts connected to a force balance. An extrusion method was used to develop the barnacle roughness, with low, medium and high artificial barnacle densities. As the height of barnacles for the three different cases was constant, barnacles with the highest density produced the highest drag coefficient.

In this study, the shape and size of each barnacle is constant. However, fouling density (centre to centre length between two neighbouring artificial barnacles) is varied. Fig. 5.1 shows the shape size and spacing for the two barnacles considered in this part of the study. A published correlation is used to estimate an equivalent sand grain roughness k_s from the barnacle fouling arrangement shown in Fig.5.1.

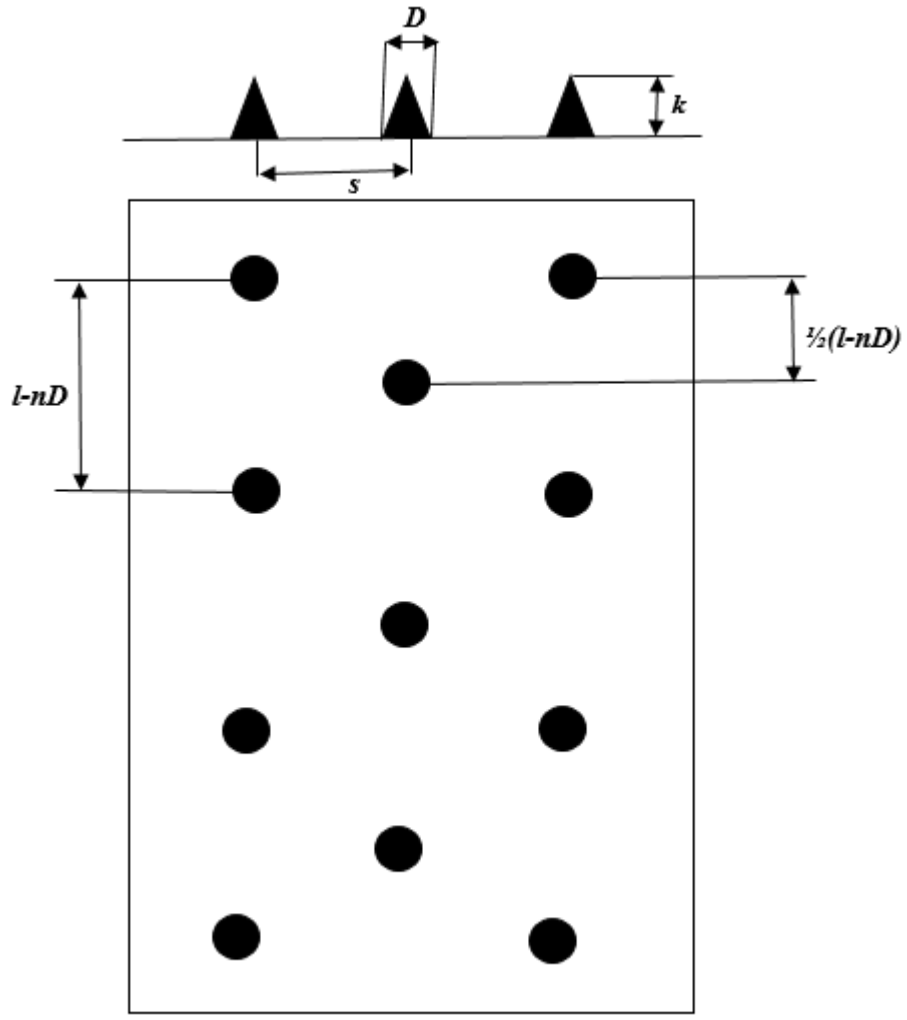

Fig.5. 1. cone shaped roughness element and spacing for the two roughness cone shapes

As shown in Fig.5.1, the *s* parameter changes with fouling density (it will increase when low density is changed to medium or medium to high density). The parameter *n* is the number of the roughness element along the side of the test plate. In order to generate a different fouling density status(low, medium and high) on a test plate, a dimensionless quantity is used;

$$\lambda = \frac{\sum \frac{\pi D^2}{4}}{lb} \tag{5.1}$$

where *D*, *l* and *b* are the barnacle diameter, length and width plate respectively. Therefore, the dimensionless factor λ has the highest value for the high density case.

3. Procedures to produce artificial barnacle

1. Barnacle scale

In the previous chapters, it was discussed that in order to determine the impact of a very slight coating roughness material on the frictional drag of a plate, some non-dimensional analysis which is related to drag coefficient, may be appropriated. However, for some roughness methods in which a single roughness element is applied, the ratio of the height of the roughness element to the boundary layer thickness can play an important role [116].

An important consideration in this study is the height of the barnacle elements relative to the boundary layer thickness. The boundary layer grows on the blade surfaces of turbine rotor blades, starting at the leading edge and reaching the thickest at the trailing edge. The skin friction coefficient increases with disturbances to the boundary layer due to roughness and the transition location moves toward the leading edge. An increase in skin friction causes an increase in the drag coefficient and thereby affects the performance of the aerofoil. Therefore, in this experiment, it is necessary to find the appropriate value of artificial barnacle height for the test plate because the interaction of artificial barnacles on the test plate should produce similar effect to roughness on the aerofoil surface.

In order to determine the required height of an artificial barnacle for the test plate, the concept of dimensional similarity was applied (dimensionless parameter) between the turbine blade and the test plate. A dimensionless parameter can be defined as the below:

$$(h_{barnacle}/\delta)_{test\ plate} = (h_{barnacle}/\delta)_{turbine\ surface}$$

In order to determine the unknown value (height of an artificial barnacle for a test plate), the barnacle height should be estimated. In Chapters 3 and 4, the barnacle height was used to calculate equivalent barnacle roughness for the fouling surface of a blade. Based on the adult *Amphibalanus Amphitrite* barnacle size, the height of a fully grown barnacle is 25mm [39] and equivalent sand grain roughness is estimated to be k_s = 0.4mm. The second step is to evaluate the boundary layer thickness of the turbine blades and the water tunnel plates. The boundary layer thickness of a full size turbine was simulated and estimated to be around 16mm around the trailing edge of rotor blade. According to previous research that was carried out by Andrewartha [110] on the same water tunnel system, boundary layer thickness was estimated 35 mm for a test plate. Therefore, the dimensionless similarity can be used to determine the unknown value (the height of an artificial barnacle for a test plate), the height of an artificial barnacle should be around 53mm.

2. Single barnacle setup

The barnacle model was obtained by 3-D scans of a real organism (Adult *Amphibalanus Amphitrite* barnacle) which was collected by the Institute of Marine and Antarctica Study (IMAS) researchers in the Tasman sea. The barnacle was scanned using a David 3D scanner Pro (version 4.5.2) at the Central Science of Laboratory (CSL). The 3D scan procedure of a sample of a real sample adult *Amphibalanus Amphitrite* barnacle is shown in Fig.5.2.

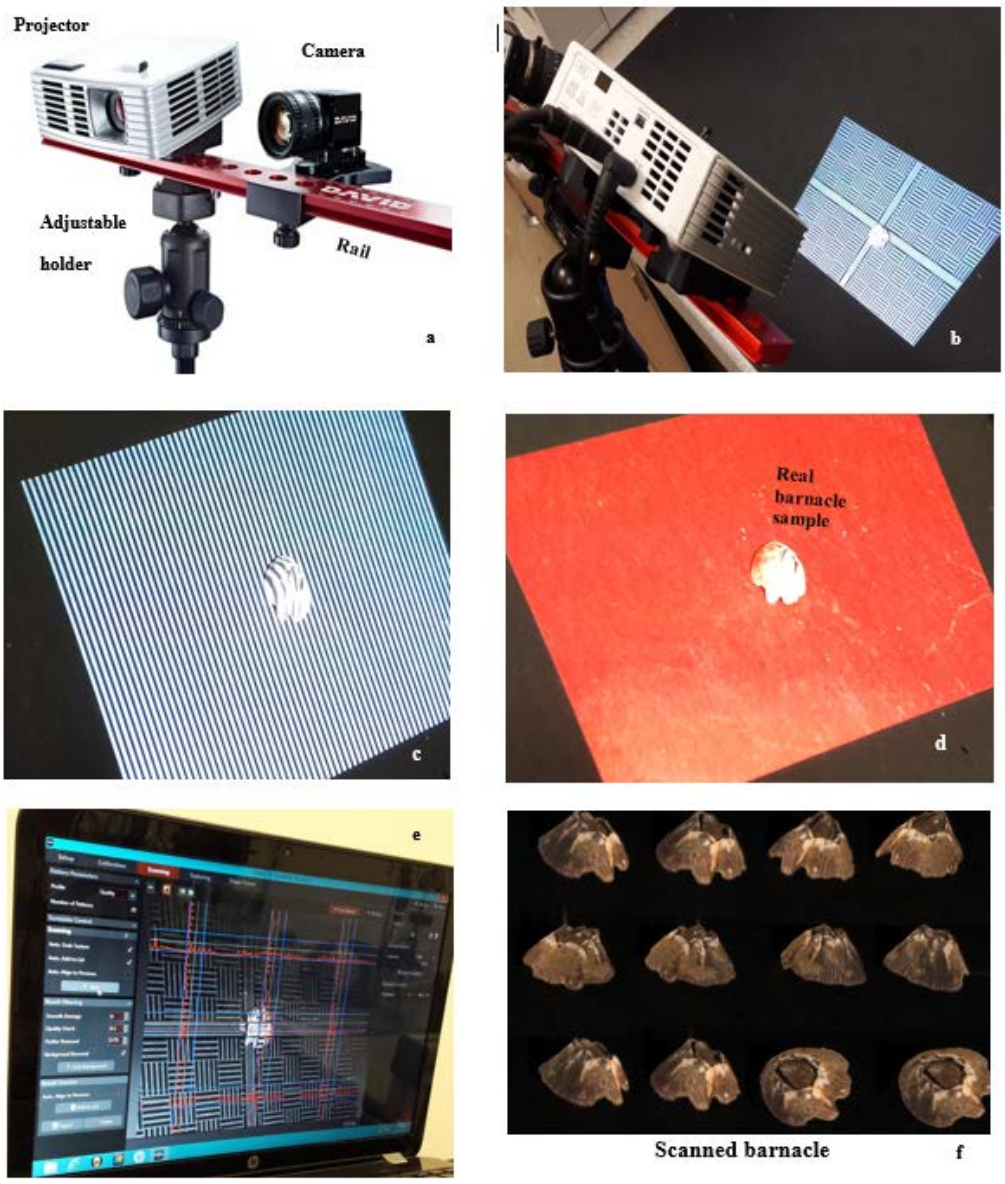

Fig.5. 2. 3D scan procedure of real sample adult barnacle

The barnacle sample was 3D printed by a UP- MINI printer. It is worth mentioning that the barnacle model was scaled up to show the boundary layer thickness on the samples. The material used for 3D sample was ABS-plastic which combines the strength and rigidity of acrylonitrile and styrene polymers with the toughness of polybutadiene rubber. Fig. 5.3 shows the ABS plastic material and the barnacle sample through the 3D printer.

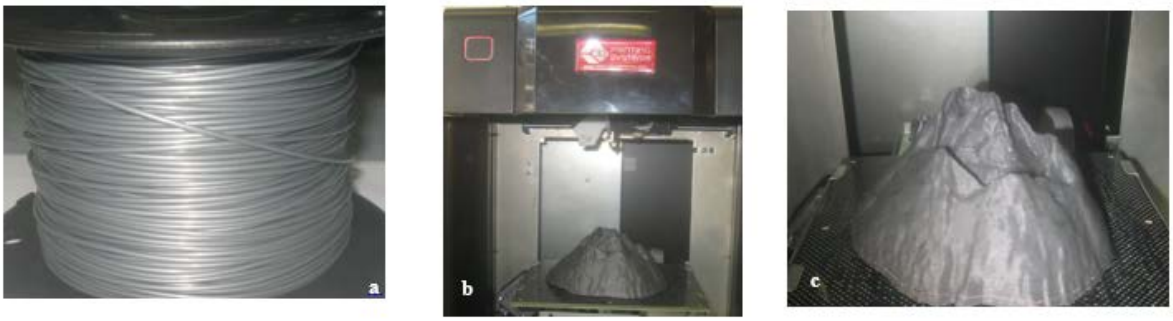

Fig.5. 3. a) the ABS plastic material b, c) the barnacle sample through the 3D printer

As three different fouling cases (low, medium and high fouling densities) are considered in this study, around 100 artificial barnacle samples for three plates are needed. In order to replicate more samples, a mould and cast technique is used.

In order to produce the barnacle's mould, silicone material was considered. PINKSIL silicone material was chosen for making the mould as it has low viscosity and more tear strength. The physical properties of PINKSIL are provided in Table.5.1[112].

Table 5. 1. The physical properties of PINKSIL [112].

Physical properties of PINKSIL silicone	
Colour	Pink
Specific gravity	1.10
Hardness	20, after 60minutes
Tensile strength (N/mm^2)	3.50
Elongation at Break (%)	400
Tear Strength (N/mm)	4.5

In the moulding process, a metal cylinder was used to surround the barnacle. The edge of the cylinder was sealed with clay material and then the barnacle sample was placed in the middle of the cylinder.

A polyester resin with a catalyst was chosen to produce an artificial barnacle. In order to generate a sample, 200mm litter resin is mixed with 2mm litter of catalyst liquid and then the mixing liquid was pour into the silicone mould. Fig.5.4 shows a sample of an artificial resin barnacle.

Fig.5. 4. a sample resin artificial barnacle

3. Barnacle array setup

The same barnacle model was used to create the array. The barnacles were arranged in a staggered fashion for all fouling density cases. The fouling density can be determined by Equation.5.1. Table 5.2 shows more details for the fouling density of the test plate.

Table 5. 2. fouling density details

	Low density	Medium density	High density
Test plate area=l*b, *l=997mm & b=597mm & t=3mm,*			
D(mm)	103	103	103
h(mm)	53	53	53
N(-)	8	14	22
λ(-)	0.148	0.259	0.407

As can be seen in Table.5.2, in all cases the size of the artificial barnacles is constant. However, the total number of samples *(N)* on a test plate is increased by changing density from low to high. The barnacles were spaced apart one another by one barnacle dimension in the x-y direction. The space between the centre to the centre of two neighbouring barnacles was a two adult barnacle diameter, one adult diameter and half diameter for low, medium and high fouling densities respectively.

In order to affix the samples on a test plate, resin and catalyst liquid were used. There was a thin layer surface of Jotamastic epoxy coating on a test plate and it was impossible to glue the barnacle on to this coating. Thus, the location of each sample on a test plate was marked and then the specific place was scratched and then glued. The load drag cell should be calibrated for each test plate (smooth and fouled plates). The load cell was calibrated insitu using a thin steel cable and a system of low friction pulleys. As the thin steel cable is located in the centreline of the test plate, there were not any barnacle samples were attached to the

centreline area of the test plate (There was no connection between thin steel cable and barnacle samples). Fig.5.5 shows the barnacle array arrangement for low, medium and high fouling densities on a test plate.

Fig.5. 5. Barnacle array arrangement for low, medium and high fouling density on a test plate

4. Experimental facilities

1. Water tunnel components

The water tunnel is driven by a Regent horizontal split-case pump (model 350-S16) with a 7kW AC 3-phase induction motor, designed for low head and high flow. The freestream velocity in the working section ranges from 0.3m/s to 2.0m/s.

De-swirl vanes are fitted immediately downstream of the pump and at the start of the return pipe to reduce swirl and secondary flows introduced by the pump. There are two diffusers to increase the flow area to the cross-section required for the two-dimensional contraction and to reduce losses in the flow conditioner. The first stage diffuser also transforms the flow from a circular to a rectangular cross-section. Cascading bends are used to turn the flow and are fitted with vanes to ensure an even flow distribution.

The flow conditioner is installed upstream of the contraction at the maximum cross-section to reduce energy losses. It consists of two sections of honeycomb and steel mesh, separated by 300mm. The honeycomb consists of closely packed 60mm long circular tubes of 6mm diameter and is used to straighten the flow and reduce turbulence in the working section.

A stainless steel mesh with a 3.15mm square aperture is used both to hold the honeycomb in place and to reduce the turbulence. The two-dimensional contraction has a contraction ratio of 3:1 and is 2m in length. It accelerates the flow to the working section, reduces turbulence, and creates uniform flow. Fig. 5.6 details the water tunnel components.

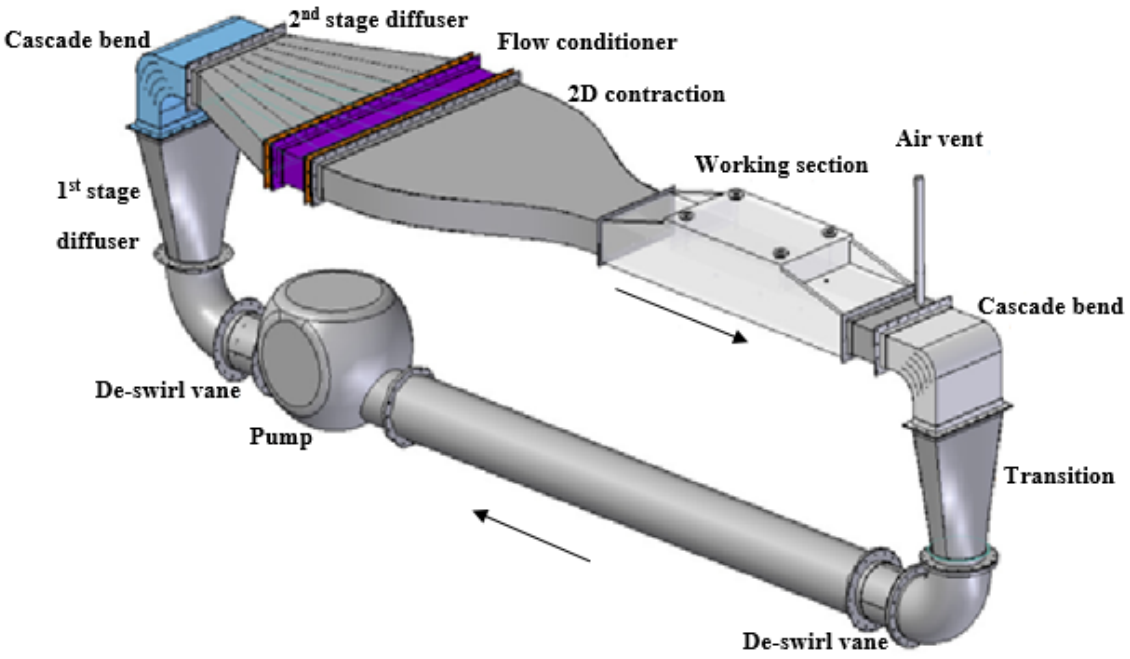

Fig.5. 6. water tunnel components [113].

The working section is constructed of 30mm thick Perspex sheet. Fig. 5.7 details the dimensions and plug locations of the working section [113].Test plates (smooth and fouled cases) measuring 997mm length and their widths being 597mm and are attached to a Perspex

backing plate which in turn is suspended by four flexures attached to the working section lid. The Perspex top panel is securely clamped to the lid of the working section and sealed using a rubber seal.

In order to control the Reynolds number and environment control, a cooling system for the water tunnel was installed for water tunnel. The temperature of the water in the water tunnel could not be maintained at a constant temperature due to the heat input from the 7kW pump and the ambient air temperature.

This inability to maintain a constant temperature means that fluid properties such as density and viscosity are variable. It is imperative that a constant Reynolds number is maintained during a boundary layer traverse to ensure that the mechanisms for interaction between the surface being tested and the near-wall boundary layer are maintained. It is also vital that measurements are able to be completed at the same Reynolds number for different test plates to allow results to be compared.

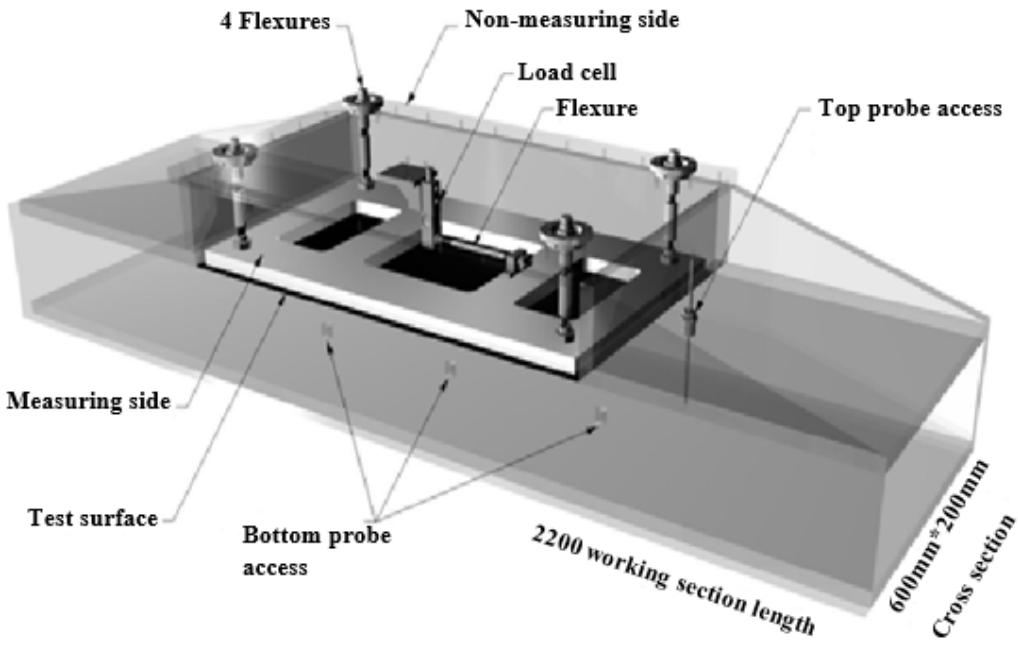

Fig.5. 7. Working section details [113].

All data were recorded by LabView programs. The water tunnel was set up to take two different categories of measurements: boundary layer pressure profiles and total drag measurements.

1. Temperature

Water temperature measurements were taken concurrently with all other measurements. This enabled water density and viscosity to be determined and hence the relevant Reynolds numbers may be accurately obtained and monitored for each set of measurements. A platinum resistance temperature probe with 4-20 mA output is upstream of the working section in the flow conditioner. The output temperatures were calibrated with a thermometer placed in the working section under both zero flow and flow conditions.

Water density and dynamic viscosity are determined from the measured absolute temperature, using the following correlations, which are polynomial fits to tabulated data for water at atmospheric pressure [114]:

$$\rho = 5.673*10^{-5}T^3 - 8.850*10^{-3}T^2 + 0.07771T + 999.8 \quad (5.2)$$

$$\mu = 6.87*10^{-7}T^2 - 5.264*10^{-5}T + 0.001773 \quad (5.3)$$

2. Pressure

Pressure measurements were obtained using three Validyne variable reluctance pressure transducers, which measure the pressure differential. A key feature of the Validyne transducers is the exchangeable diaphragm which allows the pressure range to be selected to match the experimental conditions.

The pressure transducers were connected to the Valydyne Carrier Demodulator. Two of the demodulators provide a voltage output directly to the data acquisition system. The other demodulator provides a current output which is transformed to a voltage using a purpose built current-to-voltage converter. The voltage is then shifted by a precision volt level shifter to the range required by the data acquisition system.

The pressure differential across the contraction was measured concurrently with the majority of measurements using a dedicated pressure transducer and was used to remove any temporal variations during long measurement periods.

Time averaged mean velocity was measured using a Pitot probe and static pressure tapping located in the floor of the working section. The static wall pressure tapping was located in the same plane as the Pitot probe, but was offset 50mm longitudinally from the Pitot probe centreline in the spanwise direction to enable the calculation of the local velocity without flow disturbance from the Pitot probe.

The velocity, u, can be determined from the stagnation pressure measured by the Pitot probe, P_{pitot}, and the static pressure, P_{static},

$$u = \sqrt{\frac{2(P_{pitot} - P_{static})}{\rho}} \quad (5\text{-}4)$$

3. Total drag

A floating element force balance was used to determine the total drag acting on each test plate. The test plates form the roof of the working section and are attached to a Perspex backing plate which in turn is suspended by four stainless steel flexures attached to the working section lid. The beam load cell was attached to the lid of the working section and linked by a load transfer rod to the Perspex backing of the test plate. The flexures ensure a one-dimensional transfer of force through the load transfer rod to the load cell. The load cell is connected to a stain gauge transmitter, which in turn is connected to the data acquisition system.

2. System Calibration

The pressure transducers were calibrated using water filled syringes mounted to the Mitutoyo Dial Height Gauge before running the system. The differential water level was adjusted manually by that gauge and the corresponding voltage level recorded in both the positive and negative ranges. As each transducer contains exchangeable diaphragms (pressure sensing elements), the calibration curve for each transducer is different. A typical calibration chart is given in Fig.5.8 for three pressure transducers.

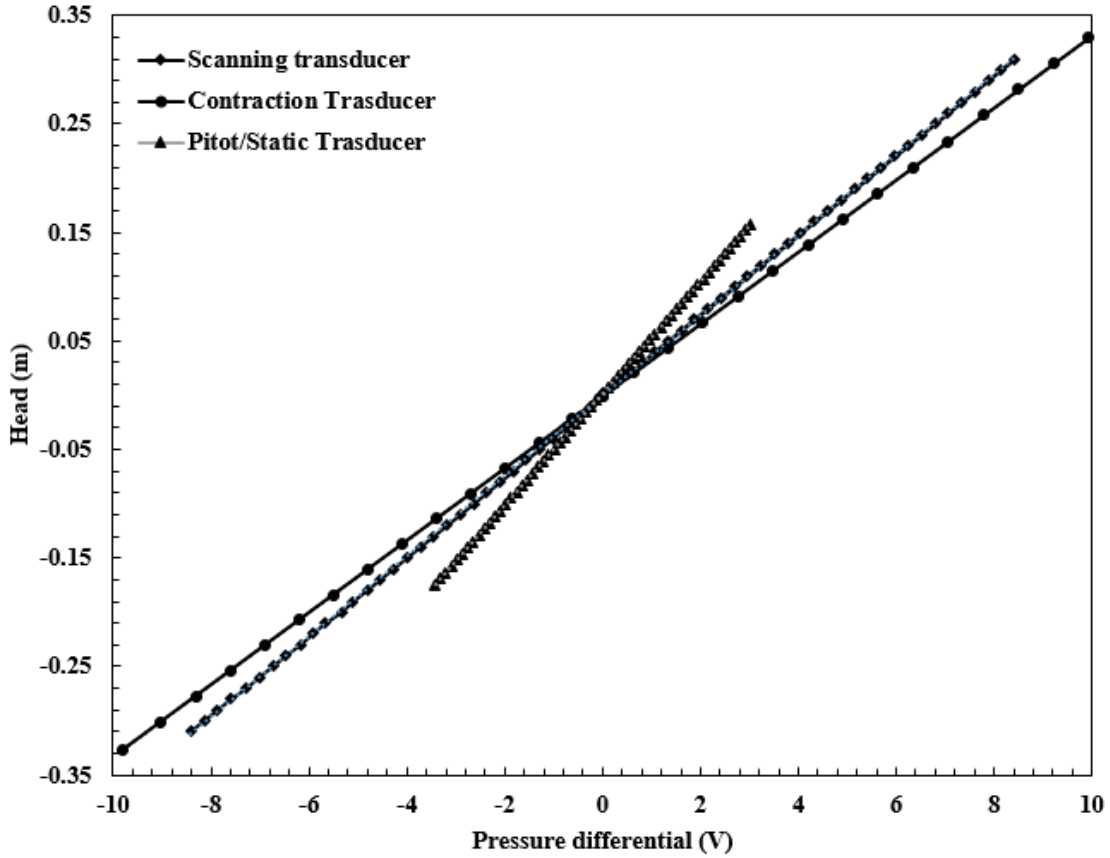

Fig.5. 8. A typical calibration of pressure transducers

The output of the load cell is a voltage, which is calibrated by applying a known force to the load cell. The load cell was calibrated insitu using a thin steel cable and a system of low friction pulleys. It is worth mentioning that this setup was the same for fouling cases and barnacle samples were not attached in the steel cable area of the test plate (Fig.5.9). Weights were added in 50gr increments, with a zero load reading taken between each loaded reading, and the voltage output recorded. A calibration was completed each time a test plate was changed over. An example of load cell calibration is given in Fig.5.10 for a load cell.

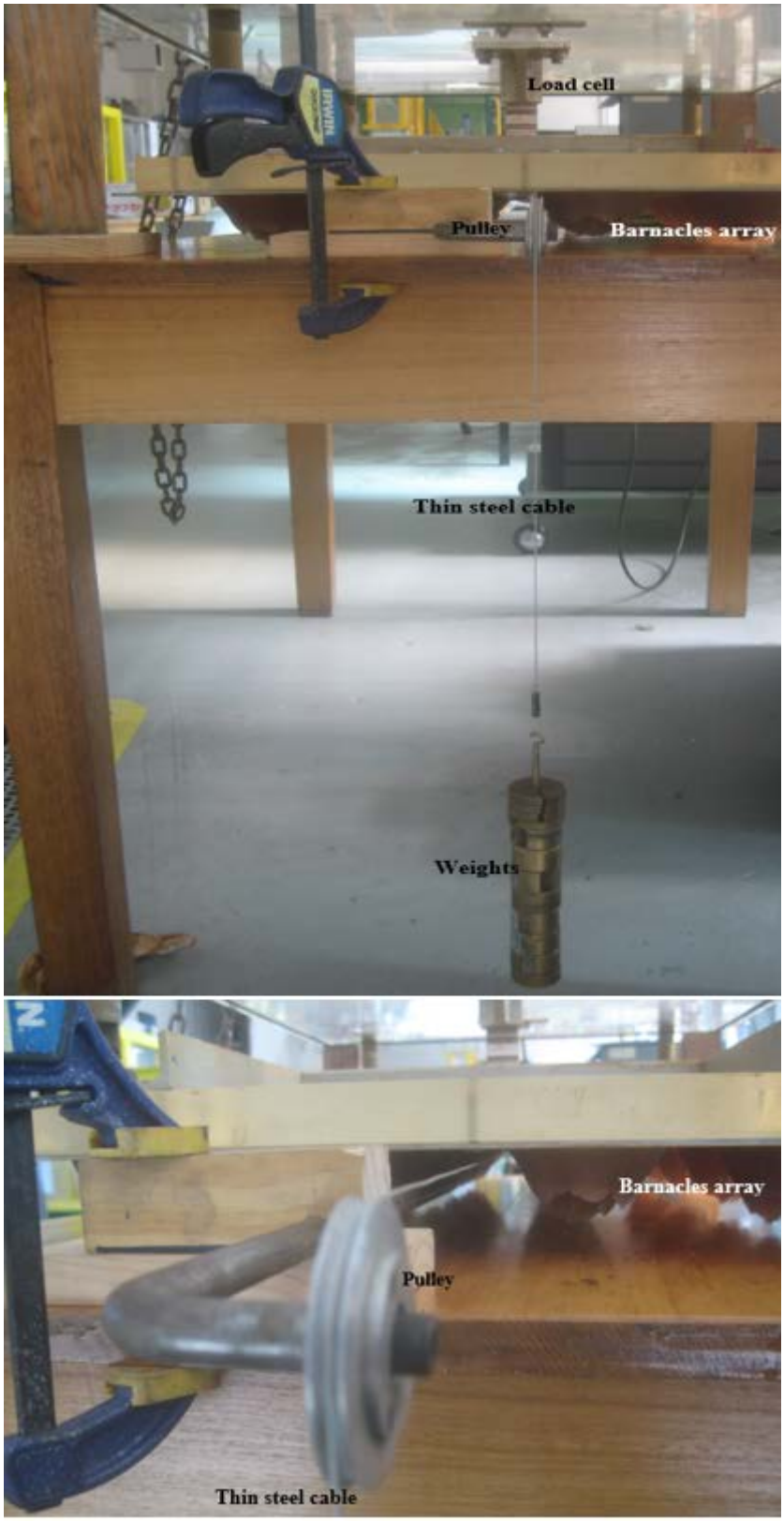

Fig.5. 9. load drag cell calibration

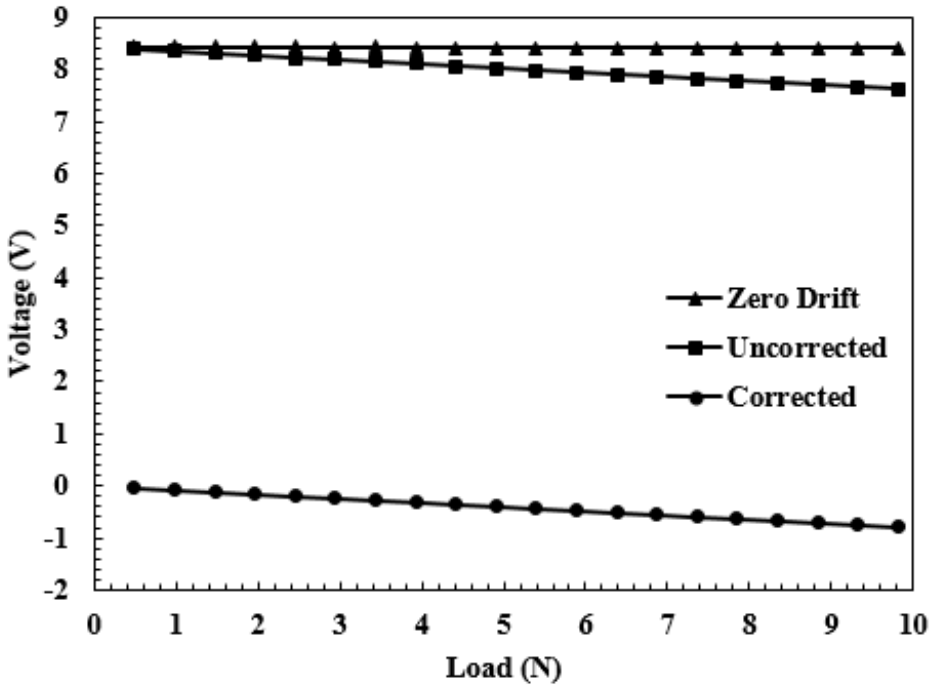

Fig.5. 10. A typical calibration of load drag cell

5. Total drag analysis

The drag coefficient results were obtained by using the floating element force balance. The drag coefficient for a smooth plate of width *b* and length *l* is defined by [116].

$$C_D = \frac{D}{0.5\rho U^2 bl} \tag{5.5}$$

The relationship between the drag coefficient and the Reynolds number for a turbulent boundary layer on a flat plate is given by the following equation [116];

$$C_D = 0.074\,\mathrm{Re}_l^{-0.2} \qquad \text{For } 5*10^5 < Re_l < 10^7 \tag{5.6}$$

Where $Re=\rho ul/\upsilon$ and u is the streamwise velocity. The streamwise velocity can be determined by equation.5.4. The dynamic and kinematic viscosity can be obtained by equations. 5.2 and 5.3.

Equation.5.6 is based on the assumption that the origin of the turbulent boundary layer is at the leading edge of the plate. However, the problem of this study is that a fully turbulent boundary layer was already established on the tunnel wall upstream of the test plate on which drag measurements were obtained. In order to solve this issue, a turbulent boundary layer in a zero pressure gradient can be postulated. It grows from a virtual origin at distance l_1 upstream from the leading edge of the test plate. Fig. 5.11 shows the boundary layer development over a test plate [113].

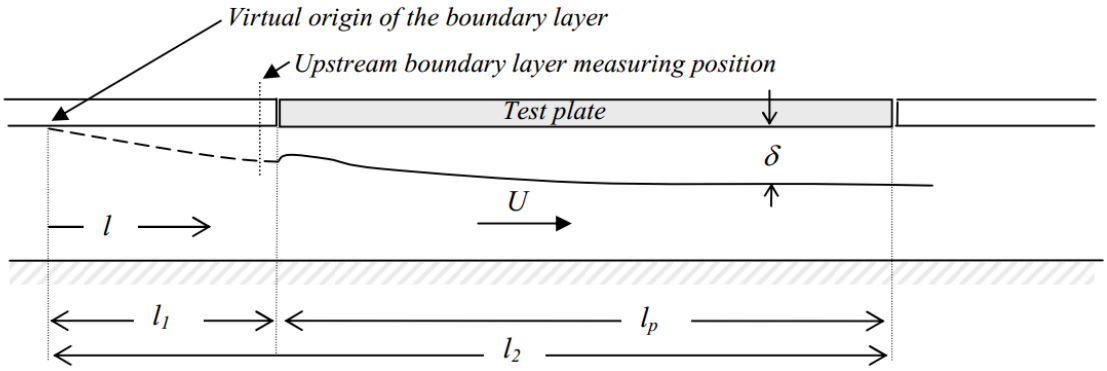

Fig.5. 11. boundary layer development over a test plate [113].

The relationship between boundary layer thickness and distance from the origin of the boundary layer is given by Schlichting [116]:

$$\delta = 0.37 Re_l^{-0.2} \tag{5.7}$$

The virtual origin of the boundary layer can be determined by varying l in Eq. 5.7 until the boundary layer thickness matches a measured boundary layer thickness at a known location. To estimate the virtual origin of the boundary layer, mean velocity profiles will be required. In the present study the virtual origin equation (Eq.5.8) which was obtained by Laser Doppler Velocimetry (LDV) by Andrewartha [110], is used to calculate the drag coefficient. The procedure of virtual origin estimation has been detailed by Andrewartha [110].

$$l_1 = 0.1842U + 0.9239 \quad (5.8)$$

For the smooth plate case only, the theoretical drag on the test plate alone could be obtained using Equation. 5.9:

$$D_{theor} = \rho b \frac{U^2}{2}(C_{D2} l_2 - C_{D1} l_1) \quad (5.9)$$

Where the drag coefficient for the region upstream of the test plate to the virtual origin (l_1) and the region including the test plate and virtual origin (l_2) are determined using the respective lengths and Equation.5.9.

However, this situation is more complex for fouling test plates. The relationship between an equivalent sand grain roughness and a rough wall skin friction coefficient for the hydraulically rough flow regime is given by Equation. 5.10 [116]:

$$C_D = (1.89 + 1.62 \log l/k_s)^{-2.5} \quad \text{for } 10^2 < l/k_s < 10^6 \quad (5.10)$$

It is worth mentioning that for very small roughness as well as plates with single protuberances, such as rivet heads, welded seams, joints, this equation can play an important role to determine the drag coefficient.

6. Results and Discussion

1. Drag measurement results for smooth case (Test validation)

The value of drag coefficients of the flat plate for a smooth painted case (Jotamastic epoxy coating on a test plate) is shown and compared with the smooth case of experimental

results from Andrewartha [114] in Fig. 5.12. It should be noted that drag measurement were conducted at 50 rpm increments in the pump speed from 150-650 rpm at 1kHz.

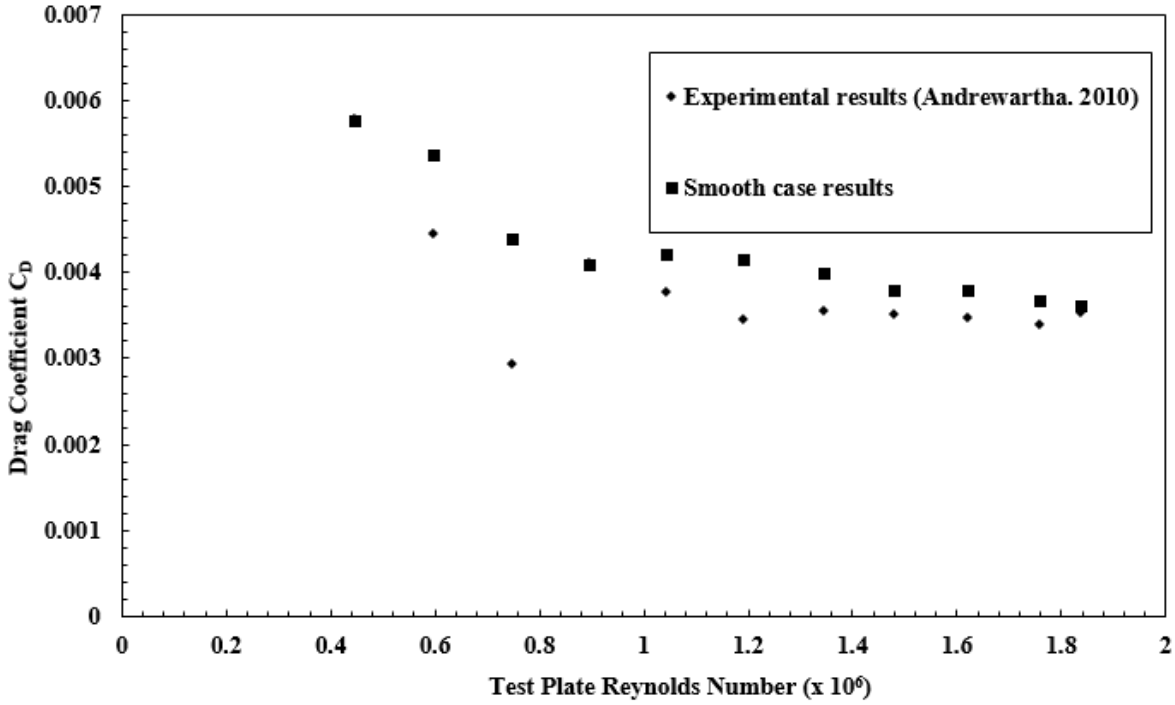

Fig.5. 12. drag force results for smooth case

Data in Fig 5.12 show the drag coefficient results for a smooth plate and the results were compared with the data from Andrewartha [110]. At the low Reynolds number ($Re<0.8*10^6$) there is a significant variation between smooth case results and Andrewartha's [110] data. However, at $Re> 0.8*10^6$ the smooth plate data compared very well with the smooth plate data and experimental results of [110]. The average relative difference between the experimental results and the data for Andrewartha [110] for $Re>0.8*10^6$ is 4.8%. Table 5.3 provides more details about the experimental results of smooth plates in a water tunnel.

Table 5. 3. results of smooth plate

Pump speed (RPM)	C_D (Smooth case)	C_D Andrewartha [110]	Relative Error(%)
150	0.005775	0.005170891	0.104670464
200	0.005368	0.003609084	0.32765373
250	0.004405	0.004056173	0.079184651
300	0.004094	0.003932308	0.039504442
350	0.004208	0.00379308	0.098500874
400	0.004154	0.003642595	0.12310224
450	0.003994	0.003733247	0.065285127
500	0.003801	0.003705432	0.025061454
550	0.003796	0.003661088	0.035663585
600	0.003685	0.003639018	0.012435395
650	0.003617	0.003646099	0.007971276

A repeatability test was performed using the smooth test plate to find the typical deviation of measured drag from the mean more easily. The uncertainty analysis of the drag coefficient of a flat plate can be rated to the extrapolation methods of resistance measurement [131] or to the uncertainty procedure of drag measurement through the wind tunnel [132]. Uncertainty associated with C_D at a given condition is caused by uncertainties in the measurement process and those induced by the curve fit procedure. This requires that the

uncertainties associated with each factor be propagated in order to arrive at a final result. The method chosen here is the Taylor series method of error propagation.

In order to find uncertainties, drag measurements were made 10 times at 11 flow Reynolds numbers. Uncertainty results for 10 repeatability tests are given in Appendix.3 and shown in Figure 5.13.

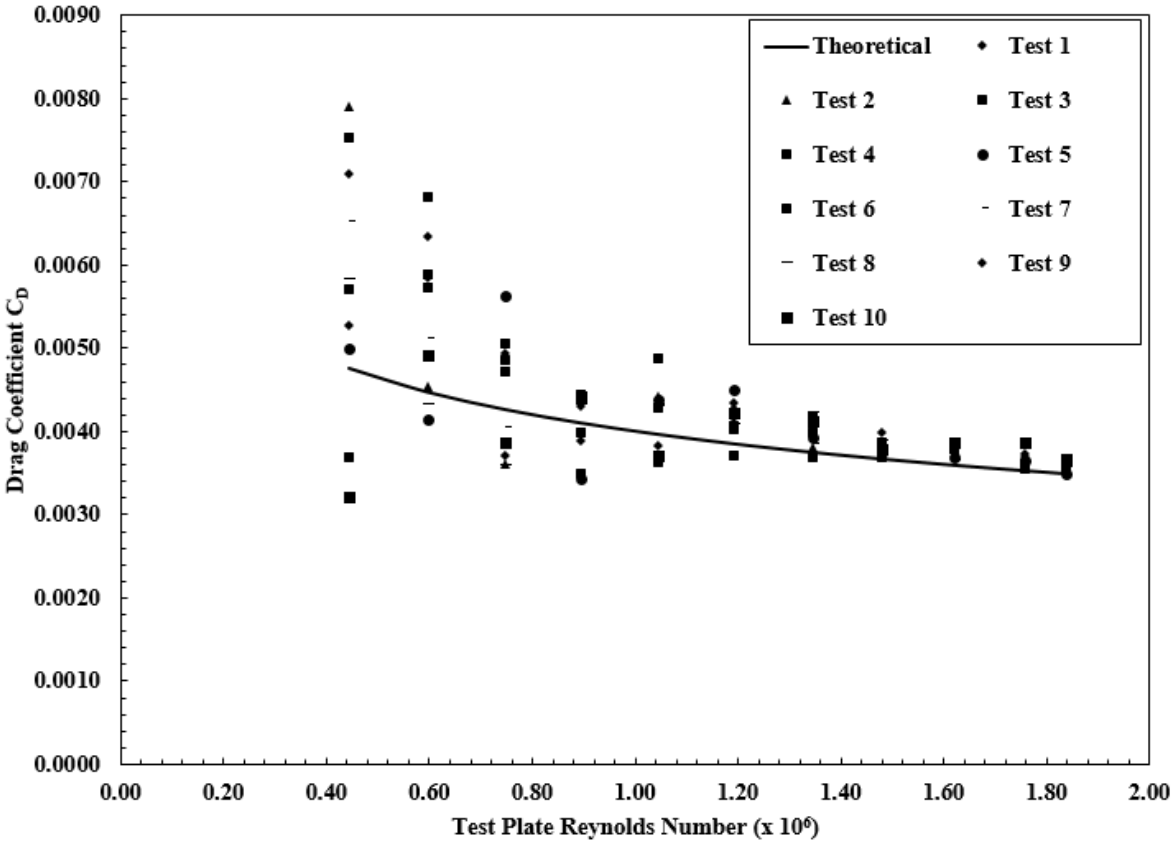

Fig.5. 13. Ten repeatability tests for drag coefficient results

2. Drag measurement results for fouling cases

Three different artificial fouled surfaces were tested in a water tunnel. The barnacles were arranged in a staggered fashion, in which the plan form roughness density was set to λ=0.148, 0.259 and 0.407 for low, medium and high density respectively. The different fouling

plates can be shown in Fig.5.14. Table. 5.4 provides more details about barnacle arrangement on a test plate:

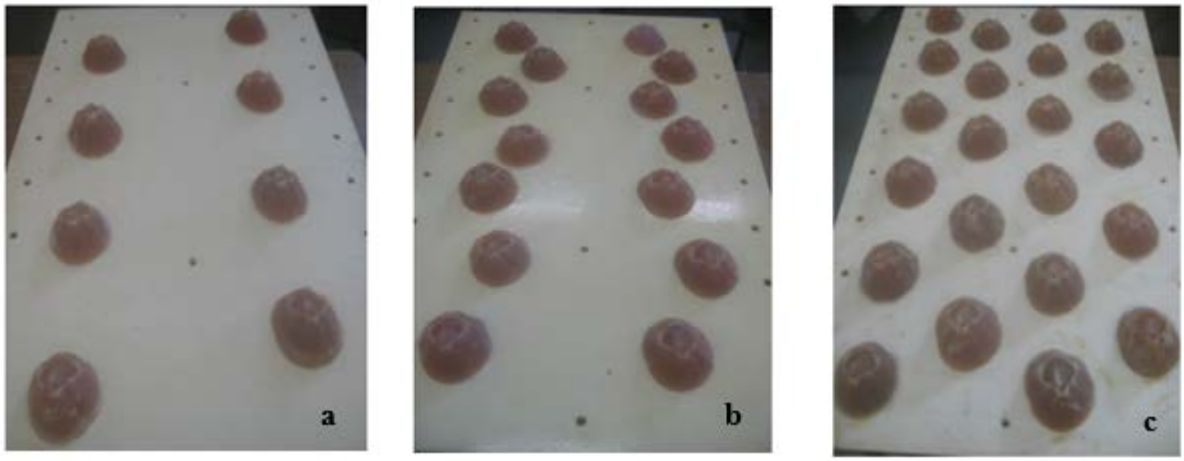

Fig.5. 14. different fouling plates a)low fouling density (λ=0.148) b) medium fouling density (λ=0.259) c) high fouling density (λ=0.407)

Table 5. 4. fouling density parameters

Density status	A_s (mm^2)	A_f (mm^2)	S (mm^2)	S_f (mm^2)	Number of row	Total barnacle	λ
Low	6211.2	29355.5	555329	8328	2	8	0.148
Medium	6211.2	29355.5	555329	8328	3	14	0.259
High	6211.2	29355.5	555329	8328	4	22	0.407

As can be seen in Table. 5.4 the fouling density is dependent on the number of barnacles and the number of rows.

According to Eq.5.10, the drag coefficient is functional of equivalent sand grain roughness height. Therefore, Eq.5.9 cannot be applied to fouled plates. As mean velocity profiles were not taken for the test plates in this study, the virtual origin equation which was obtained by Andrewartha [110] (Eq. 5.8), was used to calculate the drag coefficient for different fouling densities.

The estimate of drag coefficients for fouling plates was carried out using a "Goal Seek" technique in the Excel software. For this purpose, Excel's Goal Seek feature allows the adjustment of a value used in a drag coefficient formula to achieve a specific goal. However, there might be errors to calculate drag coefficient for a fouled plate specially, for high fouling density. This is because a virtual origin equation was used for all fouling density. (There was no appropriate data to find a boundary layer profile for fouling plates. Thus, the virtual origin equation by Andrewartha [110], was used in this research). Fig. 5.15 presents the drag coefficient data taken from the smooth painted plate and fouling plates with artificial barnacle samples with different fouling density.

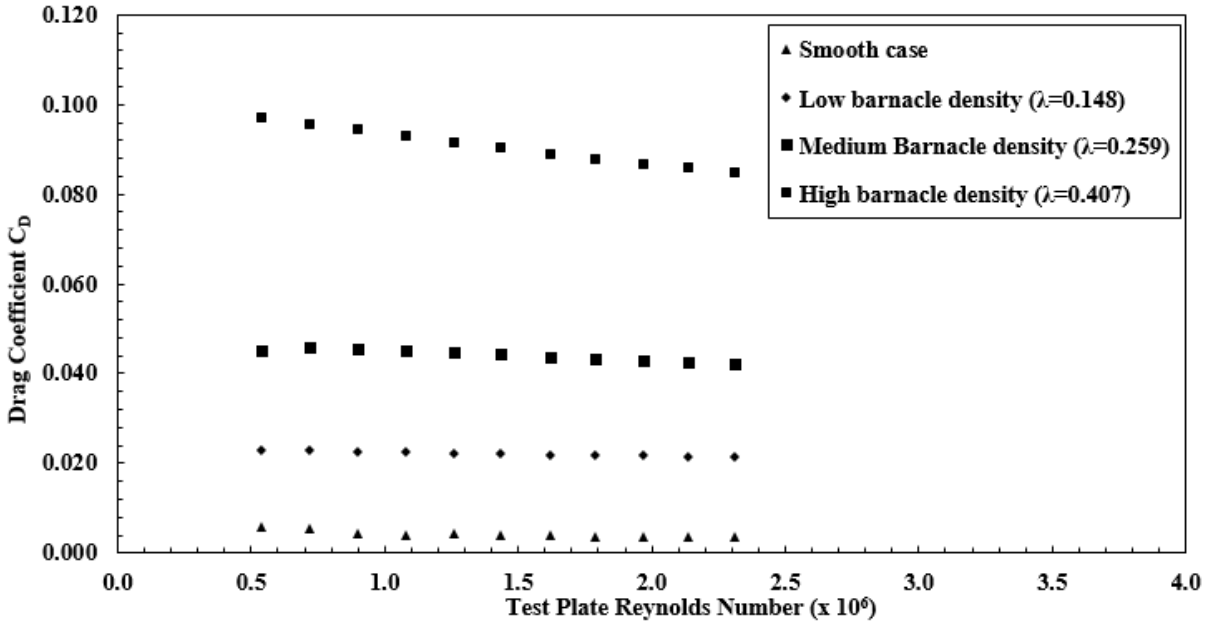

Fig.5. 15. drag coefficient results for smooth and fouled cases

As can be seen in Fig. 5.15, drag coefficient results increased with decreasing the Reynolds number. This is because of the relationship between the drag coefficient and the velocity. The relationship between the drag coefficient of the plate and velocity is inversely proportionate ($C_D=2*US_{correction}*\rho*b*l_1/U^2$). An increase in pump speed causes an increase in pitot static differential value and hence an increase in velocity.

The results of the artificial fouled test plates (Fig. 5.15) show significant increases in drag compared with the respective clean plate conditions. In addition, an increase in fouling density causes an increase in drag coefficient results. The relationship between drag coefficient and fouling density can be shown in Fig. 5.16.

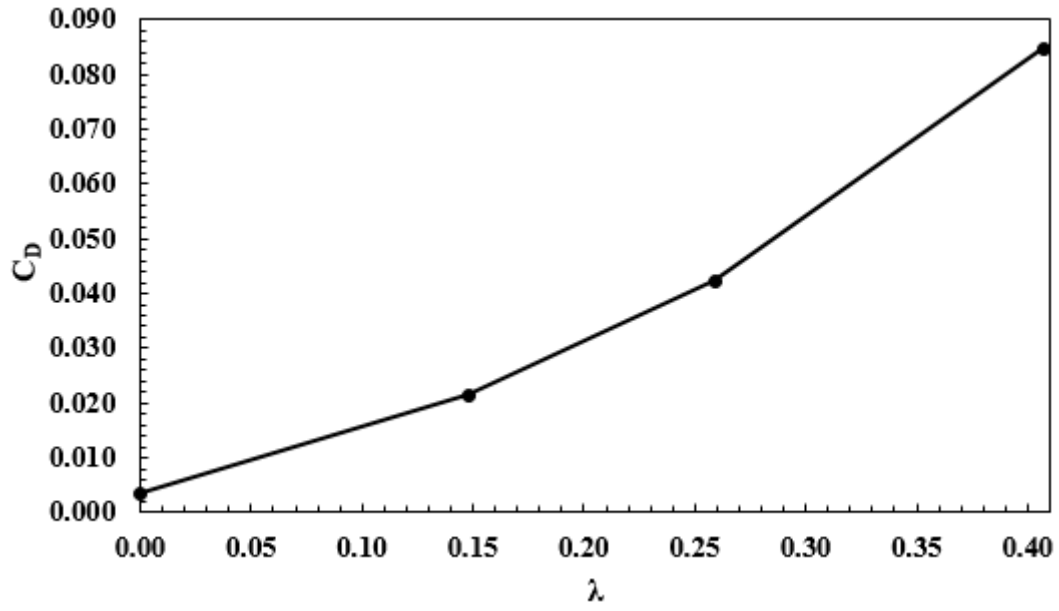

Fig.5. 16. relationship between drag coefficient results and fouling density in pump speed of 650RPM

As can be seen in Fig. 5.16, the relationship between fouling density and barnacle surface is approximately linear over the range of artificial barnacle densities tested. For a smooth plate (λ =0), the mean drag coefficient is minimum. The results reveal that fouling density increases the mean drag coefficient from 0.021 for low fouling density to 0.084 for

high fouling density. Thus, a reduction space between two neighbouring barnacles causes an increase in fouling density and hence an increased friction coefficient result. The percentage of increasing drag coefficient for different fouling density is provided in Fig. 5.17.

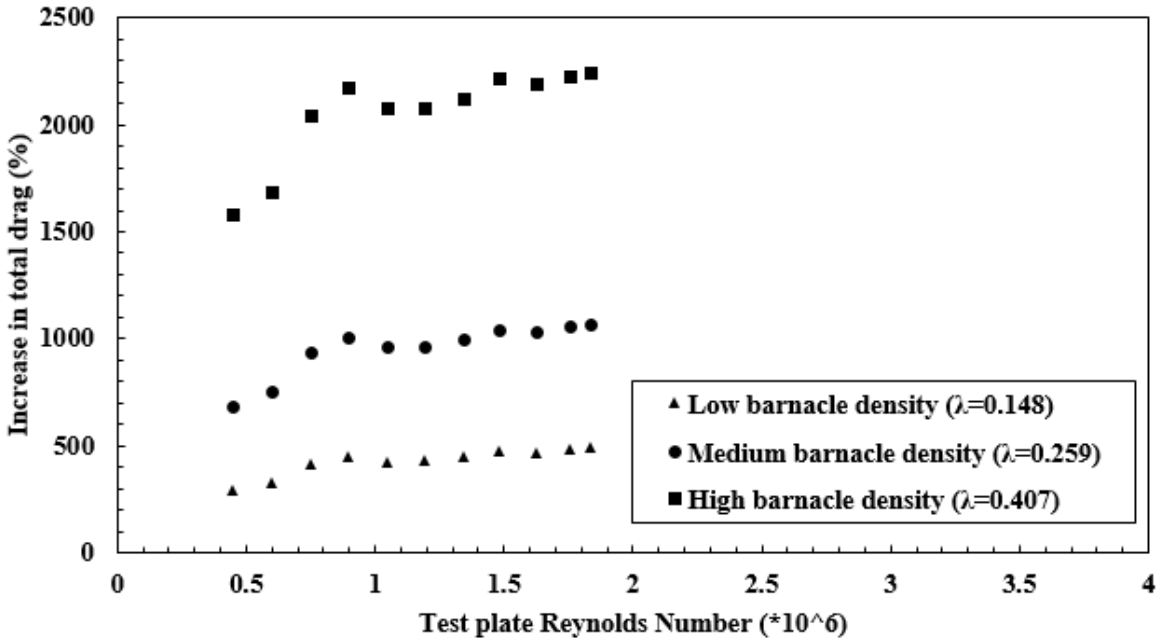

Fig.5. 17. percentage of increasing of drag coefficient due to roughness

According to theoretical drag force, the smooth test plate gives the lowest drag coefficient. As shown in Fig. 5.17, the lowest barnacle density plate produced an average 429% increase in drag coefficient over the clean plate and medium case had over a 900% increase in the drag coefficient over the smooth case. The most drag and greatest measured roughness were for a high density status which had the maximum number of barnacles.

3. Correlation for three-dimensional roughness of flat plate

Based on the measured drag coefficient for roughness cases, equation (5.10) can be used to determine sand grain roughness with very small roughness material. The flow in this method is that it assumes that the roughness is consistent for the test plate and the region

upstream of the test plate, which is not the case for rough test plates. Andrewartha [110] measured an increase of 99% in the drag coefficients of test plates due to biofilms in a recirculating water tunnel. Based on drag coefficient results, the value of sand grain roughness was obtained by this method. The results indicated that the equivalent sand grain roughness values obtained were likely to overestimate the actual roughness of the test plates.

However, the above method may not be appropriate for this research as this formula might be useful only for very small roughness particles [116]. According to Schlichting [116], in order to estimate the sand grain roughness with the above equation, it is important to consider plates with very small roughness (painted metal plates) as well as smooth plates covered with single protuberances, such as rivet heads, welded seams, joints, etc.

Many studies revealed that in order to evaluate the sand grain roughness for a single roughness element, an empirical relationship is needed for the sand grain roughness on the shape parameter factor [34,47,92,93,116,136]. Schlichting [116] indicated that the drag coefficient based on a single roughness element is functional in the largest frontal area of the roughness element perpendicular to the direction of flow. Sigal and Denberg [92], made important advances in accounting for these roughness geometry considerations for uniformly-shaped roughness elements spread in a uniform pattern over a test plate. The relationship between shape factor, Λ, and the roughness dimension has been provide by Eq. 3.3.

The equation used in this study is provided based on the three-dimensional roughness element with cone-shaped size and flat plate test [93]. The correlations for three-dimensional roughness are listed as follows:

$$\frac{k_s}{k} = \begin{cases} 1.583 * 10^{-5} \Lambda_s^{5.683} & \Lambda_s \leq 7.842 \\ 1.802 * \Lambda_s^{0.03038} & 7.842 \leq \Lambda_s \leq 28.12 \\ 255.5 * \Lambda_s^{-1.454} & 28.12 \leq \Lambda_s \end{cases} \quad (5\text{-}11)$$

Based on Eq.3.3 and Eq. 5.11, the equivalent sand grain roughness can be determined (based on the single roughness element method). Figure 5.18 shows the equivalent sand grain roughness obtained by drag coefficient results and physical dimension of roughness element for different fouling densities.

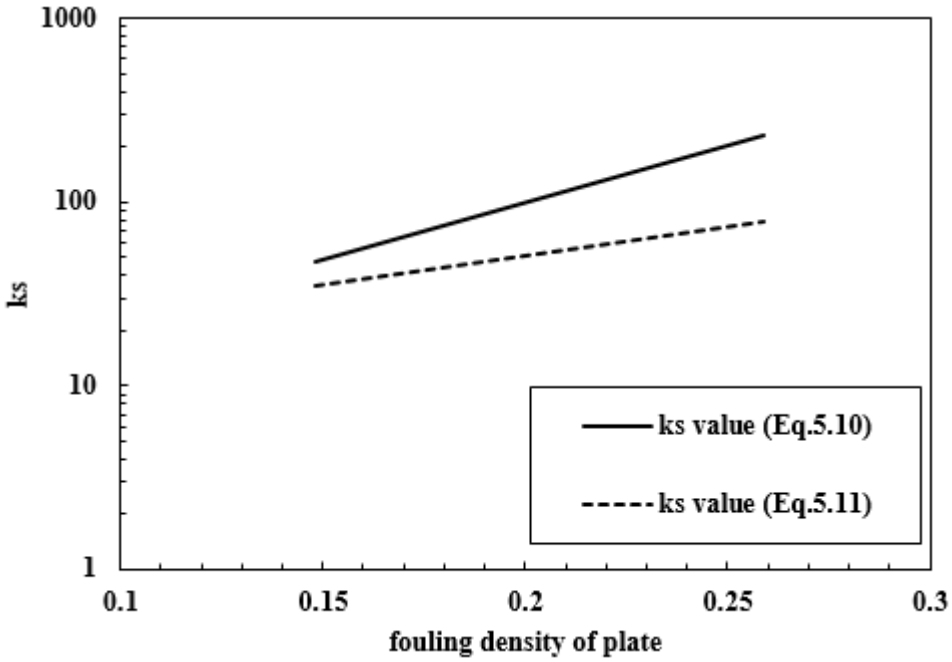

Fig.5.18, Comparison of equivalent sand grain roughness between experimental and physical dimension of roughness methods for different fouling densities

As can be seen in Fig. 5.19, an increase in fouling density parameter causes an increase in equivalent sand grain roughness value for both methods. At low density (λ=0.148) the sand grain roughness height was estimated around 47mm and 35mm by experimental drag coefficient result and geometrical formulation respectively. However, the difference of sand grain roughness value significantly increases by increasing of fouling density of plate.

For the first method (sand grain roughness obtained by drag coefficient results), the sand grain roughness value is directly proportionate by drag coefficient (Eq.5.10). As can be

seen in Fig. 5.17, the medium barnacle density plate produced over 900% increase in drag coefficient over the clean plate. In fact, the average drag coefficient results for medium case (λ=0.259) is around 0.044 which can be around two times higher than the average ones for low density status (λ=0.148). Therefore, the sand grain roughness value for medium case is significantly higher than the sand grain roughness value for low case. This scenario will be repeated for the high density status when the average drag coefficient for (λ=0.407) is around 0.09 and it will be significantly higher than medium case ((λ=0.148). Thus, the highest sand grain roughness for the first method is related to high barnacle density.

Although the second trend of Fig. 5.18 (sand grain roughness results based on geometrical formulation) is also increased, the rate of increase for this method is more reasonable. It is worth to note that the first method may not be appropriate for single roughness element as this formula might be useful only for very small roughness particles [116]. Many studies revealed that in order to evaluate the sand grain roughness for a single roughness element, an empirical relationship is needed for the sand grain roughness on the shape parameter factor [34,47,92,93,116,136].

To calculate the equivalent sand grain roughness size by geometrical formulation, k_s, the shape parameter must be known. It is worth mentioning that, in order to estimate shape parameter, Λ, single roughness dimension such as height and diameter are needed. As the shape of an artificial barnacle in this experiment was not assumed as a full cone and also the frontal size dimension of single roughness element is different with the black side, a trapezoidal shape cannot be a reasonable shape for the frontal area of single roughness (A_f). Based on the real organism of the *Amphibalanus Amphitrite* barnacle which was explained well by Poore [39], a barnacle shell is developed as a radial way. In fact, the frontal area of *Amphibalanus Amphitrite* barnacle is more similar to a triangle shape rather than trapezoidal shape. However, a frustum

cone shape is assumed in order to calculate the windward wetted area of the single roughness element (A_s). In order to calculate the total windward wetted roughness area (S_f), the total number of artificial barnacles for each plate (N) should be considered. As the shape parameter is directly depending on S_f, thus Λ is not constant and the shape factor is varied for each fouling density. The schematic diagram of the frontal area and the windward wetted area of a frustum cone shape of single barnacle are shown in Fig. 5.19. The value of sand grain roughness based on Eqs. 3.3and 5.11, are provided in Table 5.5.

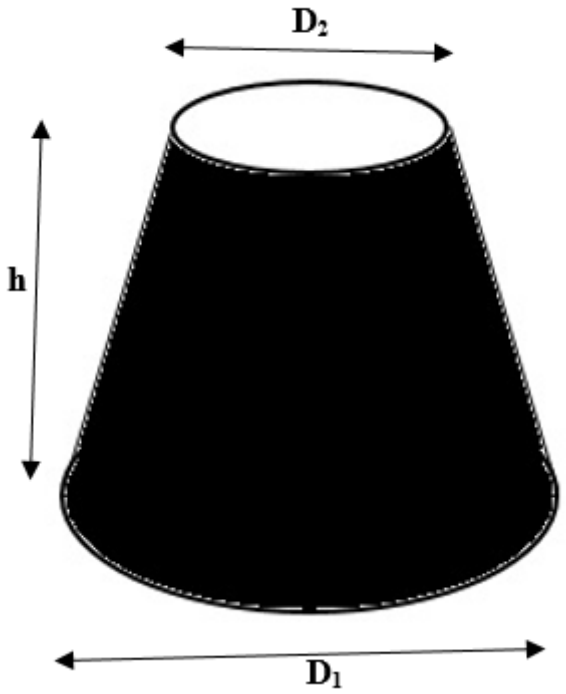

Fig.5.19. Schematic diagram of windward wetted area

Table 5. 5. Sand grain roughness parameter for three different fouling density

Barnacle height, h=57mm,	$S_{Single\ barnacle\ surface} = 8328.065 mm^2$
Barnacle diameter, D=103mm	$S_{Frontal\ area} = 29355.5 mm^2$

*Reference area=b*l=555329mm²* $S_{Single\ wetted\ area}$ *=6211.2mm²*

	Low barnacle density	Medium barnacle density	High barnacle density
λ *(Eq.5.1)*	0.148	0.259	0.407
N(Total number of barnacles)	8	14	22
Λ *(Eq. 3.3)*	63.56	36.32	23.11
Mean C_D*(Experimental results)*	0.022	0.0442	0.09
k_s *(mm)(Eq.5.11)*	34.78	78.47	112.99

The sand grain roughness results for three-dimensional cone-shaped were estimated based on equation used by Van Rij [47] and Schlichting [116]. Therefore, these results should be compared and validated with the results of Van Rij [47] and Schlichting [116]. The comparison results are shown in Fig.5.20.

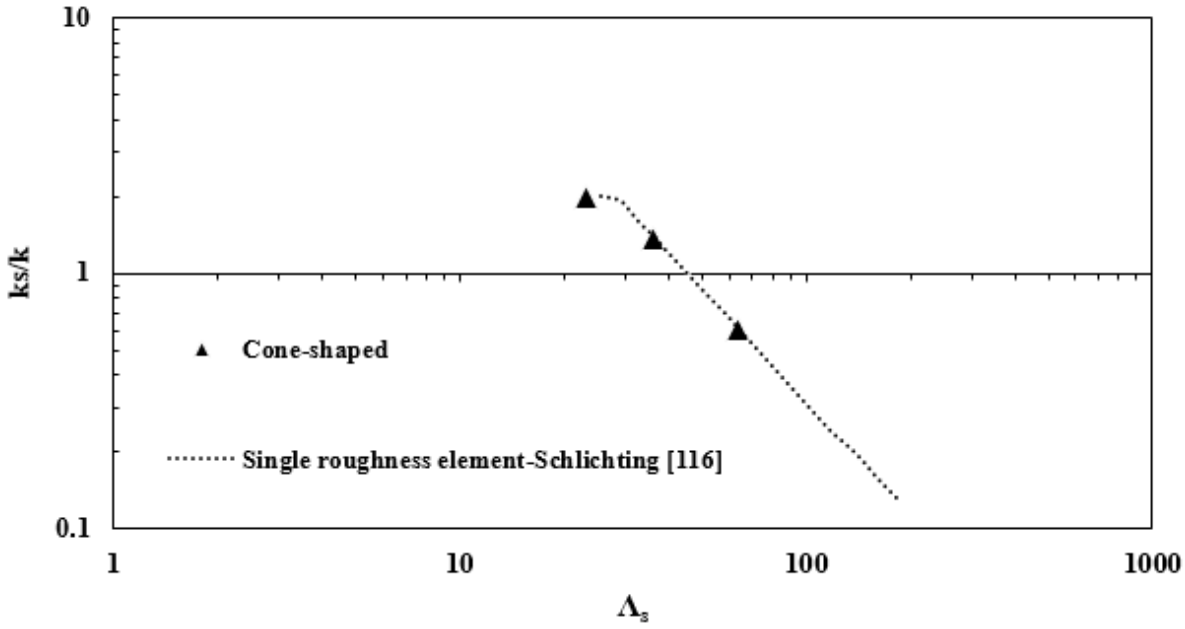

Fig.5.20. Comparison of sand grain roughness results with Eq.5.11with the experimental results of Van Rij [47] and Schlichting [116].

As can be seen in Fig.5.20, the obtained results provide a good match with the experimental data of Van Rij [47] and Schlichting [116]. Based on the shape factor results in Table 5.6, these value for low and medium densities are higher than 28.12. The ratio of sand grain roughness height to actual height was chosen by (Λ>28.12).

In order to describe the flow regime over rough boundaries, it is necessary to determine the roughness Reynolds number, k_s^+ for each test plate. There are three different flow regimes over rough surfaces: hydraulically smooth (k_s^+<5), smooth-rough transition (5<k_s^+<70) and hydraulically rough regime (k_s^+>70). Note that the roughness Reynolds number has been defined in terms of equivalent sand grain roughness height, k_s. Thus, the estimation and validation of sand grain roughness is necessary. The roughness Reynolds number can be described as , $k_s^+ = u^*.k_s/\upsilon$. Where u^* is frictional velocity and υ is kinematic viscosity of fluid. The frictional velocity can be defined as $u^* = u.(c_f/2)^{0.5}$, where the velocity, u, can be determined by Eq 5.4.

Based on drag measurement results and the roughness Reynolds number equation, k_s^+ is considerable higher than 70 for all test plates. This value was estimated at 5000 for a low-density status. As can be predicted the type of flow for all test plates is a fully rough regime as $k_s^+ > 70$. In the hydraulically rough regime, the skin friction is almost entirely dependent on form drag and eddy shedding from the protrusions [137].

7. Discussion

In this chapter, the relationship between fouling density characteristics and the drag coefficient was well established. Based on the fouling density definition which was described by Eq. 5.1, three different fouling plates were created: low, medium and high barnacle densities. The drag coefficient results were obtained by load cell drag equipment in recirculation water tunnel system. According to the experimental results which were provided in Fig. 5.15, an increase in the fouling density causes an increase in the total frictional force and hence an increase in drag coefficient results.

In order to advance the understanding of the effect of fouling density on plate performance, estimations of drag coefficients are not sufficient. According to many studies [33, 47,105-108,111], equivalent sand grain roughness is one of the most important factors to analyse of roughness characteristics. Figure 5.18 made a comparison between sand grain roughness of experimental drag tests and that value for geometrical formulations (Eq. 3.3 and 5.11). As can be clearly seen in Fig. 5.18, an increase in drag coefficient result causes an increase in sand grain roughness value. It is because of sand grain roughness is functional of drag coefficient (Eq. 5.10).

As it can be discussed, the sand grain roughness value is related to the some geometrical parameters of single roughness element as well as surface area. Schlichting [116] indicated that

the drag coefficient based on the single roughness element is functional of the largest frontal area of the roughness element perpendicular to the direction of flow. Sigal and Denberg [92], made important advances in accounting for these roughness geometry considerations of uniformly-shaped roughness elements spread in a uniform pattern over a test plate.

Based on Eq.3.3 and Eq. 5.11, the equivalent sand grain roughness was determined (based on single roughness element method). The results of the shape factor (Eq.3.3) indicated that an increase in the number of roughness elements causes a reduction in the shape factor parameter (The relationship between shape factor and total frontal area is diversely proportionate). The results of sand grain roughness (based on Eq. 5.11) agreed with experimental data of Van Rij [47] and Schlichting [116] for the cone shaped roughness element. The equivalent sand grain roughness for low density is estimated at around 34mm. It would be doubled when low density changes to medium fouling status. The sand grain roughness height increases to around 112mm once the total number of barnacles increased to 22.

However, the main challenge of this study is to find the relationship between equivalent sand grain roughness and turbine performance. As it was discussed in Chapter4, an increase in sand grain roughness value caused an increase the turbine performance. In order to predict the reduction of power turbine generation for precenting of barnacle fouling, the equivalent sand grain roughness parameter should be employed. However, the recent results of sand grain roughness cannot be used directly for a turbine blade surface.

As it was discussed, Eq.5.11 is appropriate for flat plates only. Bons [34] revealed that the equation used for a turbine blade is completely different. . Bons [34] indicated that many of the specific correlations are valid for two and three dimensional regular roughness, including bars, blocks, cones and hemisphere, etc. Bons [34] related the roughness of a surface with cone

shaped elements to equivalent sand grain roughness with equation3.2. Table 5.6 summarizes the sand grain roughness and power generation of a turbine with different fouling densities.

Table 5. 6. power generation and sand grain roughness results for turbine and flat plates

	Low barnacle density	**Medium barnacle density**	**High barnacle density**
		Flat plate	
λ (Eq.5.1)	0.148	0.259	0.407
N(Total number of barnacles)	8	14	22
Λ (Eq. 3.3)	63.56	36.32	23.11
Mean C_D(Experimental results)	0.022	0.0442	0.09
k_s (mm)(Eq.5.11)	34.78	78.47	112.99
		Turbine blade	
Λ (Eq. 3.3)	1608.6	919.2	585
k_s (mm)(Eq.3.2)	0.5	1.05	1.9
C_p(λ=6)	0.397	0.378	0.345
P(kW) (λ=6)	0.485	0.47	0.455

Table 5.6 is divided to two different parts: the first part is especial for flat plate and some useful parameters which are related to effect of tidal turbine performance, have been proved in the second part. It can be obviously seen that an increase in fouling density causes an increase in sand grain roughness results for all cases.

For the second part of table5.6, based on different fouling density, shape parameter and the sand grain roughness were obtained for a tidal turbine blade by Eq. 3.3. and 3.2. respectively. As expected, an increased ratio of fouling density causes a reduction shape factor and hence an increase in sand grain roughness. This is because of the total wetted area of a single roughness element (S_f). For high density status, the sand grain roughness is estimated at around 2mm. According to sand grain roughness results for the real organism, the *Amphibalanus Amphitrite* barnacle, equivalent height and diameter are estimated around 7.5mm and 10mm respectively. In fact, for high density status in a flat plate (λ=0.407), the equivalent sands grain roughness of tidal turbine blade with (h=7.5mm, D=10mm), was obtained 2mm.

According to sand grain roughness value obtained by Eq.3.2 and 3.3, the power coefficient of a tidal turbine model can be estimated for different fouling densities. A commercial RANS solver using a k-ω model was used to estimate the power for different simulated barnacle roughness densities on a twin-bladed turbine. In Chapter 4, it was found that the maximum power generation for both and smooth and roughened cases occurred in a tip speed ratio of 6 (λ=6). Therefore, the maximum power coefficient results were considered in this section.in order to advance understanding of barnacle roughness effect on power generation of tidal turbine, the percentage of decreasing power generation due to roughness is plotted by Fig. 5.21.

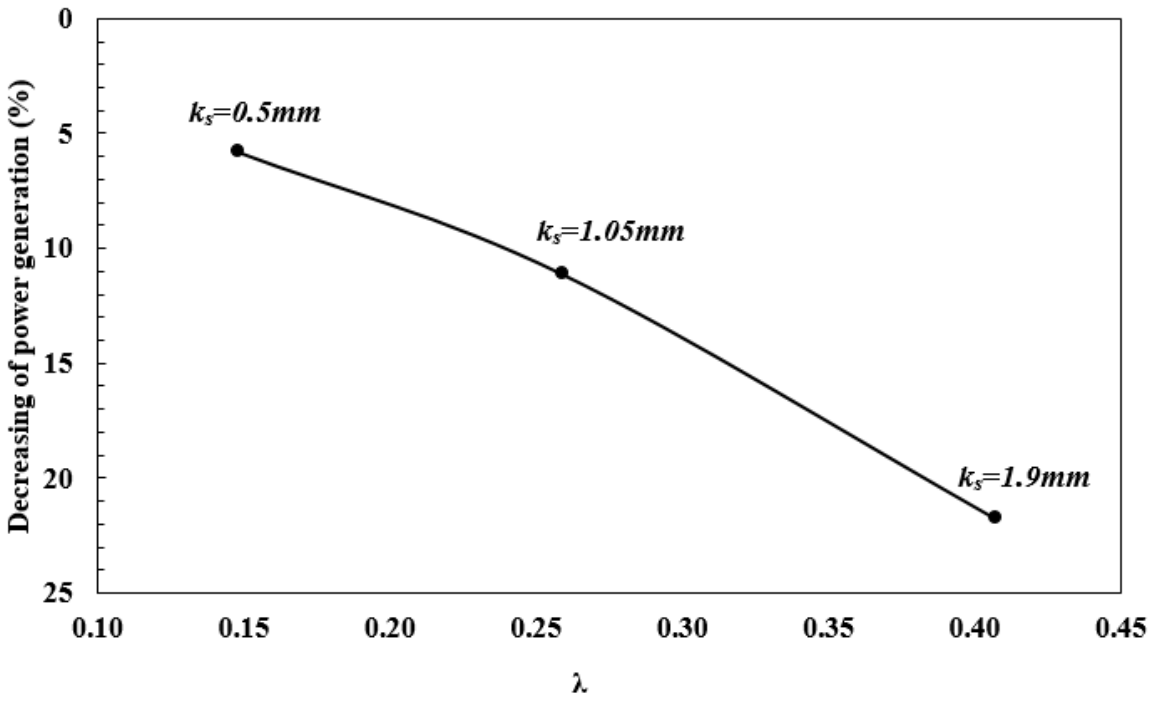

Fig. 5.21, The percentage of decreasing power generation of tidal turbine due to roughness

As was shown in Table 5.6 and Fig. 5.21, an increase in sand grain roughness causes a reduction in power coefficient results. According to theoretical hydrodynamic power of turbine, the smooth case gives the highest power coefficient. It is around 0.42.As shown in Fig. 5.21, the lowest barnacle density produced an average 5% reduction in power coefficient over the clean case. For low density status, the power coefficient is around 0.4 and there is a slight difference between low density and smooth result with the same tip speed ratio. For a medium case, the percentage is over a 10% decrease in the power coefficient over the smooth case. An increase in sand grain roughness value causes a reduction in power generation from 0.38 to 0.34. For high-density status, the percentage of decreasing of power generation is 22%.

In the case of marine renewable energy equipment, barnacle roughness density has an adverse effect on long-term performance. As was clearly explained in section 2.3, an increase in fouling density leads to an enhancement of fouling community on the marine surface. In

addition, an increase in fouling density strengthen of barnacle shell. A kind of strong shell which was produced by larva in the backside of barnacles, causes the high frictional resistance and leads to an increase of weight, subsequent potential speed reduction and loss of annual performance. Results of experimental research by Katsuyama et al. [26] in Japan revealed barnacle roughness development creates a mass imbalance profile on rotor profile of tidal turbines which can stop functioning if barnacle colonization continues.

8. Conclusion

Barnacle colonization produces roughness and increases the drag force on marine surfaces. Growing barnacles will reduce the space between themselves. In this study, artificial barnacles were arranged in a staggered fashion for all fouling densities. Three density cases were considered in this study: low, medium and high barnacle density. The barnacles were spaced apart from one another by one barnacle dimension in the x-y direction. The space between two neighbouring barnacles was the diameter of two adult barnacles, the diameter of one and half adult barnacles and the diameter of half and adult barnacle for low, medium and high fouling density respectively.

In order to investigate of the effect of fouling density on the total drag force, a floating element force balance was used. As the first step, the smooth plate results was validated against the data of Andrewartha [110]. The smooth plate data compared very well with the theoretical smooth plate data and experimental results of Andrewartha [110]. Then the drag coefficient results of fouled cases were compared versus experimental smooth result. As expected, significantly higher drag coefficients were experienced on the test plates with fouling density. As shown in Fig. 5.17, the lowest barnacle density plate produced an average 429% increase in drag coefficient over the clean plate and medium case had over 900% increase in drag coefficient over the smooth case.

An equivalent sand grain value for cone shaped roughness element was estimated using an empirical correlation for three dimensional roughness elements. Based on research by Schlichting [116], there is a relationship between the physical roughness dimension and sand grain roughness height. According to governing equations for cone-shaped roughness elements, an increase in the total number of barnacles caused an increase in the total wetted area and hence an increase in equivalent sand grain roughness. The results of roughness correlations indicated that the equivalent barnacle roughness was 34.78 mm, 78.4 mm, and 112.9 mm for low, medium and high barnacle fouling densities respectively. In addition, the numerical results obtained by empirical correlation agree with the experimental data of Van Rij [47] and Schlichting [116].

Based on governing equations (3.2 and 3.3) for tidal turbine blade and single roughness elements dimension of plate, the equivalent sand grain roughness for different fouling densities were estimated. As expected, an increased ratio of fouling density causes a reduction shape factor and hence an increase in sand grain roughness. This is because of the total wetted area of single roughness element (S_f). For high density status, the sand grain roughness is estimated at around 2mm. In addition, a commercial RANS solver using a k-ω model was used to estimate the power for different simulated barnacle roughness densities on a twin-bladed turbine.

Numerically obtained results indicated that an increase in sand grain roughness causes a reduction in maximum power generation in a tidal turbine. The minimum power coefficient occurred at a high fouling density. This was at around 0.34. the percentage of decreasing of power coefficient of tidal turbine is around 5% and 22% for low and high barnacle density status respectively.

Acknowledgment

I would like to acknowledge Dr. Jessica Walker for supporting and helping the experimental part of project. Dr. Walker spent many hours teaching me how to use the water tunnel equipment, and also provided the health and safety workshop for laser equipment. This section of research could not be finalized without her suggestions and supports.

Chapter 6

Conclusions

The purpose of this study was to investigate biofouling on tidal turbine performance. Among the various types of fouling on man-made structures, barnacles are considered to be one of the most problematic organisms. Therefore, the main objective of this study was to determine the effect of barnacles on the performance of a twin-bladed horizontal axis tidal turbine. This study presented numerical data for a model-scale 2-bladed horizontal axis marine current turbine and also experimental results for different fouling density of plate based on a floating element force balance in a water tunnel. This chapter presents the conclusions of the present study.

In Chapter 2, the characterization of marine barnacles in terms of surface roughness on the performance of marine surfaces was reviewed. Among different types of barnacle characteristics, barnacle height and density have a significant effect on the hydrodynamic parameters of surfaces colonised by barnacles. Growing barnacles will reduce the space between themselves and this increases barnacle density on a surface. Barnacle colonization produces roughness and increases drag force on marine surfaces.

Among different species of barnacles, striped barnacle (*Amphibalanus Amphitrite* barnacle) with cone shaped is chosen in this study. It is because they are most common fouling organism from Queensland to Western Australia and around the world in tropical to warm seas. In addition, the striped barnacle with cone shape, is prevalent bio-fouler of ships and marine structures.

In order to develop a useful numerical model, the effect of the conical shaped barnacle elements on a boundary layer may be represented using an equivalent sand grain roughness. Therefore, the sand grain roughness equations for three-dimensional cone shaped element was used in this study. The equation for equivalent sand grain roughness is functionally related to surface area and single roughness element dimensions. Therefore, barnacle dimension size and fouling density play directly influence the equivalent sand grain roughness. In fact, an increase in barnacle height causes an increase in sand grain roughness. Thus, adult barnacle with high fouling density on marine surface represents the worst case scenario and produces maximum equivalent sand grain roughness.

It is well understanding that the minimum size in height or density of single roughness can have an adverse effect on marine performance. The results of some relevant studies on 2D aerofoil surface revealed that the drag coefficient was increased by an average of 50% for all low barnacle density. Therefore, in order to show the effect of presence of fouling on aerofoil

performance, the minimum size of *Amphibalanus Amphitrite* barnacle height and diameter were chosen to estimate sand grain roughness in this section.

In order to determine the impact of a given very small coating roughness material on the frictional drag of a plate, some non-dimensional analysis which are related to drag coefficient, can be appropriated. The dimensionless similarity for single roughness element is the ratio of the height of the roughness element to the boundary layer thickness, h/δ. As the experimental turbine model in this study, used in this investigation was a $1/25^{th}$ scale model of a prototype turbine, and based on this, a computational model was created. In order to find sand grain roughness for aerofoil model $k_{m\text{-}s}$, the equivalent barnacle height for turbine model was needed. Therefore, dimensionless similarity (*height of single roughness element/boundary layer thickness*) between turbine prototype and model cases was applied.

As the first step, the effect of barnacle roughness on 2D aerofoil investigated. It is because marine current turbine blades typically use an aerofoil shaped cross-section for the blade profile and blade shape is critical to the aerodynamic performance of wind and tidal turbine blades. A commercial Reynolds Averaged Navier-Stokes (RANS) solver with Shear-Stress Transport (SST) turbulence model was used to simulate the flow around a two-dimensional NACA63-618 aerofoil with and without surface roughness. The model was validated against published experimental data for a smooth case. It is obvious that the smooth numerical results show good agreement with the experimental study of Walker et al. [12]. The results showed the presence of the adult barnacle fouling decreased the maximum lift coefficient by an average of 21% and lift-to-drag force ratio by an average of 60%.

In order to illustrate the effect of barnacle roughness on aerodynamic performance, the pressure distribution around the 2D aerofoil was visualized at 0° and 8° of angle of attack. The simulation results revealed the enclosed pressure coefficient area (the enclosed area between

the pressure coefficient curves for each surface is equal to the normal force coefficient of aerofoil) decreases with presence of the simulated barnacle fouling. It can be noted that an increase in fouling height causes a reduction in normal force coefficient. This contributes to a reduction in lift force by an average of 22% and 25% for fouling case at angles of attack of 0° and 8° respectively.

The turbulent kinetic energy increases with fouling height and produced a greater region of turbulent activity in the wake. As shown in the Fig. 3.12, the absolute value of turbulence kinetic energy increased over the upper surface of aerofoil when sand grain roughness was added on surface. In fact a thicker turbulent boundary layer was apparent on the upper aerofoil surface when sand grain roughness was present. With increase in turbulence kinetic energy, the separation point moved to the leading edge and turbulence flow occurred over most of the upper surface.

The effect of cone shaped barnacle roughness on a twin-bladed axial tidal turbine was investigated numerically. The marine current turbine model consisted of a twin-bladed rotor with a diameter of 0.8m. This is representative of a $1/25^{th}$ scale model of a full size turbine. A commercial Reynolds Averaged Navier-Stokes (RANS) solver with k-ω turbulence model was used to simulate the flow around a three-dimensional tidal turbine blade with and without surface roughness. The numerical results for smooth case agreed well with the experimental published data [12]. The numerical results revealed the barnacle roughness decreased the peak power coefficient from 0.42 to 0.37 at the design tip-speed ratio of 6. This represents a decrease in turbine output power of 12%.

The effect of barnacle roughness on total drag force and the turbulent boundary layer on a test plate covered with artificial barnacles was studied experimentally in a water tunnel using a floating element force balance. In order to generate the fouling density on a flat plate,

artificial models were affixed and replicated with different fouling density on the flat plate. The height of single roughness element is constant for all fouling status. Fouling density is defined as a ratio of the total barnacle surface area to the surface area of a flat plate. Artificial barnacle samples were used to generate the fouled plates.

As the boundary layer is measured for smooth and fouled plates, it is necessary to know the relationship between boundary layer thickness and height of roughness of plate. Based on dimensionless similarity for single roughness element [116], the ratio of the height of single roughness element to the boundary layer thickness can play a vital role to estimate equivalent artificial barnacle height for the test plate. Therefore, the ration of boundary layer thickness of plate to height of barnacle was chosen as the dimensionless similarity. The unknown value is the height of artificial barnacle for flat plate. According to previous research which carried out by Andrewartha [110] on the same water tunnel system, boundary layer thickness of flat plate was estimated 35mm for smooth plate. For turbine system, the maximum height of a real organism (*Amphibalanus Amphitrite*) barnacle is 15mm [84]. Thus, the relevant height of artificial barnacle is around 53mm for a test plate.

The artificial barnacle models tested were obtained using a novel method of scanning real barnacles, 3D printing and then moulding them using an epozy resin. As barnacle roughness density is one of the most problematic parameters for marine surfaces, fouling density was chosen for the experimental study. Fouling density is defined as the ratio of the total barnacle surface area on a test plate to test plate area. Three fouled plates were tested with low (λ=0.148), medium (λ=0.259) and high (λ=0.407) barnacle fouling density.

The drag results reveal significantly higher drag coefficients were experienced on the test plates with increase fouling density. As shown in Fig. 5.17, the lowest barnacle density plate produced an average 429% increase in drag coefficient over the clean plate and medium

case had over 900% increase in drag coefficient over the smooth case. In fact, the drag results indicate an increase in fouling density causes an increase in drag coefficient result.

In addition, the results of roughness correlations and sand grain roughness by experimental study indicated that an increase in fouling density parameter causes an increase in equivalent sand grain roughness value for both methods. At low density (λ=0.148) the sand grain roughness height was estimated around 47mm and 35mm by experimental drag coefficient result and geometrical formulation respectively. However, the difference of sand grain roughness value significantly increases by increasing of fouling density of plate.

Based on governing equations (geometrical formulations)for tidal turbine blade and single roughness elements, an increase in sand grain roughness causes a reduction in power coefficient results. According to theoretical hydrodynamic power of turbine, the smooth case gives the highest power coefficient. It is around 0.42. As shown and discussed, the lowest barnacle density produced an average 5% reduction in power coefficient over the clean case. For low density status, the power coefficient is around 0.4 and there is a slight difference between low density and smooth result with the same tip speed ratio. For a medium case, the percentage is over a 10% decrease in the power coefficient over the smooth case. An increase in sand grain roughness value causes a reduction in power generation from 0.38 to 0.34. For high-density status, the percentage of decreasing of power generation is 22%.

In the case of marine renewable energy equipment, barnacle roughness density has an adverse effect on long-term performance. As was clearly explained in section 2.3, an increase in fouling density leads to an enhancement of fouling community on the marine surface. In addition, an increase in fouling density strengthen of barnacle shell. A kind of strong shell which was produced by larva in the backside of barnacles, causes the high frictional resistance and leads to an increase of weight, subsequent potential speed reduction and loss of annual

performance. Results of experimental research by Katsuyama et al. [26] in Japan revealed barnacle roughness development creates a mass imbalance profile on rotor profile of tidal turbines which can stop functioning if barnacle colonization continues.

REFERENCES

[1] Annual Report 2010: Implementing agreement on ocean energy systems; OES-IA: Lisbon, Portugal. Available online: http://www.ocean-energy-systems.org/library/annual_reports/

[2] Annual Report 2011: Implementing agreement on ocean energy systems; OES-IA: Lisbon, Portugal. Available online: http://www.ocean-energy-systems.org/library/annual_reports/

[3] Bedard. R, Jacobson. P.T, Previsic. M, Musial. W, Varley. R. 2010. An overview of ocean renewable energy technologies. Oceanography. 23: 22-23.

[4] Review and analysis of ocean energy systems development and supporting policies. OES-IA: Ireland. June 2006. Available online: http://mhk.pnnl.gov/wiki/index.php/Review_and_analysis_of_ocean_energy_systems_development_and_supporting_policies

[5] Bahaj. A.S, Myers. L.E. 2003. Fundamentals applicable to the utilization of marine current turbines for energy production. Renewable Energy. 28: 2205-2211.

[6] Gross. R, Leach. M, Bauen. A. 2003. Progress in renewable energy. Environ. Int. 29: 105-122.

[7] Tidal energy today: estimate of global potential tidal resources. Available online: http://tidalenergytoday.com/2015/02/17/estimate-of-global-potential-tidal-resources/

[8] Townsin. R.L. 2003. The ship hull fouling penalty. Biofouling. 19:9-15.

[9] Lewthwaite. J.C, Molland. A.F, Thomas. K.W. 1984. An investigation into the variation of ship skin frictional resistance with fouling. The National Academies of Sciences, Engineering , and Medicine: Washington, DC, USA. Pp. 269-284.

[10] Schultz. M.P, Bendick. J.A, Holm. E.R, Hertel. W.M. 2011. Economic impact of biofouling in a naval surface ship. Biofouling. 27: 87-98.

[11] International Maritime Organisation. 2011. A transparent and reliable hull and propeller performance standard; MEPC; IMO: London, UK. Pp. 1-6.

[12] Walker. J. M. Flack. K. A. Lust. E. E. Schultz. M. P. and Luznik. L., 2014. Experimental and numerical studies of blade roughness and fouling on marine current turbine performance. Renewable Energy. 66: 257-267.

[13] Lee J H, Park S, Kim D H, Rhee S H, Kim M C. (2012). Computational methods for performance analysis of horizontal axis tidal stream turbines. Applied Energy; 98: 512-523.

[14] Somerscales E, Knudsen E J, (1981). Fouling of heat transfer equipment. Hemisphere pub.

[15] Sakmani A S, Lam W H, Hashim R, Chong H Y. (2013). Site selection for tidal turbine installation in the Strait of Malacca. Renewable and Sustainable Energy Reviews; 21: 590-602.

[16] Apolinario M, Couthino R, Hellio C, Yebra D. (2009). Understanding the biofouling of offshore and deep-sea structures; Woodshead publishing: Cambridge, UK.

[17] Yebra M, Rasmussen N, Weinell, Pederson T. (2010). Marine fouling and corrosion protection for off-shore ocean. International Conference on ocean Energy; Bilbao, Spain.

[18] Clare A, Aldred N. (2009). Surface colonisation by marine organisms and its impact on antifouling research. Advanced in marine antifouling coatings and technologies; Oxford: Woodhead Publishing, P: 46-79.

[19] Stafslien S, Daniels J, Bahr J, Chisholm B, Ekin A, Webster D, Orihuela B, Rittschof D. (2012). An improved laboratory reattachment method for the rapid assessment of adult barnacle adhesion strength to fouling-release marine coatings. Journal of Coatings Technology and Research; 9(6): 651-665.

[20] Tribou M, Swain G. (2010). The use of proactive in-water grooming to improve the performance of ship hull antifouling coatings. Biofouling; 26(1): 47-56.

[21] Schultz M P. (2007). Effects of coating roughness and biofouling on ship resistance and powering. Biofouling; 23(5): 331-341.

[22] Hui C Y, Long R, Wahl K J, Everett R K. (2011). Barnacles resist removal by crack trapping. Journal of The Royal Sociaty Interface; 8(59): 868-879.

[23] Wood E F, Allen F, Scientific C. (1958). Common marine fouling organisms of Australian waters. Department of the Navy, Navy office.

[24] Redfield A, Hutchins L, Deevy E, Ayers J, Turner H, Laidlaw F, Ferry J, Todd D. (1952). Marine fouling and its prevention. Rep. for Bur. Ships, US Navy Dep. By Woods Hole Oceanogr. Inst., Woods Hole, Mass.

[25] Drake J M, Lodge D M. (2007). Hull fouling is a risk factor for intercontinental species exchange in aquatic ecosystems. Aquatic Invasions; 2(2): 121-131.

[26] Katsuyama I, Kobayashi S, Igawa S, Kyozuka Y, Ida M. (2014). Biofouling of model turbines for tidal current power generation and the effect of anti-fouling paint. Sessile organisms; 31:1-5.

[27] Orme J, Masters I, Griffiths R. (2001). Investigation of the effect of biofouling on the efficiency of marine current turbines. Proceedings of the Marine Renewable Energy conference:, March 27-28: Newcastle, UK.

[28] Thomason J, Hills J, Clare A, Neville A, Richardson M. (1998). Hydrodynamic consequences of barnacle colonization. Recruitment, Colonization and Physical-Chemical Forcing in Marine Biological Systems, Springer:191-201.

[29] Schultz M P, Kavanagh C J, Swain G W, (1999). Hydrodynamic forces on barnacles: Implications on detachment from fouling-release surfaces. Biofouling; 13(4): 323-335.

[30] Koehl M. (2007). Mini review: hydrodynamics of laval settlement into fouling communities. Biofouling; 23(5): 357-368.

[31] Khor Y, Xiao Q. (2011). CFD simulations of the effects of fouling and antifouling. Ocean Engineering; 38(10): 1065-1079.

[32] Hunt M J, Alexander C G. (1991). Feeding mechanisms in the barnacle Tetraclita squamosa (Bruguiere). Journal of Experimental Marine Biology ana Ecology; 154(1): 1-28.

[33] Schultz M P, Swain G W. (2000). The influence of biofilms on skin friction drag. Biofouling; 15(1-3): 129-139.

[34] Bons J P. (2002). St and Cf augmentation for real turbine roughness with elevated freestream turbulence. ASME Turbo Expo: Power for Land, Sea, and Air, American Society of Mechanical Engineers.

[35] Henderson. J. and Lucas. J., 1971. Larval development and metamorphosis of Acanthaster planci (Asteroidea). Nature. 232(5313): 655-657.

[36] Maruzzo. D. n. Aldred. A. S. Clare and Hoeg. J. T., 2012. Metamorphosis in the cirripede crustacean Balanus Amphitrite. PLoS One. 7(5): e37408.

[37] Oliveria. D. and Granhag. L., 2016. Matching Forces Applied in underwater Hull cleaning with Adhesion Strength of Marine Organisms. Journal of marine Science and Engineering. 4(4):66.

[38] He. L. Zhang. G. Quian. P.Y., 2013. Characterization of two 20kDa-cement protein (cp20k) homologues in Amphibalanus Amphitrite. PLoS One. 8(5): e64130.

[39] Poore G. 2010. Barancles. Published by Museum Victoria publishing. ISBN: 9780980381351.Victorian naturalist 2010. 127.

[40] Wang Q, Chen J, Pang X, Li S, Guo X. (2013). A new direct design method for the medium thickness wind turbine airfoil. Journal of Fluids and Structures; 43: 287-301.

[41] Timmer W, Schaffarczyk A. (2004). The effect of roughness at high Reynolds numbers on the performance of aerofoil DU97-W300Mod. Wind Energy; 7(4): 295-307.

[42] Ahmed M R. (2012). Blade sections for wind turbine and tidal current turbine applications current status and future challenges. International Journal of Energy Research; 36(7): 829-844.

[43] Hee Jo C, Yim J, Hee K, Rho Y. (2012). Performance of horizontal axis tidal current turbine by blade configuration. Renewable Energy; 42: 195-206.

[44] Petrone G, de Nicola C, Quagliarella D, Witteveen J, Laccarino G. (2011). Wind turbine performance analysis under uncertainty. Proceeding of 49th AIAA Aerospace Sciences Meeting.

[45] Li D, Li R, Yang C, Wang X. (2010). Effects of surface roughness on aerodynamic performance of a wind turbine airfoil. Proceeding of Power and Energy Engineering Conference (APPEEC), Asia- Pacific, IEEE.

[46] Khalfallah M, Koliub A M, (2007). Effect of dust on the performance of wind turbines. Desalination; 209(1): 209-220.

[47] Flack K A, Schultz M P, (2010). Review of hydraulic roughness scales in the fully rough regime. Journal of Fluids Engineering; 132(4): 041203.

[48] Sagol E, Reggio M, Ilinca A. (2013). Issues concerning roughness on wind turbine blades. Renewable and Sustainable Energy Reviews; 23: 514-525.

[49] Bettermann D. (1965). Contribution a l'etude de la couche limite turbulente le long de plaques rugueuses. Centre National de la Recherche Scientifique Laboratoire d'Aerothermique.

[50] Gregory N, O'reilly C. (1973). Low-speed aerodynamic characteristics of NACA 0012 aerofoil section, including the effects of upper-surface roughness simulating hoar frost. HM Stationery Office.

[51] Timmer W. (2009). An overview of NACA 6-digit airfoil series characteristics with reference to airfoils for large wind turbine blades. AIAA Paper 2009; 268:.

[52] Corten G P, Veldkamp H F. (2001). Insects cause double stall. Copenhagen: EWEC.

[53] Keho M F, Bragg M B. (1997). Airfoil boundary-layer development and transition with large leading-edge roughness. AIAA Journal; 35(1): 75-84.

[54] Ramsay R, Hoffmann M, Gregorek G. (1999). Effects of grit roughness and pitch oscillations on the S809 airfoil: Airfoil performance report, Revised (12/990. Tech. Rep. December, National Renewable Energy Laboratory (NREL).

[55] Zhang Y, Igarashi T, Hu H. (2011). Experimental investigations on the performance degradation of a low-Reynolds-number airfoil with distributed leading edge roughness. AIAA Paper 2011; 1102:.

[56] Ren N, Ou J. (2009). Dust effect on the performance of wind turbine airfoils. Journal of Electromagnetic Analysis and Applications; 1: 102.

[57] Freudenreich K, Kaiser K, Schaffarczyk A, Winkler H, Stahl B. (2004). Reynolds number and roughness effects on thick airfoils for wind turbines. Wind Engineering; 28(5): 529-546.

[58] Pascazio M, Autric J, Favier D, Maresca C. (1996). Unsteady boundary-layer measurement on oscillating airfoils: transition and separation phenomena in pitching motion. AIAA Paper; 96-0035.

[59] Schreck S J, Faller W E, Helin H E, (1998). Pitch rate and Reynolds number effects on unsteady boundary-layer transition and separation. Journal of Aircraft; 35(1): 46-52.

[60] Brodeur R R, Van Dam C, (2001). Transition prediction for a two-dimensional reynolds-averaged navier-stokes method applied to wind turbine airfoils. Wind Energy; 4(2): 61-75.

[61] Dalili N, Edrisy A, Carriveau R. (2009). A review of surface engineering issues critical to wind turbine performance. Renewable and Sustainable Energy Reviews; 13(2): 428-438.

[62] Ma D, Zhao Y, Qiao Y, Li G, (2015). Effects of relative thickness on aerodynamic characteristics of airfoil at a low Reynolds number. Chinese Journal of Aeronautics; 28(4): 1003-1015.

[63] Kerho M. (1995). Effect of large distributed roughness near an airfoil leading edge on boundary layer development and transition. University of Illinois at Urbana-Champaign.

[64] Van Rooij R, Timmer W. (2003). Roughness sensitivity considerations for thick rotor blade airfoils. Journal of Solar Enegy Engineering; 125(4): 468-478.

[65] Bai T, Liu J, Zhang W, Zou Z. (2014). Effect of surface roughness on the aerodynamic performance of turbine blade cascade. Propulsion and Power Research; 3(2): 82-89.

[66] Montis M, Niehuis R, Fiala A. (2010) Effect of surface roughness on loss behaviour, aerodynamic loading and boundary layer development of a low-pressure gas turbine airfoil. ASME Turbo Expo 2010: Power for Land, Sea, and Air, American Society of Mechanical Engineeris.

[67] Montis M, Niehuis R, Fiala A. (2010) Aerodynamic measurements on a low pressure turbine cascade with different levels of distributed roughness. ASME Turbo Expo 2010: Power for Land, Sea, and Air, American Society of Mechanical Engineeris.

[68] Turner A, Hubbe-Walker S, Bayley F. (2000). Fluid flow and heat transfer over straight and curved rough surfaces. International Journal of Heat and Mass Treansfer; 43(2): 251-262.

[69] Korkut E, Atlar M. (2012). An experimental investigation of the effect of foul release coating application on performance, noise and cavitation characteristics of marine propellers. Ocean Engineering; 41: 1-12.

[70] Wan B, Nishikawa E, Uchida M. (2002). The experiment and numerical calculation of propeller performance with surface roughness effects. Kansai Ship Building Association Journal; (238): 49-54.

[71] Kojima H, Toda K, Yamamoto M. (2002). Computation of aerodynamic performance of airfoil with surface roughness. Engineering Turbulence Modelling and Experiments 5. W.R. Fueyo. Oxford, Elsevier Science Ltd: 629-636.

[72] Huang C, Yang K, Liu Q, Zhang L, Bai J, Xu J, (2011). A study on performance influences of airfoil aerodynamic parameters and evaluation indicators for the roughness sensitivity on wind turbine blade. Science China Technological Sciences; 54(11): 2993-2998.

[73] Batten W M J , Bahaj A S, Molland A F, Chaplin J R. (2008). The prediction of the hydrodynamic performance of marine current turbines. Renewable Energy; 33(5): 1085-1096.

[74] Goundar J N, Ahmed M R. (2013). Design of a horizontal axis tidal current turbine. Applied Energy; 111: 161-174.

[75] Ng K W, Lam W H, Pichiah S. (2013). A review on potential applications of carbon nanotubes in marine current turbines. Renewable and Sustainable Energy Reviews; 28: 331-339.

[76] Chen L, Lam W H. (2015). A review of survivability and remedial actions of tidal current turbines. Renewable and Sustainable Energy Reviews; 43: 891-900.

[77] Soares C G, Garbatov Y, Zayed A, Wang G. (2009). Influence of environmental factors on corrosion of ship structurs in marine atmosphere. Corrosion Science; 51(9): 2014-2026.

[78] Antikainen P, Peuranen S. Ice loads, case study. BOREAS V, (2000). Wind power production in cold climates. Proceedings of an International Conference, Levi, Finland.

[79] Jasinski W J, Noe S C, Selig M S, Bragg M B. (1998). Wind turbine performance under icing conditions. Journal of Solar Enegy Engineering; 120(1): 60-65.

[80] Talhaug L, Vindteknik K, Ronsten G, Horbaty R, Baring-Gould I, Lacroix, Peltola E, (2005). Wind energy projects in cold climates. Executive Committee of the International Energy Agency Program for Research and Development on Wind Energy Conversion Systems: 1-36.

[81] Titah-Benbouzid H, Benbouzid M. (2015). Marine renewable energy converters and biofouling: a review on impacts and prevention. EWTEC 2015.

[82] Polagye B, Thomson J. (2010). Screening for biofouling and corrosion of tidal energy device materials:in-situ results for Admiralty Inlet, Puget Sound, Washington, Northwest National Marine Renewable Energy Centre 2010.

[83] Hills J M, Thomason J C, (1996). A multi-scale analysis of settlement density and pattern dynamics of the barnacle *Semibalanus balanoides*. Marine Ecology Progress Series; 138: 103-115.

[84] Frannkel P. Development and testing of marine current turbine's SeaGen 1.2 MW tidal stream turbine. Internaltional Conference on Ocean Energy 2010; Bilbao, Spain.

[85] Ferrer. E, Munduate. X, (2009). CFD predictions of transition and distributed roughness over a wind turbine aerofoil. In 47th AIAA aerospace sciences meeting.

[86] Ren. N, Ou. J, (2009). Numerical simulation of surface roughness effect on wind turbine thick aerofoils. Asia-Pacific Power and Energy Engineering conference.

[87] Patel. VC, Yoon. JY, (1195). Application of turbulence models to separated flow over rough surfaces. Journal of fluid engineering. 117(2):234.

[88] Durbin. PA, Medic. G, Seo. JM, Eaton. JK, Song. S, Rough wall modification of two layer k-epsilon.

[89] Knopp. T, Eisfeld. B, Calvo. Jb, (2009). A new extension for k-w turbulence model to account for wall roughness. International journal of heat and fluid flow. 30:54-65.

[90] Villalpando. F, Reggio. M. Ilinca. A. (2012). Numerical study of flow around iced wind turbine aerofoil. Engineering applications of computational fluid mechanics. 6(1): 39-45.

[91] Dirling. J. R., 1973. A method for computing rough wall heat transfer rates on re-entry nosetips. 8th Thermophysics Conference. Palm Springs, CA, USA.

[92] Sigal. A. and Danberg. J., 1990. New correlation of roughness density effect on the turbulent boundary layer. AIAA journal. 28(3): 554-556.

[93] Van Rij. J. A. Belnap. B. and Ligrani. P., 2002. Analysis and experiments on three-dimensional, irregular surface roughness. Transactions-American Society of Mechanical Engineers Journal of Fluid Engineering. 124(3):671-677.

[94] Menter. F. R., 1994. Two- equation eddy-viscosity turbulence models for engineering applications. AIAA journal. 32(8): 1598-1605.

[95] Langtry. R. and Menter. F., 2005. Transition modelling for general CFD applications in aeronautics. 43rd AIAA Aerospace Sciences Meeting and Exhibit. Reno, Nevada.

[96] Richardson. L.F., 1911. The approximate arithmetical solution by finite differences of physical problems involving differential equations, with an application to the stresses in a masonry dam. Philosophical Transactions of the Royal Society of London. Series A, containing papers of mathematical or physical character: 307-357.

[97] Richardson. L. F. and Gaunt. J. A., 1927. The differed approach to the limit. Part I. Single lattice. Part II. Interpenetrating lattices. Philosophical Transactions of the Royal society of London. Series A, containing papers of mathematical or physical character: 299-361.

[98] Richardson. L. F., 2007. Weather prediction by numerical process. Cambridge University Press.

[99] Mineur. F. Cook. E. J. Minchin. D. Bohn. K. Macleod. A. Kaggs. C. A., 2012. Changing coats: marine aliens and artificial structures. Oceangraphy and marine biology. 50: 189-234.

[100] Ghararli. K. and Johnson. D.A., 2012. Numerical modelling of an S809 airfoil under dynamic stall, erosion and high reduced frequencies. Applied Energy. 93:45-52.

[101] Pourazam. P, Caracoglia. L, Lackner. M, and Moddarres-Sadeghi. Y., 2015. Stochastic analysis of flow-induced dynamic instabilities of wind turbine blades. Journal of Wind Engineering and Industrial Aerodynamics. 137: 37-45.

[102] Corten. GP, Veldkamp. HF, (2001). Insects can halve wind turbine power. Nature: 412-14.

[103] Crisp. D, Walker. G, Yule. A., 1985. Adhesion and substrate choice in mussels and barnacles. Journal of Colloid and Interface Science. 104(1):40-50.

[104] Kamino. K., 2016. Barnacle underwater attachment biological adhesives. 153-176-springer.

[105] Schultz, M. and Swain. G.,1999. "The effect of biofilms on turbulent boundary layers." Journal of Fluids engineering **121**(1): 44-51.

[106] Schultz, M. P. ,2000. "Turbulent boundary layers on surfaces covered with filamentous algae." Journal of fluids engineering **122**(2): 357-363.

[107] Schultz, M. P. 1998., The effect of biofilms on turbulent boundary layer structure, Florida Institute of Technology Melbourne, FL.

[108] Schultz, M. P., 2004. "Frictional resistance of antifouling coating systems." Journal of fluids engineering **126**(6): 1039-1047.

[109] Swift, M. R., Fredriksson. D.W, Unrein. A, Fullerton. B, Patursson. O and Baldwin. K., 2006. "Drag force acting on biofouled net panels." Aquacultural Engineering **35**(3): 292-299.

[110] Andrewartha, J. M.,2010. The effect of freshwater biofilms on turbulent boundary layers and the implications for hydropower canals, University of Tasmania.

[111] Barros. J.M, Murphy. E.A, Schultz. M.P. (2016). Particle Image Velocimetry measurements of the flow over barnacles in a turbulent boundary layer. 18th International Symposium on the Application of Laser and Imaging Techniques to Fluid Mechanics.

[112] Barnes, T. D. S. ,2017. "PINKSIL Skin Safe-Fast Set Moulding System RTV Silicone Rubber." Technical Data Sheet, from www.barnes.com.au/index.php?controller=attachment&id_attachment=560.

[113] Barton, A., Sargison. J, Brandner. P and Walker. G., 2007. A force balance to measure the total drag of biofilms on test plates. 16th Australasian Fluid Mechanics Conference (AFMC), School of Engineering, The University of Queensland.

[114] Cengel, Y, Michael, B., 2005, Thermodynamics-an Engineering Approach. McGraw-Hill, ISBN 0-07-310768-9.

[115] Dynamics, D. 2009. "Laser doppler anemometry - measurement principles."

[116] Schlichting, H. and Gersten. K., 2016. Boundary-layer theory, Springer.

[117] Turan. O, Demirel. K, Day. S, and Tezdogan. T. (2016). Experiemntal determination of added hydrodynamic resistance caused by marine biofouling on ships. Transportation research procedia, Vol. 14, pp. 1649-1658.

[118] Mosaad. M.A. (1986)Marine propeller roughness penalties. PhD thesis. University of Newcastle upon Tyne, UK.

[119] Owen. D, Demirel. Y.K, Oguz. E, Tezdogan. T, and Incecik. A. (2018). Investigating the effect of biofouling on propeller characteristics using CFD, Ocean Engineering. Vol. 159, PP. 505-516.

[120] Dermirel. Y.K, Uzun. D, Zhang. Y, Fang. H.C. Day. A.H, and Turan. O. (20170. Effect of barnacle fouling on ship resistance and powering. Biofouling, Vol. 33. Pp. 819-834.

[121] Demirel. Y.K, Tura. O, and Incecik. A. 920170, Predicting the effect of biofouling on ship resistance using CFD, Applied Ocean research, Vol. 62. Pp. 100-118.

[122] Barnsely. M.J, Wellicome. J.F. (1990). Final report on the 2nd phase of development and testing of a horizontal axis wind turbine test rig for the investigation of stall regulation aerodynamics.

[123] Dvorak. F.A. 919690. Calculation of turbulent boundary layers on rough surfaces in pressure gradients. AIAA journal. Pp. 1752-1759.

[124] Simpson. R.L. (1973). A generalized correlation of roughness densityeffects on the turbulent boundary layer. AIAA journal. Pp. 242-244.

[125] Bos. F.M, Lentink. D, Van Oudheusden. B.W, Bijl. H. (2008). Influence of wing kinematics on aerodynamic performance in havering insect flight. Journal of Fluid Mechanics. Pp. 341-368.

[126] ANSYS CFX User's Guide Release 15.0, ANSYS Inc., Canonsburg (2013).

[127] Examinig Spatial (Grid) Convergence, NPAR Alliance CFD Verification and Validation Web Site. https://www.grc.nasa.gov/WWW/wind/valid/tutorial/spatconv.html

[128] Jo. C.H, Lee. J.H, Rho. Y.H, Lee. K.L. (2014). Perforamnce analysis of a HAT tidal current turbine and wake flow characteristics. Renewable Energy. Vol 65. Pp. 175-182.

[129] Tian. L, Zhao. N, Wang. T. Zho. W, Shen. W. (2018). Assessment of inflow boundary conditions for RANS simulations of neutral ABL and wind turbine wake flow. Journal of wind engineering and industrial aerodynamics. Vol. 179. Pp. 215-228.

[130] Tummala. A, Velamati. R.K, Sinha. D.K, Indraja. V, Krishna. V.H. (2016). A review on small scale wind turbines. Renewable and sustainable energy reviews. Vol. 56. Pp. 1351-1371.

[131] ITTC 2002b. Uncertainity analysis, example for resistance test. ITTC procidures and guidelines, procidure 7.5-02-02-02, Revision 01.

[132] Peters. S.E, (1980). A method to calculate uncertainties of drag coefficient wind tunnel data. Air force armament lab eglin AFB FL.

[133] Gillmer. T.C, Johnson. B. (1982). Introduction to naval architecture. Annapolis, MD:US Naval institute.

[134] Granville. P.S. (1958). The frictional resistance and turbulent boundary layer of rough surfaces. Journal of Ship Research. Vol.2. pp. 52-74

[135] Granville. P.S. (1987). Three indirect methods for the drag characterization of arbitrary rough surfaces on flat plates. Journal of Ship Research. Vol 31(1), pp. 70-77.

[136] Bogard. D.G, Schmidt. D.L, Tabbita. M. (1996). Characterization and laboratory simulation of turbine aerofoil surface roughness and associated heat transfer. ASME international gas turbine and aeroengine congress and exhibition. V004T09A044-V004T09A044.

[137] Nikuradse. J. (1933). Law of flow in rough pipes-Translation of Stomungsgesetze in rahen rohren. NACA report 1929.

[138] Schetz, J.A. (1993). Boundary layer analysis, Prentics-Hall Inc., New Jersey.

[139] Shkedy, Yehoshua, Safriel, Uriel, Tamar, Keasar (1995). Life-history of Balanus amphitrite and chthamalus stellatus recruited to settlement panels in the mediterranean coast of Israel. Israel Journal of Zoology 41:147-161.

[140] Shalla, Salma. H, Ghobashy. Abdul. Hartnoll. Richard (1995). Studies on the biology of Balanus amphitrite Darwin from lake Timsah in the Suez Canal. Crustaceana. 68:503-517.

APPENDICES

A.1. NACA63-618 aerofoil points for Chapter 3

#Group	Point	X-cord (m)	Y-cord (m)	Z-cord(m)
1	1	0.95048	0.01293	0
1	2	0.90103	0.02531	0
1	3	0.85147	0.038	0
1	4	0.80178	0.05073	0
1	5	0.75191	0.0633	0
1	6	0.70187	0.07534	0
1	7	0.65164	0.08655	0
1	8	0.60125	0.09667	0
1	9	0.55069	0.10541	0
1	10	0.5	0.11251	0
1	11	0.44919	0.11767	0
1	12	0.39829	0.12056	0
1	13	0.34734	0.12086	0
1	14	0.2964	0.11822	0
1	15	0.24549	0.11273	0
1	16	0.19469	0.10418	0
1	17	0.14404	0.09219	0
1	18	0.09367	0.07586	0
1	19	0.06868	0.06542	0
1	20	0.04393	0.05268	0
1	21	0.01965	0.03616	0
1	22	0.00797	0.02491	0
1	23	0.00361	0.01878	0
1	24	0.00156	0.01511	0
1	25	0	0	0
1	26	0.00844	-0.01211	0

1	27	0.01139	-0.01458	0
1	28	0.01703	-0.01849	0
1	29	0.03035	-0.025	0
1	30	0.05607	-0.03372	0
1	31	0.08132	-0.03998	0
1	32	0.10633	-0.04484	0
1	33	0.15596	-0.05181	0
1	34	0.20531	-0.05642	0
1	35	0.25451	-0.05903	0
1	36	0.3036	-0.0599	0
1	37	0.35266	-0.05906	0
1	38	0.40171	-0.0563	0
1	39	0.45081	-0.05197	0
1	40	0.5	-0.04633	0
1	41	0.54931	-0.03971	0
1	42	0.59875	-0.03241	0
1	43	0.64836	-0.02475	0
1	44	0.69813	-0.01702	0
1	45	0.74809	-0.0096	0
1	46	0.79822	-0.00297	0
1	47	0.84853	0.00238	0
1	48	0.89897	0.00571	0
1	49	0.94952	0.00603	0
1	50	1	0	0

A.2. Blade geometry details for Chapter 4.

Model	R=0.4 m	NACA 63-618					
Section number	Radius	Pre-Twist	Chord	% Thick	thickness	Pitch Axis	c/R
	(m)	(deg)	(m)	(t/c)	t (m)	(x/c)	
0	0.0000	12.86	0.00000	100.00	0.03200	0	0.0000
1	0.0460	12.86	0.03200	100.00	0.03200	0.5	0.0800
2	0.0580	12.86	0.03920	80.00	0.03136	0.4813	0.0980
3	0.0700	12.86	0.04680	62.90	0.02944	0.4366	0.1170
4	0.0820	12.86	0.05440	46.00	0.02502	0.3834	0.1360
5	0.0895	12.86	0.06000	36.30	0.02178	0.3387	0.1500
6	0.0970	12.86	0.06440	29.80	0.01919	0.3	0.1610
7	0.1045	12.86	0.06816	25.40	0.01731	0.27	0.1704
8	0.1120	12.19	0.06728	22.90	0.01541	0.27	0.1682
9	0.1195	11.52	0.06613	21.00	0.01389	0.27	0.1653
10	0.1270	10.84	0.06511	19.60	0.01276	0.27	0.1628
11	0.1345	10.17	0.06410	18.50	0.01186	0.27	0.1602
12	0.1420	9.50	0.06308	18.00	0.01135	0.27	0.1577
13	0.1540	8.71	0.06136	18.00	0.01104	0.27	0.1534
14	0.1660	8.02	0.05968	18.00	0.01074	0.27	0.1492
15	0.1780	7.43	0.05800	18.00	0.01044	0.27	0.1450
16	0.1900	6.91	0.05628	18.00	0.01013	0.27	0.1407
17	0.2020	6.45	0.05460	18.00	0.00983	0.27	0.1365
18	0.2140	6.04	0.05288	18.00	0.00952	0.27	0.1322
19	0.2260	5.68	0.05116	18.00	0.00921	0.27	0.1279
20	0.2380	5.35	0.04940	18.00	0.00889	0.27	0.1235
21	0.2500	5.05	0.04768	18.00	0.00858	0.27	0.1192
22	0.2620	4.77	0.04592	18.00	0.00827	0.27	0.1148
23	0.2740	4.51	0.04412	18.00	0.00794	0.27	0.1103
24	0.2860	4.26	0.04232	18.00	0.00762	0.27	0.1058
25	0.2980	4.03	0.04048	18.00	0.00729	0.27	0.1012
26	0.3100	3.80	0.03864	18.00	0.00696	0.27	0.0966
27	0.3220	3.57	0.03680	18.00	0.00662	0.27	0.0920
28	0.3340	3.35	0.03488	18.00	0.00628	0.27	0.0872
29	0.3460	3.13	0.03296	18.00	0.00593	0.27	0.0824
30	0.3580	2.90	0.03104	18.00	0.00559	0.27	0.0776
31	0.3700	2.67	0.02904	18.00	0.00523	0.27	0.0726
32	0.3820	2.43	0.02704	18.00	0.00487	0.27	0.0676
33	0.3940	2.18	0.02504	18.00	0.00451	0.27	0.0626
34	0.4000	2.06	0.02404	18.00	0.00433	0.27	0.0601

A.3. Uncertainty results for 10 repeatability test for Chapter 5.

Pump speed (rpm)	Approximate Velocity (m/s)	Mean C_D	Std Deviation	Std Error
150	0.52	0.00577	0.001554	0.000491441
200	0.69	0.00536	0.000895	0.000283124
250	0.86	0.0044	0.000725	0.000229144
300	1.04	0.00409	0.000387	0.000122372
350	1.21	0.0042	0.00038	0.000120051
400	1.38	0.00415	0.000213	6.73992E-05
450	1.56	0.00399	0.000173	5.47723E-05
500	1.72	0.0038	0.000097	3.06793E-05
550	1.89	0.00379	0.000075	2.39588E-05
600	2.05	0.00368	0.000128	4.05309E-05
650	2.22	0.00361	0.000065	2.0843E-05